Ore Geology Reviews 72 (2016) 402–433

Contents lists available at ScienceDirect

Ore Geology Reviews

journal homepage: www.elsevier.com/locate/oregeorev

Late Mesozoic molybdenum mineralization on Hainan Island, South China: Geochemistry, geochronology and geodynamic setting

D.R. Xu [a,*], C.J. Wu [a,*], G.C. Hu [a,b], M.L. Chen [c], Y.R. Fu [c], Z.L. Wang [d], H.Y. Chen [a], P. Hollings [e]

[a] Key Laboratory of Mineralogy and Metallogeny, Guangzhou Institute of Geochemistry, Chinese Academy of Sciences, Guangzhou 510640, China
[b] University of Chinese Academy of Sciences, Beijing 100049, China
[c] Hainan Bureau of Geology, Haikou 570206, China
[d] School of Geosciences and Info-Physics, Central South University, Changsha 410083, China
[e] Department of Geology, Lakehead University, 955 Oliver Road, Thunder Bay, ON P7B 5E1, Canada

ARTICLE INFO

Article history:
Received 12 September 2014
Received in revised form 28 July 2015
Accepted 28 July 2015
Available online 12 August 2015

Keywords:
Mo mineralization
Hainan Island
Late Mesozoic
Tectonic setting
Granites

ABSTRACT

Hainan Island has become an important molybdenum (Mo) producer in East China, with the proven and measured metal Mo reserves of >0.29 Mt and >0.69 Mt, respectively. The known Mo-related deposits and occurrence which genetically might be attributed to porphyry- and hydrothermal vein types are hosted predominantly within the Cretaceous granitoids. These granitoids belong to high-K calc-alkaline, metaluminous to weakly peraluminous I-type series, and have geochemical affinities to arc-related basalts as defined by SiO_2 (57.40–77.34 wt.%) and K_2O (2.45–6.28 wt.%) contents, A/CNK ratios (mostly 0.86–1.10), depleted K, Ba, Nb, Sr, P and Ti, and enriched Rb, Th, Pb, Zr and La, and LREE-enriched REE patterns ($La/Yb_N = 7.1–66.3$) with pronounced negative Eu anomalies to no Eu anomalies ($Eu/Eu^* = 0.35–1.08$). The highly variable geochemical compositions might be linked to magmatic processes. The LA-ICP-MS U–Pb dating on zircon have revealed three stages of magma emplacement for the Cretaceous Mo-hosting granitoids during ca. 113–108 Ma, ca. 100–94 Ma and ca. 90–70 Ma, respectively. The initial $^{87}Sr/^{86}Sr$ ratios (from 0.70567 to 0.71208) and $\varepsilon_{Nd}(t)$ values (from −3.9 to −6.9) suggest that the host granitoids were sourced from an enriched subcontinental lithospheric mantle that had been metasomatized by fluids and/or melts released from ancient, subducted oceanic crust under an extension-induced setting. This setting is most favorable to variable degree of magma mixing between mantle-derived and crust-derived melts.

With the second event as most important and the third event likely recording the youngest Mo mineralization in East China, the Re–Os dating of molybdenite from two types of Mo deposits on Hainan Island has identified three Mo mineralizing events occurring at ca. 112 Ma, ca. 106–95 Ma and ca. 89–72 Ma. They are consistent with the episodes of the Cretaceous magmatism. The Re concentrations of molybdenites and $\delta^{34}S$ values of sulfides (1.36–5.73‰ and average 4.3‰) commonly indicate that the metal Mo is of hybrid origin between mantle and crust but with variable degree of hybridization. Given that the subduction of the Paleo-Pacific plate beneath the eastern Asian margin dominated the Late Mesozoic tectonism of South China, and that Hainan Island has been a part of the Cathaysia Block since Late Permian, the widespread Cretaceous extension and associated Mo mineralizing event(s) on Hainan Island might be a response to episodic rollback of the subducted slab, which led to the underplating of mantle-derived basaltic melts and associated deep crustal melting. Moreover, this tectono-magmatic scenario likely resulted in the migratory pluses of Mo metallogenesis and the change of metal Mo sources from northeast to southwest Hainan Island.

1. Introduction

Hainan Island, located on the northern margin of the South China Sea (Fig. 1a), has long been known for its Fe- and Au reserves, such as the large-scale, Shilu hematite-rich Fe–Co–Cu ore district (Xu et al., 2013, 2014a, 2015) and the Gezhen- and Baolun-type gold ore deposits (e.g., Hou et al., 1996; Ding et al., 2005), and therefore previous research into metallogenesis on Hainan Island mainly focused on this two ore deposit-types. Recent exploration suggests that there is significant potential for molybdenum (Mo) mineralization on Hainan Island, because eight Mo-related deposits and one occurrence have been identified (Fig. 1b and Appendix A1). Among these, the Luokuidong deposit (Fig. 1b and Appendix A1) is one of the most exciting discoveries in South China, accounting for proven Mo reserves of more than 254,346 tons, with an average grade of 0.05% (HBG: Hainan Bureau of Geology, in press).

* Corresponding authors.
E-mail addresses: xuderu@gig.ac.cn (D.R. Xu), wuchuanjun321@126.com (C.J. Wu).

http://dx.doi.org/10.1016/j.oregeorev.2015.07.023
0169-1368/

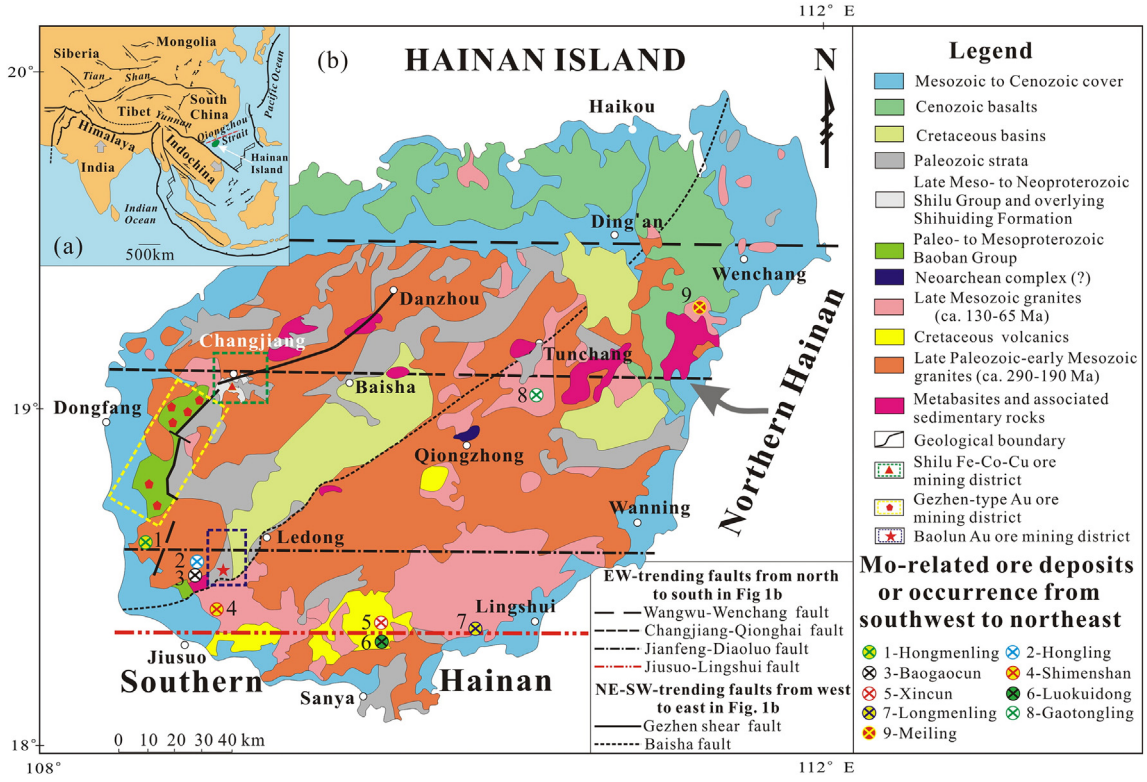

Fig. 1. (a) Location map (modified after Xu et al., 2014a) and (b) geological sketch map showing major stratigraphic and magmatic units, structures and molybdenum (Mo)-related ore deposits or occurrence on Hainan Island (modified after Xu et al., 2013, 2014a).

China is currently the largest Mo producer in the world with most of the metal Mo reserves located in East China, where reserves of metals Mo, W, Sn, Bi and Sb rank among the largest worldwide (USGS, 2011). The major types of Mo ore systems in East China contain porphyry, porphyry–skarn, skarn, and hydrothermal vein, which produced the giant East China Mesozoic metallogenic province and its constituent metallogenic belts or regions (Mao et al., 2011a). Mao et al. (2011a) and Zeng et al. (2013) suggested that the majority of the Mo deposits in East China formed during the Mesozoic between 240 Ma and 80 Ma, and might be linked to multiple tectono-magmatic events, involving far-field-subduction, plate collisions, crustal thickening, post-collision collapse, and extension/rifting or lithospheric thinning, and associated crust–mantle processes (Hua et al., 2003; Zhou et al., 2006). Over the last century, the majority of studies have focused on the Mo deposits as isolated units at the ore-field scale, rather than research involving all the coeval Mo ore deposits at the regional scale (e.g., Mao et al., 2011a,b; Li et al., 2012; Zeng et al., 2013). Especially, most of the published, Chinese and international papers have contributed to the genesis and associated tectonic settings of Mo ore deposits in the South China, Middle-Lower Yangtze River Valley, East Qinling–Dabie, Interior of North China Craton, Yan–Liao and Northeast China (Mao et al., 2011a). Consequently, the importance of Mo mineralization on Hainan Island has been underestimated. It is necessary to place more emphasis on the Mo-related deposits on Hainan Island, in order to evaluate the nature of the Mo mineralization, and more importantly to pinpoint the link between the Mo mineralizing events and the Mesozoic tectonic development of East China. In this contribution, we carried out analysis on geochemistry and Nd–Sr isotopes of host rocks, and sulfur isotope of sulfide minerals, as well as LA-ICP-MS U–Pb dating on zircon from host rocks and Re–Os dating on molybdenite from the Mo-related deposits on Hainan Island. The aim of the paper is to precisely and accurately define the timing of granitic magmatism and associated Mo mineralization, and to elucidate the Mo metallogenetic events and their corresponding geodynamic settings.

2. Geological setting

South China comprises the Yangtze Block in the northwest and the Cathaysia Block in the southeast (Li et al., 2002a). Traditionally, Hainan Island has been regarded as the southwestern extent of the Cathaysia Block, adjacent to the northern Indochina Block (Fig. 1a; Li et al., 2002a, 2008a,b; Metcalfe, 2013). Except for the unconfirmed Devonian and Jurassic (HBGMR, 1997), the stratigraphy is dominated by Paleozoic successions that outcrop as isolated units dispersed over the island, whereas Precambrian strata are relatively rare and mostly occur in western Hainan Island (Fig. 1b). Hainan Island is covered mostly by Permian to Cretaceous intrusive and extrusive rocks which comprise ca. 50% of the land area (Fig. 1b). Based on zircon SHRIMP, LA-ICP-MS and conventional U–Pb, mica (biotite, muscovite and sericite) and amphibole K–Ar and Ar–Ar, and whole rock Rb–Sr dating methods (Wang et al., 1991; Hou et al., 1996; Li et al., 2006; Wang et al., 2011, 2012; Zhang et al., 2011a; Tang et al., 2013; Jiang and Li, 2014; HBG, in press; and references therein), the intrusions can be grouped into the Late Carboniferous to Permian (ca. 300–250 Ma), the Triassic (ca. 250–200 Ma), the Middle to Late Jurassic (ca. 173–150 Ma) and the Cretaceous (ca. 131–70 Ma). Two sets of fault systems dominate the tectonic configuration of Hainan Island, the NE-trending Gezhen and Baisha faults occurring from west to east, and the E-trending Wangwu–Wenchang, Changjiang–Qionghai, Jianfeng–Diaoluo and Jiusuo–Lingshui crustal scale faults passing through the island from north to south (Fig. 1b). Because of its unusual tectonic setting, i.e., situated at the intersection of the Eurasian, Indian–Australian and Pacific plates (Fig. 1a), Hainan Island was subjected to complex tectonic development accompanied by multiple deformation, magmatism and metamorphism which led to many metalliferous ore deposits containing Fe, Co, Cu, Pb, Zn, Au, Ag, W, Sn and Mo (Xu et al., 2013).

The suggested position of the Cathaysia Block including Hainan Island (Li et al., 1995, 1999) before the late Mesoproterozoic assembly of the Rodinia supercontinent, implies that a united, Paleoproterozoic or older crystalline basement (Li et al., 2008a; Wang et al., 2015)

which mainly comprised amphibolitic gneisses, granulites and charnockites of granulite facies metamorphism (Zhang et al., 1997), likely underlies Hainan Island. Paleoproterozoic to Mesoproterozoic rifting (HBGMR, 1997; Zhang et al., 1997) led to the deposition of the ca. 1.80–1.45 Ga Baoban Group (HBGMR, 1997; Ma et al., 1997) in a spreading back-arc or inter-arc basin (Xu et al., 2013). This is consistent with the protoliths to the Baoban Group, a suite of flysch, clastic–sedimentary rocks containing pelites, siltstones, thin-bedded siliceous rocks and minor greywackes, interlayered with mafic and intermediate to mafic volcanic and pyroclastic rocks (HBGMR, 1997). Nevertheless, the Baoban Group has been identified mainly in the hanging wall of the NE-trending Gezhen shear fault (Fig. 1b). At ca. 1450 Ma, mixed S- and I-type granites were emplaced within the Baoban Group (Xu et al., 2013), which led Li et al. (2008a) to suggest that the Cathaysia Block was part of western Laurentia before and during the late Mesoproterozoic assembly of Rodinia (Li et al., 2002a).

During the late Mesoproterozoic Grenvillian orogeny, which led to the formation of Rodinia supercontinent, a more extensive South China Block (SCB) was likely formed when the Cathaysia and the Yangtze Blocks were amalgamated during the South China Jinningian event (Li et al., 2008b). On Hainan Island, this orogeny not only initiated the development of the NE-trending Gezhen shear fault and regional metamorphism to amphibolite and granulite facies of the Baoban Group (Fig. 1b; HBGMR, 1997; Ma et al., 1997), but also likely caused the sedimentation of the Late Mesoproterozoic to Early Neoproterozoic Shilu Group and overlying Shihuiding Formation (ca. 1.08–0.83 Ga) in a marine, retro-arc foreland basin (Xu et al., 2014a, 2015; Wang et al., 2015). As a result, the Baoban Group was metamorphosed to migmatitic gneisses, plagioclase–amphibole gneisses and quartz–mica schists (Ma et al., 1997), which host a series of the shear zone-related Gezhen-type Au deposits (Fig. 1b; Hou et al., 1996). The contact relationship between the Shilu Group and the underlying Baoban Group is rarely observed due to the thick Quaternary cover. At the end of the Jinningian event (HBGMR, 1997), the Shilu Group and overlying Shihuiding Formation were subjected to regional metamorphism of greenschist facies. Both the Shilu Group, comprising metamorphosed neritic siliciclastics and sedimentary carbonates, and the Shihuiding Formation, containing a suite of low-grade, terrigenous clastic sedimentary rocks, only appear in the Shilu area and host the banded iron formation (BIF)-type Fe–Co–Cu ore district (Fig. 1b; Xu et al., 2013, 2014a, 2015). However, Li et al. (2008a) suggested an age of ca. 1440–1430 Ma for deposition of the Shilu Group in a rift environment, and an age of ca. 1200–1000 Ma for the Shihuiding Formation in a foreland basin. Therefore, the depositional times and tectonic settings of both the Shilu Group and overlying Shihuiding Formation need to be further constrained.

By the Cambrian, following the Neoproterozoic (ca. 830–740 Ma) breakup of Rodinia (Li et al., 1999), the separated SCB from Rodinia drifted close to the Australian continent within the newly forming East Gondwana (Li et al., 2008b). Significantly the Cambrian neritic to littoral, P–Mn-bearing siliciclastic rocks and sedimentary carbonates which contain *Trilobite* fossils, comparable to those in Queensland, northeastern Australia (Zeng et al., 1992), were deposited in the Sanya area of the southern Hainan Island at this time (Fig. 1b). This indicates that Hainan Island was a part of East Gondwana (Xu et al., 2014b). Conformably overlying the Cambrian rocks are the Lower Ordovician to Middle Silurian, marine volcaniclastic sedimentary rocks in the northern Hainan Island or neritic–littoral to terrestrial clastic rocks and sedimentary carbonates in southern Hainan Island (HBGMR, 1997). These rocks also host many metalliferous ore deposits, such as the large-scale Baolun quartz vein-type Au ore deposit within the Lower Silurian succession (Fig. 1b). During the Middle Ordovician to Late Silurian, the Cathaysia and Yangtze Blocks, which had been rifted apart during the Neoproterozoic, collided for the second time and re-formed the SCB (Li et al., 2008b). On Hainan Island, this collisional event, i.e., the South China Caledonian orogeny (Wang et al., 2013), has been recorded by deformation of the early Paleozoic rocks, and a high-angular unconformity between the early Paleozoic and the overlying Carboniferous units (HBGMR, 1997). However, the Devonian rocks as well as the Silurian granites, which are widespread in the SCB (Shu et al., 2014a), have not been found on Hainan Island (HBG, in press). This leads to a multivariant division of Hainan Island into two terranes which belong to either the Cathaysia or the Indochina Blocks (Metcalfe et al., 1994; Li et al., 2002b). Subsequently, Hainan Island, together with the SCB, was separated from the Gondwana during the Late Devonian (Metcalfe, 2013), and then moved northward and merged into the southeast Asian continental margin during the Permian, resulting in a prominent unconformity between the late Paleozoic and Early Triassic strata (HBGMR, 1997).

During the late Paleozoic, rifting occurred along the present Changjiang–Qionghai fault in the northern Hainan Island (Fig. 1b), eventually forming an oceanic basin due to continuous extension as shown by the presence of metamorphosed mid-ocean ridge basalts which likely represent the relics of the east Paleo-Tethyan oceanic crust (Li et al., 2002b). The presence of the oceanic basin resulted in the deposition of Carboniferous and Permian volcaniclastic rocks and sedimentary carbonates (Fig. 1b), and the formation of a conformable contact between the Carboniferous and the Permian successions (HBGMR, 1997). In the late Paleozoic to early Mesozoic, closure of the ocean basin and subsequent collision between the two separated massifs resulted in the formation of the Shilu mélange (Hsü et al., 1990) with voluminous Indosinian to early Yanshanian granites (ca. 300–200 Ma) emplaced on the Island. The disappearance of the Paleo-Tethyan oceanic crust in the early Mesozoic was likely coeval with the formation of the Pangea supercontinent (ca. 250 Ma; Wang et al., 2013).

After the Middle Jurassic the SCB, including Hainan Island, likely lay in an extensional back-arc setting (Zhou et al., 2006) due to subduction and slab roll-back of the Paleo-Pacific plate beneath the South China continental margin. The Cretaceous (ca. 130–70 Ma) granites and mafic dikes, and the coeval volcanic rocks on Hainan Island, indicate that this extensional event commenced in the Early Cretaceous (Xu et al., 2013). This was heralded by the formation of Late Jurassic–Late Cretaceous NE-trending terrestrial clastic red beds in inland lakes (Zeng et al., 1992; HBGMR, 1997). Late Cretaceous to Cenozoic rifting led not only to the Cenozoic depressions/sags and large-scale volcanism on Hainan Island and its peripheral areas, but ultimately to the South China Sea oceanic crust (Xu et al., 2013).

3. Ore geology and deposit classification

Based on the standard of Zeng et al. (2013), the known eight Mo-related ore deposits and one occurrence on Hainan Island (Fig. 1b; Appendix A1) are the large-scale (100,000–500,000 tonnes Mo) Luokuidong Mo deposit, the medium-scale (10,000–100,000 tonnes Mo) Shimenshan Mo–Pb–Zn–Ag and Longmenling Mo deposits, the small-scale (<10,000 tonnes Mo) Baogaocun Mo, Xincun Mo, Gaotongling Mo, Meiling Cu–Mo and Hongmenling Mo–W–Pb–Zn deposits, and the Hongling occurrence. The known deposits have proven and measured Mo reserves of more than 0.29 Mt and 0.69 Mt, respectively, with average grades ranging from 0.05 wt.% to 0.24 wt.% (Appendix A1). Aside from that the Luokuidong and Xincun deposits are hosted by both the granitoids consisting of monzogranites, porphyritic granites, rhyolitic porphyries, granite porphyries and quartz-orthophyres, and the continental volcanic rocks composed of rhyolitic and dacitic porphyroclastic rocks, andesites and andesitic breccia, and the Meiling deposit was installed within granodiorites, granodioritic porphyries and explosive breccias, the remaindering deposits and occurrence occurred within granitoids comprising syenogranites, (porphyritic) monzogranites, (plagio)granite porphyries, porphyritic granites, and granodiorites (Appendix A1). Moreover, the host rocks to the majority of the deposits are Cretaceous in age, except for the Hongmenling deposit present within both the Triassic and Cretaceous rocks (Appendix A1 and Figs. 1b and 2a). Regionally, the Mo mineralization seems to occur in

northeastern and southwestern Hainan Island, and is commonly controlled by the E- and NE-trending faults (Fig. 1b). At the deposit scale (Appendix A1; Figs. 2b–f and 3), Mo mineralization generally occurred as vein-like, lenticular and tabular orebodies that are associated with the N-, E-, NW to NNW-, NW to NWW-, and NE-trending secondary fissures/fractures, and/or controlled by caldera or breccia pipe. As the predominant ore mineral, molybdenite is often present as blades, laths, clots and/or foliated, flaky, radial or acicular aggregates (Fig. 4a–g) either disseminated in host rocks or in quartz veins, veinlets and stockworks crosscutting host rocks, or as monocrystal interstitial to gangue minerals, or as thin smears filled in fissures of host rocks. Other ore minerals such as pyrite, chalcopyrite, sphalerite, galena, chalcocite, arsenopyrite, magnetite, hematite, specularite, wolframite, scheelite, bismuthinite, and cassiterite are highly variable and often present as intergrowths with molybdenite (Figs. 3h and 4d). The complex gangue minerals are K-feldspar, plagioclase, quartz, muscovite, biotite, sericite, chlorite, epidote, and calcite, with zircon, rutile, titanite, ilmenite, apatite, fluorite, tourmaline, topaz, and andalusite as accessory minerals (Appendix A1; Figs. 3 and 4a–g). The Mo ores display granolepidoblastic, euhedral to subhedral, granular, poikilitic, porphyritic, emulsion, cataclastic and metasomatic textures, and massive, banded, nodular, disseminated, vein and brecciated structures (Figs. 3 and 4a–g).

Two types of Mo-related ore deposits have been recognized on Hainan Island (Appendix A1), based on the host rocks, ore-controlling structures, ore metal associations, orebody morphologies and ore occurrences, ore and gangue minerals, and alteration patterns as well as their comparisons with that of both Chinese and worldwide, typical Mo ore deposit-types (Lowell and Guilbert, 1970; Mutschler et al., 1981; Westra and Keith, 1981; White et al., 1981; Landtwing et al., 2002; Seedorff and Einaudi, 2004; Cannell et al., 2005; Seedorff et al., 2005; Ludington and Plumlee, 2009; Gruen et al., 2010; Lawley et al., 2010; Laznicka, 2010; Mao et al., 2011b; Zeng et al., 2013). The porphyry mineralization, which might be assigned for the Meiling, Hongmenling, Shimenshan, Luokuidong and Baogaocun deposits, genetically is associated mostly with porphyry stocks/dikes and/or breccias (e.g., in Meiling) (Figs. 1b, 2b–e and 5a–d). Laterally and vertically this type mineralization roughly shows alteration zoning outward from silicification and potassic (K-feldspar and biotite) or greisen Mo ore zone at core, through phyllic (sericitic, silica and pyritic) Mo–(Cu–W) ore zone or argillic (kaolinite) zone, to propylitic (chloritic, epidote and carbonate) (Pb–Zn–Ag) ore zone (Appendix A1; Figs. 3a and e, 4a and 5a–d). The molybdenite in lenticular, vein-like, tabular (e.g., in Luokuidong) and/or ring-like (e.g., in Meiling) orebodies generally occurs as flaky, foliated and/or acicular aggregates or as laths or blades either located in quartz veins, veinlets and/or stockworks or disseminated in host rocks (Figs. 2b–e, 3a–b and d–g, and 5a–d). Like the hydrothermal vein mineralization (Pirajno, 2009; Mao et al., 2011b; Zeng et al., 2013; Appendix A1), the orebodies of the Xincun, Longmenling and Gaotongling deposits (Figs. 1b, 2f, 3c and h, 4b and d, and 5e) are generally present as quartz veins that fill secondary fractures or fissures and mostly hosted by granitoids and partly by rhyolitic porphyries (e.g., Xincun), or as disseminations in host rocks. Despite widespread and strong, alteration occurrence of this deposit-type (Appendix A1; Fig. 3c and h) is strictly controlled by faults which not only resulted in linear rather than zoned envelope-type (e.g., Seedorff et al., 2005) alteration but also superimposition of various alterations along fracture zones. As a result, the Mo grade always decreases from the centers to the margins of the altered fracture zones.

The suggested classification of Mo-related deposits on Hainan Island is somewhat problematic. For example, the ambiguity of lateral and vertical alteration–mineralization zoning as well as the rare occurrence of stockwork molybdenite indicate that the present porphyry ore system on Hainan Island is atypical when compared with the characteristic features of typical porphyry Mo mineral systems as described and reported by Lowell and Guilbert (1970), Westra and Keith (1981), White et al. (1981), Landtwing et al. (2002), Seedorff and Einaudi (2004), Cannell et al. (2005), Seedorff et al. (2005), Ludington and Plumlee (2009), Laznicka (2010), Mao et al. (2011b) and Zeng et al. (2013). To some

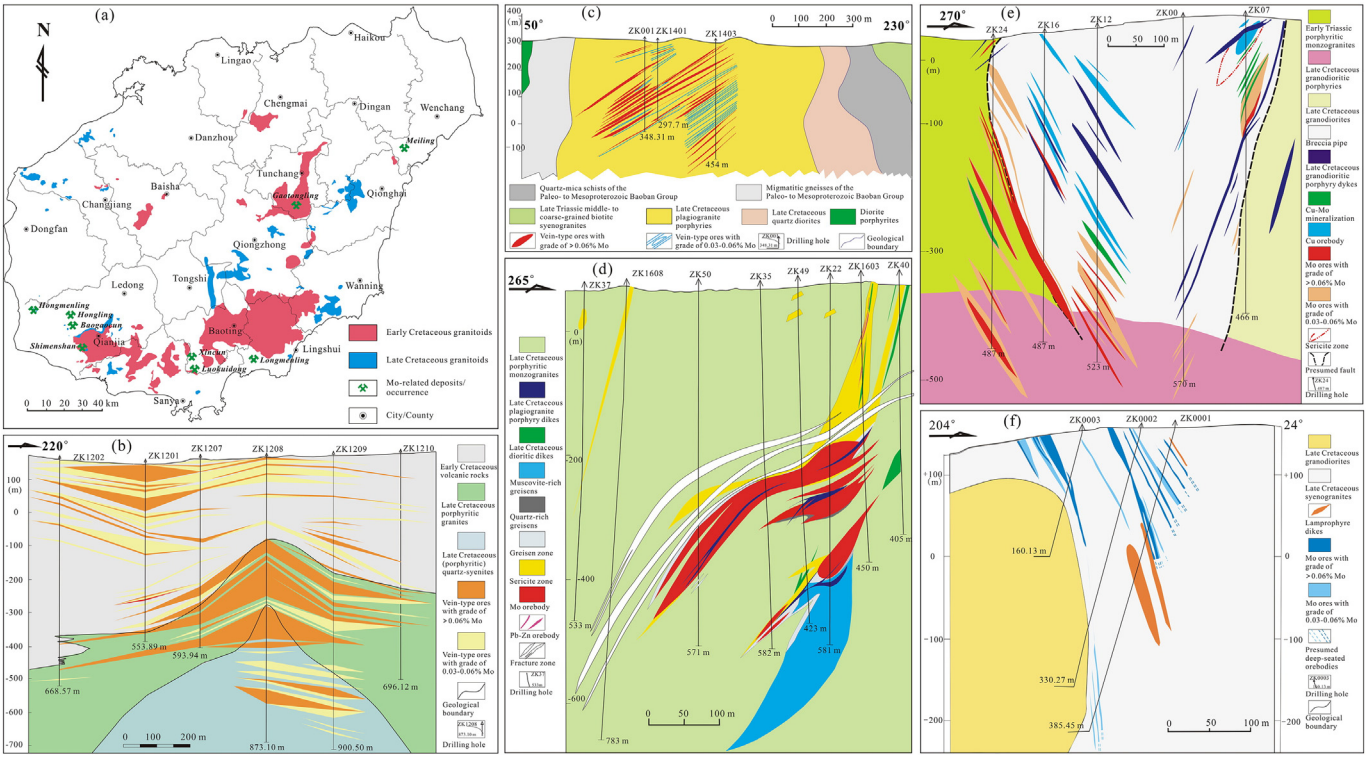

Fig. 2. (a) Sketch map showing distributions of the Cretaceous granitoids related to Mo mineralization on Hainan Island, and (b–f) Cross sections of the selected Mo-related deposits depicting geometries, attitudes, host rocks and associated alterations of Mo mineralization. Panels (b), (c), (d), (e) and (f) are from the Luokuidong, the Baogaocun, the Shimenshan, the Meiling, and the Gaotongling deposits, respectively.

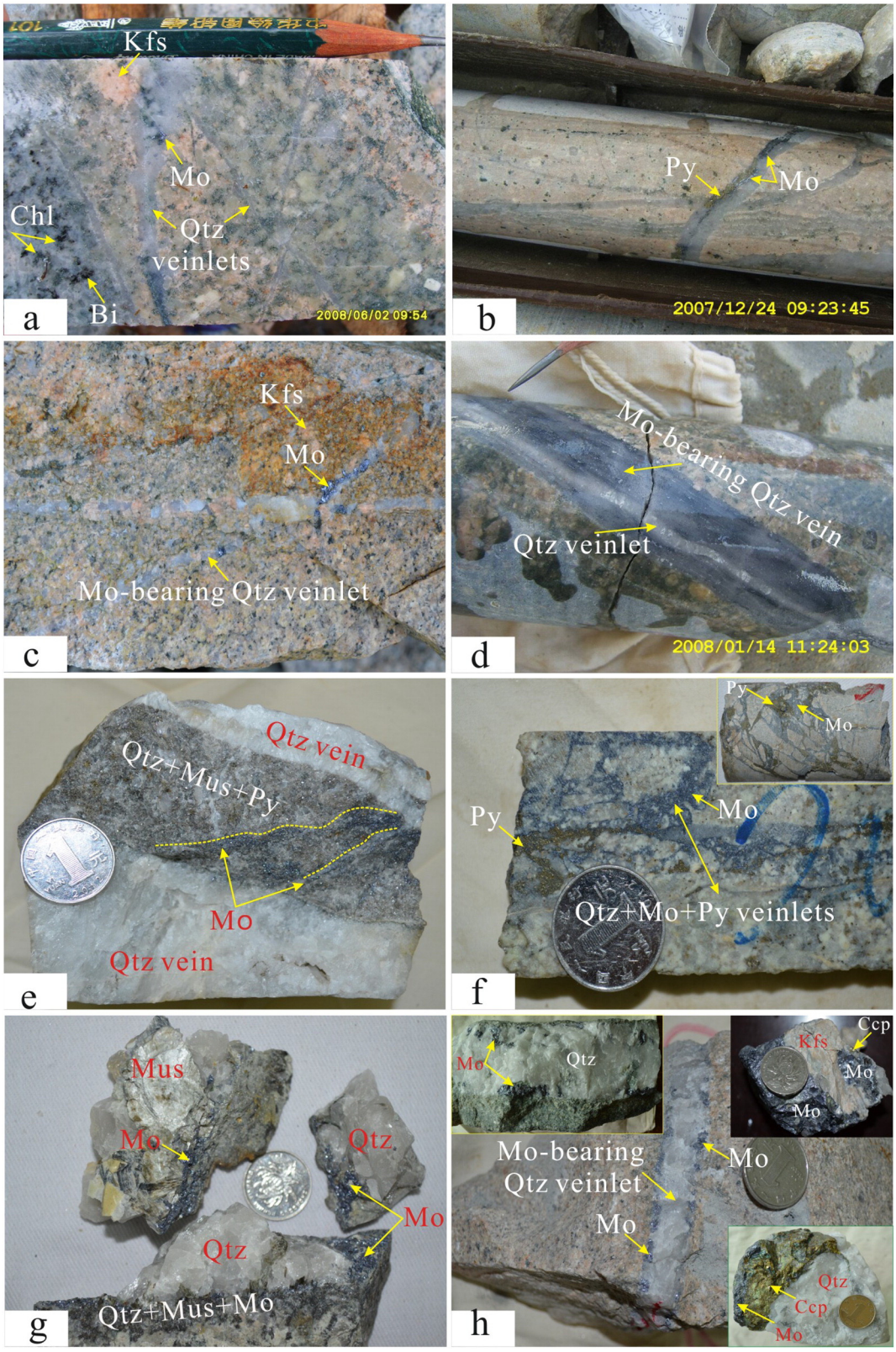

Fig. 3. Photographs illustrating occurrences of molybdenites and associated alterations from the Mo-related ore deposits on Hainan Island. (a) Stockwork veinlets comprising quartz (Qtz) + molybdenite (Mo) in plagiogranite porphyries from the Baogaocun deposit, note altered minerals K-feldspar (Kfs), biotite (Bi) and chlorite (Chl); (b) stockwork veinlets comprising quartz (Qtz) + molybdenite (Mo) + pyrite (Py) in porphyritic granites from the Luokuidong deposit; (c) molybdenite (Mo)-bearing quartz (Qtz) veinlets in syenogranites from the Gaotongling deposit, note altered mineral K-feldspar (Kfs); (d) banded quartz vein composed of alternating quartz (Qtz)-rich and molybdenite (Mo)-rich veinlets in porphyritic granites from the Luokuidong deposit; (e) molybdenite (Mo) veinlets in quartz (Qtz) + sericite (Ser) + pyrite (Py) veins intercalated with quartz (Qtz) veins from the Shimenshan deposit; (f) stockwork veinlets comprising quartz (Qtz) + molybdenite (Mo) + pyrite (Py) in brecciated granodioritic porphyries from the Meiling deposit; (g) molybdenite (Mo) as intergrowth with muscovite (Mus) in quartz (Qtz) veins in porphyritic granites from the Hongmenling deposit; (h) molybdenite (Mo)-bearing quartz (Qtz) veinlet in granodiorites from the Gaotongling deposit, note molybdenites (Mo) as intergrowth with chalcopyrite (Ccp) and K-feldspar (Kfs) in the top and lower right corners. Coins and pencil in the Figure represent sizes.

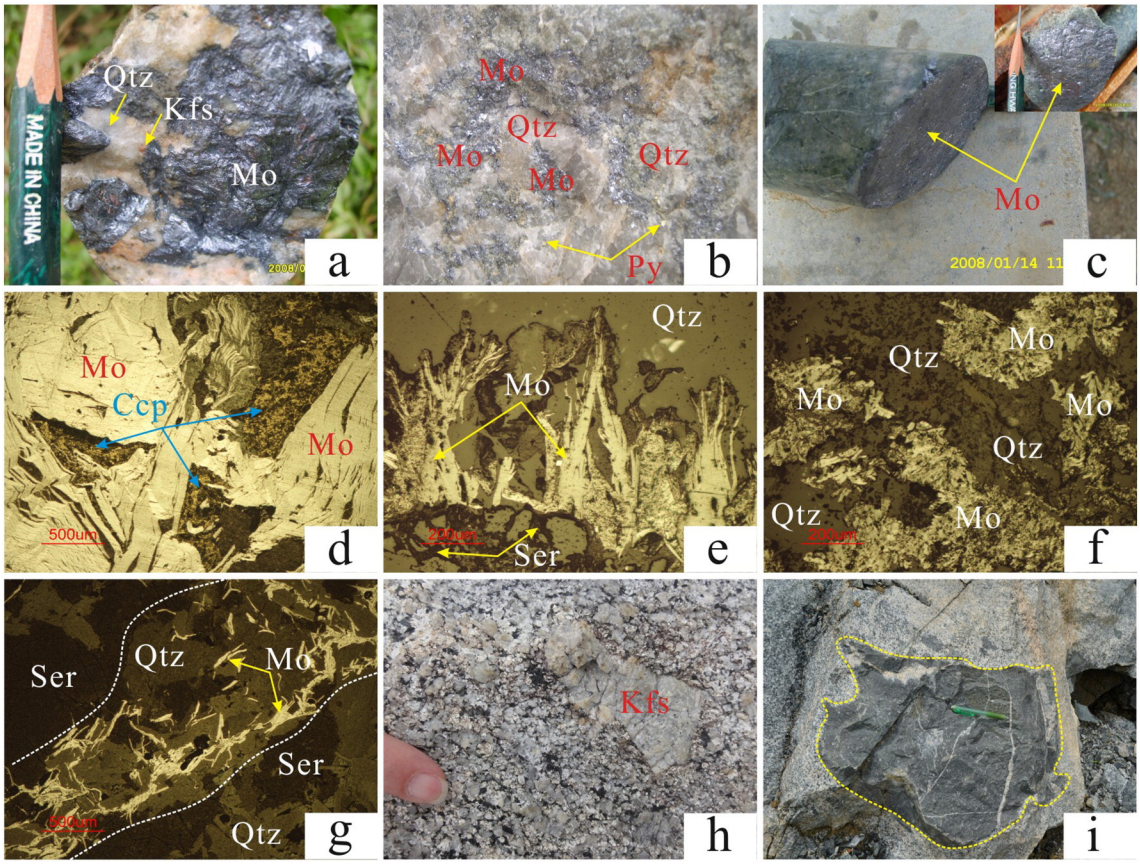

Fig. 4. Photographs and photomicrographs showing compositions, textures and structures of the Mo ores and associated granitoids. (a) Radial/nodular molybdenite (Mo) aggregates as intergrowth with quartz (Qtz) and K-feldspar (Kfs) in plagiogranite porphyries from the Baogaocun deposit; (b) molybdenite (Mo) as intergranular aggregates between quartz (Qtz) grains disseminated in quartz (Qtz) + pyrite (Py) vein from the Longmenling deposit, (c) molybdenite (Mo) as thin smears of fissure surfaces (left and right from the Luokuidong and the Baogaocun deposits, respectively); (d) molybdenite (Mo) as clots intergrown with chalcopyrite (Ccp) from the Gaotongling deposit; (e) molybdenite (Mo) as foliated aggregates in quartz (Qtz) + sericite (Ser) vein from the Hongmenling deposit; (f) molybdenite (Mo) as foliated and acicular aggregates in quartz (Qtz) vein from the Meiling deposit; (g) acicular molybdenite (Mo) in quartz (Qtz) + sericite (Ser) vein from the Shimenshan deposit; (h) K-feldspar (Kfs) megacrystal in porphyritic monzogranites from the Qianjia pluton; (i) mafic enclave in granodiorites from the Gaotongling deposit. Pencils and finger in the Figure represent sizes. Panels (d) to (f) are taken from reflect-light.

extent, this likely resulted from relatively low-level exploration and exploitation for most of the Mo-related deposits on Hainan Island which led to non-comprehensive field data. Fortunately, the genetic categories of the porphyry Mo deposits associated with lithogeochemistry and tectonic setting of the granitoid host rocks have also been proposed by Sillitoe (1980), Westra and Keith (1981), Carten et al. (1993), Seedorff et al. (2005), and Ludington and Plumlee (2009). In comparison with the Climax-type porphyries (Westra and Keith, 1981; White et al., 1981; Ludington and Plumlee, 2009; Lawley et al., 2010), the Cretaceous Mo-hosting granitoids on Hainan Island generally contain lower Rb (<250 ppm), Nb (<20 ppm) and Ta (<1.5 ppm) concentrations, higher Sr (>140 ppm) and Zr (>120 ppm) contents, and moderately negative Eu anomalies (*see* Section 5). However, these trace-element signatures are comparable to that of the intrusions which host the MAX porphyry Mo ore deposit and associated Pb–Zn–Ag mineralization in SE British Columbia, Canada (Lawley et al., 2010). This suggests that on Hainan Island most of the Mo-related deposits might be regarded as the low-grade, subduction-related, fluorine-poor porphyry Mo deposits associated with calc-alkaline intrusions (Sillitoe, 1980; Carten et al., 1993), consistent with the Cretaceous ore-bearing granitoids on Hainan Island that are high-K calc-alkaline, metaluminous to weakly peraluminous I-type series (see Section 5).

4. Sampling and analytical methods

Seventy-one, unaltered and unweathered granitoid samples from the Cretaceous Mo-hosting plutons were selected for the present study. Among these, 50 samples come from the Early Cretaceous plutons in Tunchang, Ledong, Baoting and Lingshui areas, and the remainder from the Late Cretaceous pluton in Ledong area (Fig. 2a). These fresh samples contain broad lithologies composed of syenogranites, granodiorites, granites, monzogranites, granodioritc porphyries, granite porphyries, quartz monzonites, and diorites (Appendix A2). Bulk-rock analyses for major and trace elements, and rare earth elements (REE) were carried out at the State Key Laboratory of Isotope Geochemistry, Guangzhou Institute of Geochemistry, Chinese Academy of Sciences (SKLIG GIG-CAS). Major elements were measured using Rigaku RIX 2000 X-ray fluorescence spectrometry following the method of Li et al. (2006), and the precision was better than 1%. Trace element and REE analyses were conducted on a Perkin-Elmer Elan 6000 inductively coupled plasma mass spectrometer (ICP-MS). The analysis followed the procedure described by Li et al. (2006) and Wang et al. (2012). The precision for trace elements was generally better than 5%. Several USGS (W-1 and W-2) and Chinese standard references (GSR-1, GSR-2 and GSR-3) were repeatedly measured with the samples, giving values that were generally within ±2% and ±5% (RSD) of the certified values for major and trace elements, respectively.

Twenty-seven representative host granitoids were selected for Nd–Sr isotope measurements. Among these, five samples come from the Late Cretaceous pluton, and the remaindering from the Early Cretaceous plutons. Nd–Sr isotopic components were measured using a Micromass Isoprobe MC-ICPMS at the SKLIG GIG-CAS. $^{88}Sr/^{86}Sr = 0.1194$ and $^{146}Nd/^{144}Nd = 0.7219$ were adopted to calibrate mass bias, respectively. The NBS SRM987 and Shin Etsu standard

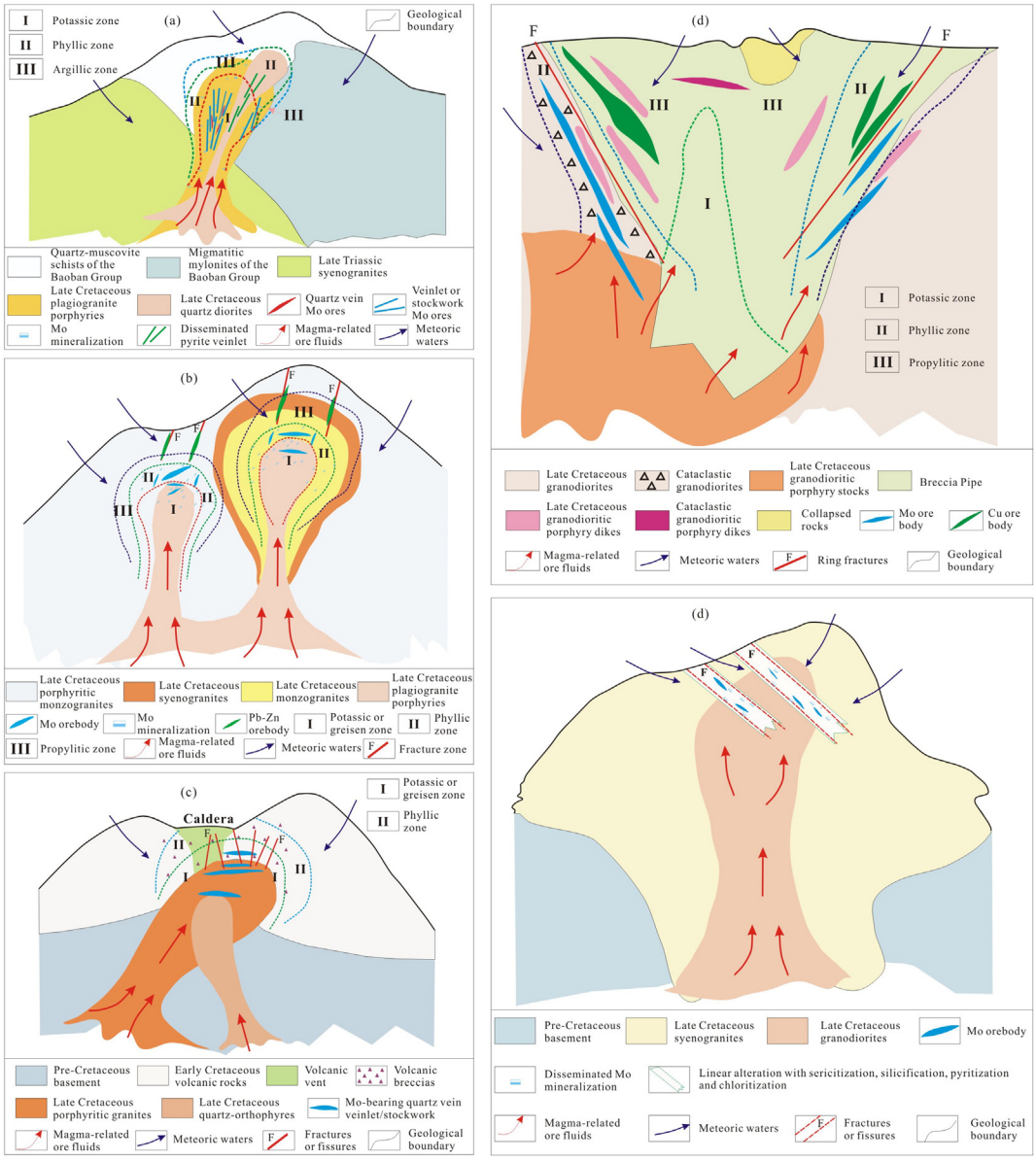

Fig. 5. Conceptual metallogenic models for the selected Mo-related ore deposits showing host rocks, Mo-related mineralization and associated alterations. Panels (a), (b), (c), (d), and (e) are for the Baogaocun, the Shimenshan, the Luokuidong, the Meiling, and the Gaotongling deposits, respectively.

solutions were repeatedly measured with the samples to monitor the analytical quality, which yielded an average of 0.710247 ± 17 (2σ) for $^{87}Sr/^{86}Sr$ and 0.512125 ± 12 (2σ) for $^{143}Nd/^{144}Nd$. A detailed description on analytical methods has been given by Li et al. (2006).

In order to determine the crystallization ages of host rocks and thereby to constrain the Mo mineralizing events on Hainan Island, samples GTL-4 and GTL-9 from the Gaotongling, and sample SM-1 from the Shimenshan deposits were undertaken on LA-ICP-MS U–Pb dating of zircon. After using conventional magnetic and heavy liquid separation methods, zircons were handpicked under a binocular microscope, mounted in epoxy disks, polished to expose their internal structures, and then analyzed by a LA-ICP-MS system comprising an Agilent 7500a ICP-MS coupled with a Resonetics RESOlution M-50 (193 nm ArF-Excimer) laser source at the SKLIG GIG-CAS. Both optical photomicrographs and cathodoluminescent (CL) images were taken as a guide to selection of U–Pb dating spots. Sample mounts were placed in a specially-designed double volume sample cell flushed with Ar and He. Laser ablation was operated at a constant energy (80 mJ cm^{-3}) at a repetition rate of 8 Hz and a spot diameter of 31 μm. The ablated aerosol was carried to the ICP source by He–Ar gas via a Squid system to smooth signals. External standard glass NIST SRM 610 and standard zircon TEMORA were used for external calibration (Black et al., 2003; Wang et al., 2012). ^{29}Si was used as the internal calibrant. Common Pb was corrected by using ComPbCorr#3_17 (Andersen, 2002). Concordia diagrams and ages were obtained using Isoplot/Ex (3.0) (Ludwig, 2003). The data reduction of U–Pb dating was performed by an in-house program ICPMSDataCal (Liu et al., 2008). Uncertainties on individual analyses are reported at one sigma level (1σ) and the weighted mean ages for pooled $^{206}Pb/^{238}U$ results are quoted at 95% confidence level.

To identify Mo mineralizing ages and to provide insight into the origin of ore metal Mo, Re–Os analyses on fourteen molybdenite samples were also carried out. Among these, six samples are collected from the Gaotongling deposit, two from the Hongmenling deposit, two from the Meiling deposit, two from the Shimenshan deposit, and the remainder from the Hongling occurrence. The Re–Os analyses were undertaken at the SKLIG GIG-CAS. Sun et al. (2010) and Li et al. (2013) described molybdenite Re–Os analytical methods and results, in detail. Here, two important points were highlighted as follows: (1) to ensure removal of Os as OsO_4, the concentrated HNO_3 was used to digest molybdenite and the step for Re–Os sample dissolution and preparation was

repeated twice, and (2) to eliminate memory effects of Os, the ICP-MS sampling system was flushed by 0.5% $H_2NNH_2 \cdot H_2O$ in 10% ethanol and 5% HNO_3 alternately, until the counts of ^{190}Os dropped to background level regardless of Os introduction. In addition, sulfur isotope analyses were also performed on twelve sulfide (molybdenite, pyrite and chalcopyrite) separates, which were verified to form during the same metallogenic epoch by detailed hand specimens and photomicrograph observation. Among these, four molybdenite and three chalcopyrite separates were from the Gaotongling deposit, and two molybdenite plus three pyrite separates were from the Shimenshan deposit. The sulfide separates were analyzed using a CF-IRMS (EA-IsoPrine Euro3000, GV instruments) mass spectrometer with an Elemental Analyzer sample injector at the State Key Laboratory of Environmental Geochemistry, GIG-CAS. Standards GBW04414 (Ag_2S, $\delta^{34}S_{CDT} = -0.07 \pm 0.13‰$) and GBW04415 ($Ag_2S$, $\delta^{34}S_{CDT} = 22.15 \pm 0.14‰$) were used for calibration. The sulfur isotope ratios are reported as $\delta^{34}S$ relative to the CDT (Canon Diablo Troilite). The precision of the $\delta^{34}S$ determinations is better than ±0.2‰.

5. Analytical results

5.1. Geochemical compositions

Appendix A2 lists the major- and trace element compositions of the analyzed 71 samples. For comparison, eighteen analyses of major-, trace- and REE elements for the Early Cretaceous granitoids from the Gaotongling deposit in Tunchang area as reported by Wang et al. (2012) are also listed in Appendix A2. The Cretaceous Mo-hosting granitoids on Hainan Island are intermediate to felsic and have variable but relatively high contents of SiO_2 (57.40%–77.34 wt.%), Al_2O_3 (11.95–17.46 wt.%), K_2O (2.45–6.05 wt.%), Na_2O (2.33–5.21 wt.%), CaO (0.65–5.91 wt.%) and FeO_T (0.49 to 6.81 wt.%), and variable but relatively low contents of TiO_2 (0.09–1.07 wt.%), MgO (0.11–3.46 wt.%), MnO (0.01–0.15 wt.%) and P_2O_5 (0.01–0.35 wt.%). The broad chemical compositions are consistent with their petrographic characteristics. Nevertheless, there are positive correlations of Al_2O_3 with FeO_T ($R^2 = 0.39$), CaO ($R^2 = 0.56$), MgO ($R^2 = 0.47$), TiO_2 ($R^2 = 0.45$) and P_2O_5 ($R^2 = 0.41$), negative correlations with SiO_2 ($R^2 = -0.74$) and K_2O ($R^2 = -0.23$), and no correlation with Na_2O (Fig. 6). On Fig. 7a, the samples predominantly fall within the high-K calc-alkaline field, with minor within the shonshonitic field. The ratios of A/CNK (0.86–1.17) and A/NK (1.11–2.45) (Appendix A2) cluster most of the samples into the transition between metaluminous and weakly peraluminous fields (Fig. 7b). Despite undistinguishable, the Late Cretaceous samples show slightly low Al_2O_3, CaO, FeO_T, MgO, $Mg^{\#}$, MnO, TiO_2 and P_2O_5, and slightly high SiO_2 and ($K_2O + Na_2O$), and ratios of Na_2O/K_2O, relative to the Early Cretaceous samples (Appendix A2; Figs. 6–7).

Likewise, the trace element and REE concentrations are also highly variable among the Mo-hosting granitoids. Appendix A2 and Fig. 8a–b show that the Cretaceous granitoids have $\sum$REE concentrations ranging from 51 ppm to 385 ppm, and are characterized by variable enrichment of LREE relative to HREE ($La/Yb_N = 7.1–66.3$) and strongly negative Eu to no Eu anomalies ($Eu/Eu^* = 0.35–1.08$). Primitive mantle-normalized trace element spider diagrams (Fig. 8c–d) exhibit that the granitoids are enriched in Rb, Th, La, Pb, Zr and Sm, and depleted in Ba, K, Nb, Sr, Ti and P. However, there are some differences in trace element composition between the Early Cretaceous and the Late Cretaceous granitoids. For example, the Late Cretaceous samples have variable but lower large ion lithophile elements (LILEs) such as Sr and Ba, and transition metal elements (TMEs) including Cr, Co, Ni and V, and variable but higher Y, relative to the Early Cretaceous samples (Appendix A2). Consequently, the Early- and Late Cretaceous samples with relatively low Y and high Sr show geochemical affinities to typical adakitic rocks (Defant and Drummond, 1990; Wang et al., 2012).

5.2. Geochronology

5.2.1. LA-ICP-MS U–Pb dating on zircon

Zircon crystals from the investigated granitoids are achromatous and transparent, euhedral to subhedral and prismatic. These zircon grains are ~80 to 200 μm in length and ~50 to 100 μm in width, and display finely oscillatory zoning in CL imaging (Fig. 9a–c), suggesting a magmatic origin (e.g., Corfu et al., 2003; Fedo et al., 2003). This is consistent with the Th/U values greater than 0.1 in all zircons analyzed (Th/U = 0.15–1.37; Appendix A3).

Zircon grains from three granitoid samples were dated by LA-ICP-MS method. A total of 13 analyses were performed on 13 zircon crystals from sample GTL-4 (Appendix A3), with two rejected due to discordance. Eleven concordant to nearly concordant analyses gave age range from 89.19 ± 2.25 Ma to 237.58 ± 3.43 Ma (Appendix A3). Excluding three analyses (spots 6, 12 and 23) due to large deviations from the others, the remaining eight yielded a weighted mean $^{206}Pb/^{238}U$ age of 100.8 ± 2.4 Ma (MSWD = 2.8; Fig. 9a), which is interpreted as the crystallization age of the granitic magma. A total of 20 analyses were performed on 19 zircon grains from sample GTL-9, with four discarded because of discordance (Appendix A3). One analysis (spot 8) was also rejected for its poor quality of data. The remaining 15 analyses define an age range from 96.31 ± 1.54 Ma to 194.02 ± 2.81 Ma. Excluding one analysis (spot 3) due to large deviation from the others, the remaining 14 analyses yield a weighted mean $^{206}Pb/^{238}U$ age of 100.2 ± 1.7 Ma (MSWD = 2.7; Fig. 9b), which is interpreted as the crystallization age of the granitic magma. The two weighted mean ages from the Gaotongling deposit are consistent with each other within analytical error. A total of 24 analyses on zircon grains (Appendix A3) were obtained from sample SM-1, with four rejected due to discordance. The remaining 20 concordant to nearly concordant analyses lie between 84.06 ± 0.98 Ma and 111.25 ± 1.78 Ma. Excluding two analyses (spots 6 and 11) due to large deviations from the others, the remainder give a weighted mean $^{206}Pb/^{238}U$ age of 91.7 ± 1.9 Ma (MSWD = 7.4; Fig. 9c). The relatively large MSWD value might be ascribed to different degrees of radiogenic Pb loss in this sample. Alternatively, we employed the *TuffZirc* age of ca. 94 Ma (Fig. 9d) to represent the crystallization age of granitic magma which is insensitive for Pb inheritance and Pb loss (e.g., Ludwig and Mundil, 2002; Ludwig, 2003).

5.2.2. Re–Os dating of molybdenite

Because of possessing the unique crystallochemical property of accommodating rhenium (Re) at the ppm level and containing little or no initial (common) osmium (Os) (Bingen and Stein, 2003; Selby and Creaser, 2004), and because of the Re–Os system behaving as a closed system at the scale of the molybdenite phase through penetrative high-grade metamorphism (Stein et al., 1998), molybdenite has become a robust chronometer whose value reaches far beyond the dating and understanding of ore genesis (Du et al., 1993, 1994; Stein et al., 2001; Stein and Bingen, 2002; Bingen and Stein, 2003; Zimmerman et al., 2008). Re–Os data which consist of ^{187}Re and ^{187}Os concentrations are used to determine ages and total Re and total Os concentration data. Common Os was found to be negligible in all the molybdenite analyses and thus, the total Os is reported as radiogenic ^{187}Os produced by the in situ decay of parent ^{187}Re (Du et al., 1994; Stein et al., 2001). The model age (t) can be calculated from the basic age equation of $t = (1/\lambda) \ln(1 + {}^{187}Os/{}^{187}Re)$, where λ is the decay constant of $^{187}Re = 1.666 \times 10^{-11}\ a^{-1}$ cited from Smoliar et al. (1996). Re–Os data including the calculated model ages for fourteen molybdenite samples from different deposits are presented in Appendix A4 and plotted in Fig. 10a. For the purpose of comparing between deposits and thereby tracking the evolution of Mo metallogenesis and related tectonic processes on Hainan Island, Appendix A4 also lists the Re–Os data reported by Liao et al. (2008), Wang and Liao (2012), and Li et al. (2014).

Six molybdenite samples from the Gaotongling deposit yielded model ages ranging from 98.46 ± 0.95 Ma to 105.9 ± 1.4 Ma

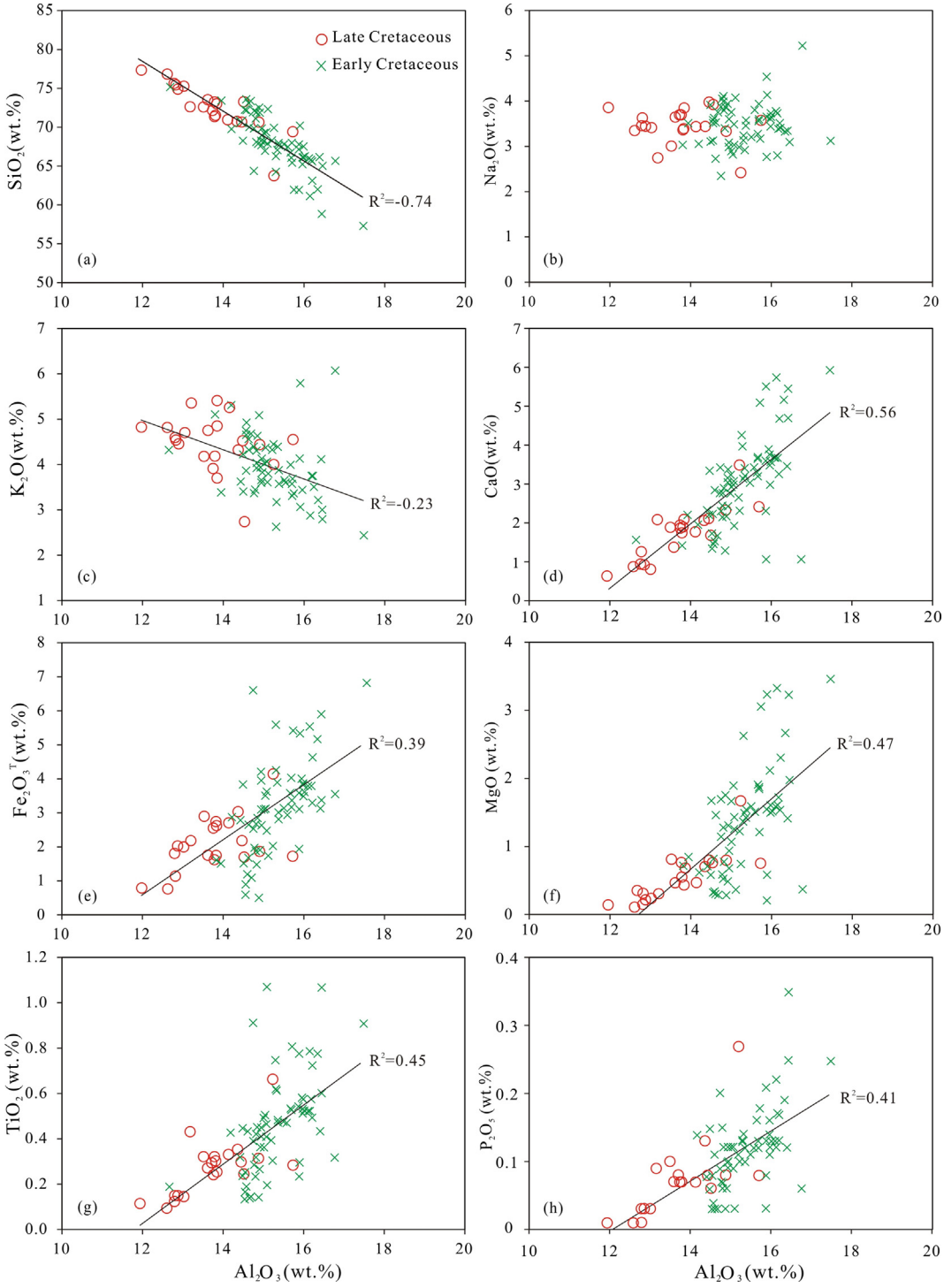

Fig. 6. Variation diagrams of Al_2O_3 with major oxides for the granitoids associated with Mo mineralization on Hainan Island.

(Appendix A4). Excluding sample GTL-1 due to its comparatively large deviation from others, the remainder define a well-constrained isochron age of 102.5 ± 1.8 Ma (2σ, MSWD = 2.0), with the initial $^{187}Os/^{188}Os$ value of −0.33 ± 0.14 (Fig. 10a) as calculated using Isoplot software (Ludwig, 2003). The low $^{187}Os/^{188}Os$ ratio suggests that there is no measurable normal Os in the measured molybdenites, and demonstrates that the Re–Os chronometer is reliable in locking in the age of Mo mineralization (Stein et al., 2001; Bingen and Stein, 2003). Thus the isochron age of 102.5 ± 1.8 Ma can be interpreted to be the mineralizing age of the Gaotongling deposit. From the same deposit, an isochron age of 98.4 ± 2.5 (2σ, MSWD = 1.7) was also yielded by five molybdenite samples with the model ages from 97.9 ± 1.2 Ma to 102.4 ± 1.5 Ma (Liao et al., 2008), consistent within analytical error with the present results (Appendix A4 and Fig. 10a). Correspondingly, the Re concentrations for the Gaotongling molybdenite fall in a range from 3.2 ppm to 13.3 ppm (Appendix A4).

Eight Re–Os analyses of molybdenite from the Hongmenling, Hongling, Shimenshan and Meiling deposits/showing yielded model ages of 71.9 ± 1.6 Ma and 72.1 ± 0.9 Ma, 100.9 ± 0.8 Ma and 99.2 ± 1.3 Ma, 77.8 ± 1.3 Ma and 80.4 ± 0.9 Ma, and 104.6 ± 1.2 Ma and 104.4 ± 1.4 Ma, respectively (Appendix A4). Li et al. (2014) also reported three molybdenite model ages of 99.8 ± 1.1 Ma, 99.6 ± 0.5 Ma and

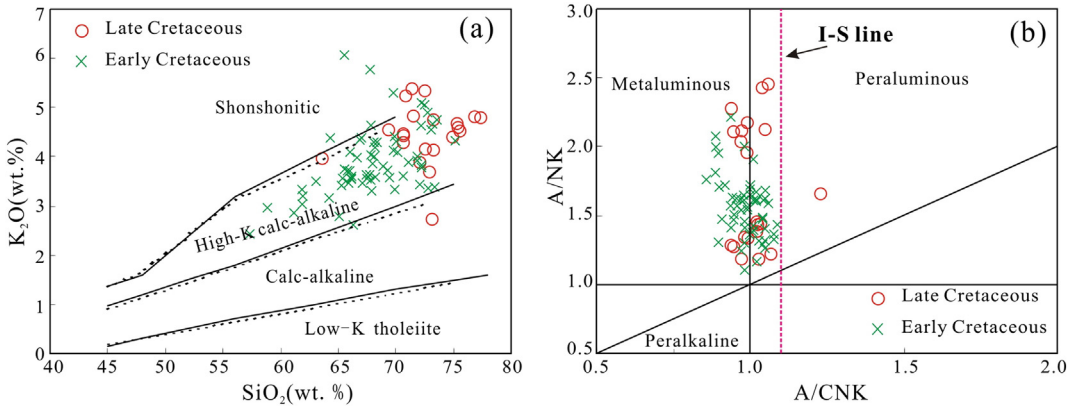

Fig. 7. Geochemical classification diagrams for the granitoids associated with Mo mineralization on Hainan Island. (a) SiO_2–K_2O diagram after Rickwood (1989) and (b) A/CNK vs. A/NK diagram after Maniar and Piccoli (1989).

100.1 ± 1.3 Ma for the Luokuidong deposit, one model age of 103.9 ± 1.0 Ma for the Baogaocun deposit, and two model ages of 88.6 ± 1.0 Ma and 80.2 ± 0.6 Ma for the Shimenshan deposit. In addition, Wang and Liao (2012) obtained six model ages ranging from 112.3 ± 4.2 Ma to 95.6 ± 0.9 Ma for molybdenite from the Xincun deposit, in which five age determinations provide an isochron age of 97.7 ± 0.13 Ma (MSWD = 1.03 and initial $^{187}Os/^{188}Os = -0.17 \pm 0.24$). Correspondingly, the Re concentrations are 1.05 ppm to 1.67 ppm for the Shimenshan deposit, 0.31 ppm and 0.35 ppm for the Hongmenling deposit, 135.7 ppm and 142.4 ppm for the Hongling occurrence, 28.39 ppm to 31.54 ppm for the Luokuidong deposit, 35.25 ppm for the Baogaocun deposit, 9.15 ppm and 25.85 ppm for the Meiling deposit, and 5.49 ppm to 99.67 ppm for the Xincun deposit (Appendix A4).

5.3. Nd–Sr and sulfur isotopic components

The initial Nd–Sr isotopic ratios have been back-calculated by employing the crystallization ages of 92–96 Ma and 98–107 Ma for the Late Cretaceous and the Early Cretaceous granitoids, respectively. To reduce the effect of Sm/Nd fractionation, the calculation formula for T_{DM2} (i.e., two-stage Nd depleted mantle model age) was adopted from Li and McCulloch (1996). The measured Nd–Sr isotopic compositions include those cited from Wang et al. (2012), and the calculated $\varepsilon_{Nd}(t)$ and $^{87}Sr/^{86}Sr_i$ values, and T_{DM2} ages are presented in Appendix A5. The Late Cretaceous samples exhibit initial $^{87}Sr/^{86}Sr$ ratios ranging from 0.70730 to 0.70834, with $\varepsilon_{Sr}(t)$ values between +47 and +57, $\varepsilon_{Nd}(t)$ values between −4.8 and −6.3, and T_{DM2} ages between 1.29 Ga

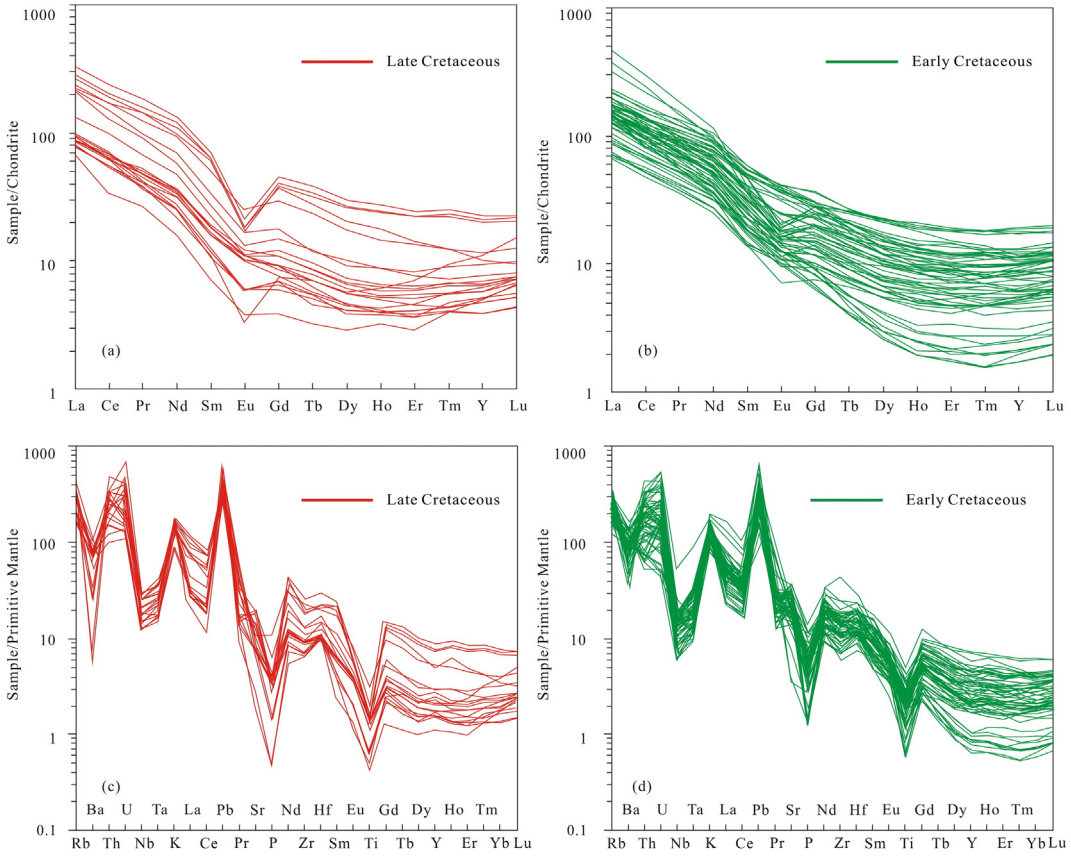

Fig. 8. Chondrite-normalized REE patterns (a–b) and primitive mantle-normalized trace element diagrams (c–d) for the Mo-hosting granitoids on Hainan Island. Chondrite- and primitive mantle-normalized values are from Sun and McDonough (1989).

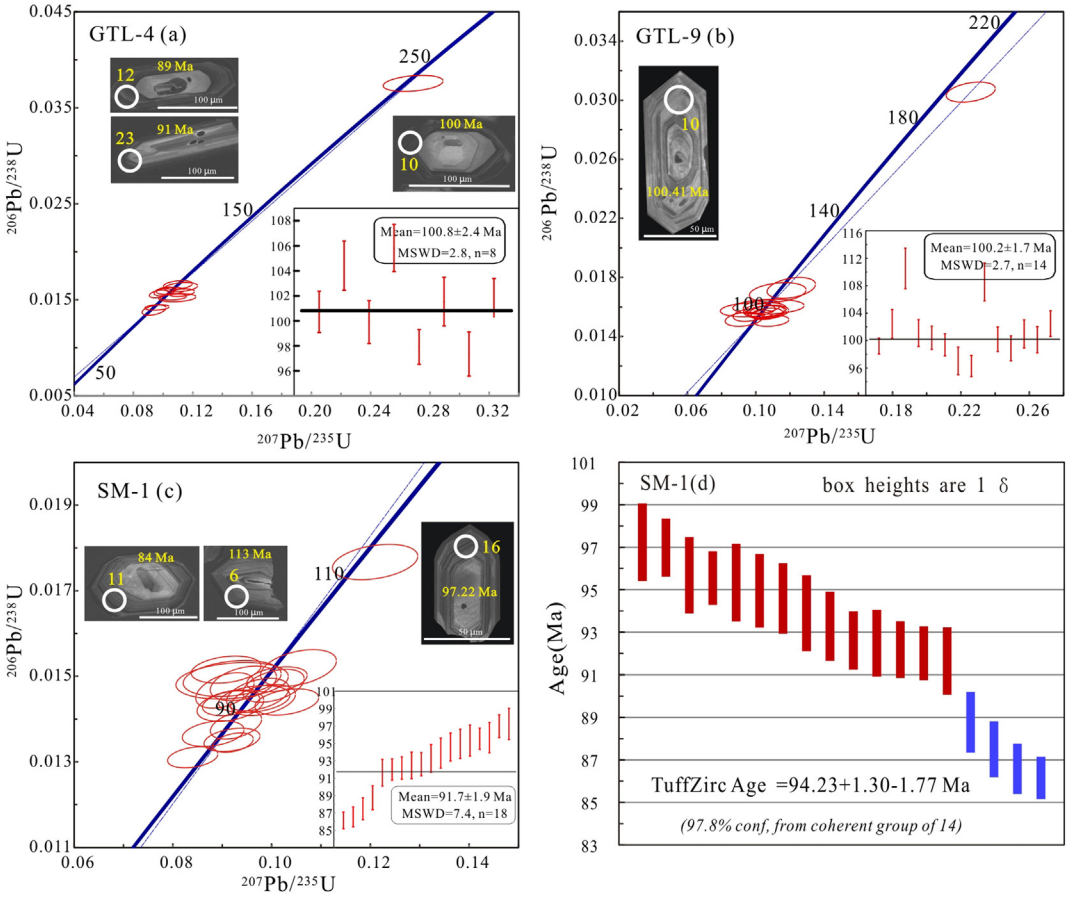

Fig. 9. U–Pb concordia diagrams for zircons from the Mo-hosting granitoids in the Gaotongling (a–b) and Shimenshan (c) deposits. Because of relatively large MSWD value, a *TuffZirc* age was employed to represent the crystallization age of sample SM-1 (d). Both the weighted mean $^{206}Pb/^{238}U$ ages and the representative cathodoluminescence (CL) images of zircons are also given in the Figure. Each analyzed spot with serial number and age value is marked by a white, solid circle.

and 1.41 Ga (avg. 1.35 Ga). Undistinguishable from the Late Cretaceous granitoids, the Early Cretaceous samples give initial $^{87}Sr/^{86}Sr$ ratios spreading from 0.70567 to 0.71208, with $\varepsilon_{Sr}(t)$ values between +18 and +109, $\varepsilon_{Nd}(t)$ values between −3.8 and −6.9, and T_{DM2} ages between 1.03 Ga and 1.46 Ga (avg. 1.27 Ga).

Sulfur isotopic components plus the previously published data by Liao et al. (2008) for molybdenite, chalcopyrite and pyrite separates are presented in Appendix A6. The $\delta^{34}S$ values of sulfide minerals from the Gaotongling deposit are between 1.36‰ and 5.50‰ (average 3.84‰), whereas that from the Shimenshan deposit range from 4.77‰ to 5.73‰ (average of 5.32‰). Molybdenite from both the Gaotongling and the Shimenshan deposits exhibits approximately consistent $\delta^{34}S$ ranges from 4.39‰ to 5.50‰, whereas three chalcopyrite samples from the Gaotongling give variable $\delta^{34}S$ values of 1.36‰, 2.93‰ and 3.86‰, respectively. In addition, the $\delta^{34}S$ values of pyrite separates from both the Gaotongling and the Shimenshan deposits are 2.9 to 3.0‰, and 4.77 to 5.73‰, respectively.

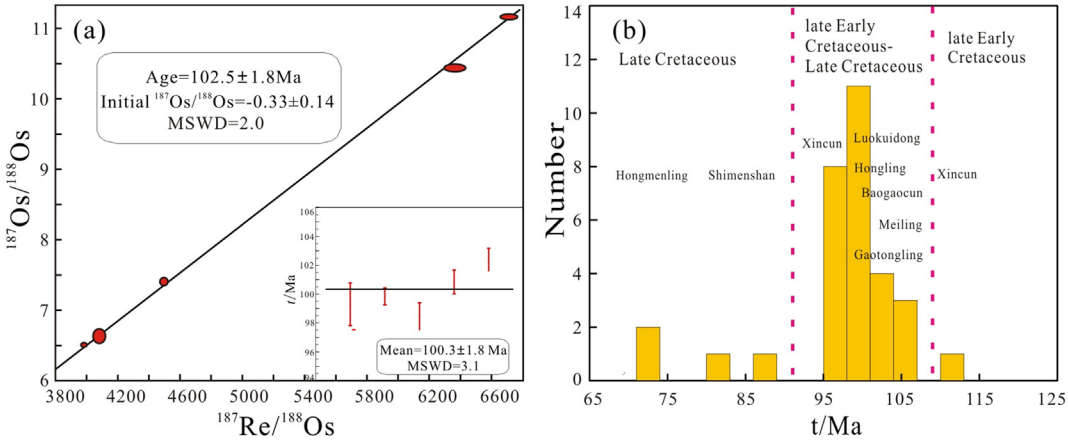

Fig. 10. (a) Re–Os isochron age attached by weighted mean age for molybdenites from the Gaotongling deposit, and (b) histogram of Re–Os model ages for molybdenites from the eight Mo-related deposits and one occurrence on Hainan Island.

6. Discussion

6.1. Timing of magmatism and associated Mo mineralization: implication for youngest Mo metallogenetic event in East China

Zircon has the ability to withstand multiple episodes of weathering, transportation, diagenesis, and metamorphism up to amphibolite facies, and thus possesses an inherently stable U–Pb isotopic system (Lee et al., 1997; Corfu et al., 2003; Fedo et al., 2003). Likewise, the Re–Os chronometer in molybdenite has been shown to be remarkably robust and remain intact even if earlier-formed molybdenite may recrystallize during subsequent orogenic events, and thus can survive high-grade metamorphism, intense deformation and hydrothermalism (Raith and Stein, 2000; Stein and Bingen, 2002; Bingen and Stein, 2003; Stein et al., 2001, 2003). Thereby the integration of zircon U–Pb dating with the molybdenite Re–Os chronometer can provide unequivocal age results to pinpoint magmatic and mineralizing events that have been superimposed over a long geological history.

The consistent weighted mean ages of ca. 100 Ma yielded by two granitoid samples from the Gaotongling deposit (Fig. 9a–b) are ca. 8 Ma younger than 107.6 ± 1.5 Ma reported by Wang et al. (2012) and ca. 5 Ma older than 95.6 ± 1.6 Ma given by Chen et al. (2008), using the same dating method. This suggests that the Mo-hosting pluton in Tunchang area might have been emplaced periodically at least in two stages of ca. 108 Ma and ca. 100–96 Ma. Two concordant ages of 110.5 ± 3.0 Ma (spot 5) and 108.6 ± 2.8 Ma (spot 14) in sample GTL-9 thus likely record the early phase of magmatic emplacement (Appendix A3). In contrast, four concordant ages of 97.0 ± 2.0 Ma (spot 12) and 96.3 ± 1.5 Ma (spot 13) in sample GTL-9, and 97.9 ± 1.3 Ma (spot 19) and 97.4 ± 1.7 Ma (spot 22) in sample GTL-4 (Appendix A3) appear to mark the second stage of emplacement. However, two youngest concordant ages of 89.2 ± 2.3 Ma (spot 12) and 90.9 ± 1.2 Ma (spot 23) for two zircon grains in sample GTL-4 are significant and likely represent the latest stage of plutonism. These two zircon crystals have Th/U ratios of 0.15 and 0.45, and show finely oscillatory zoning in CL imaging (Appendix A3 and Fig. 9a), suggesting a magmatic origin. In contrast, two zircons with two older ages of ca. 238 Ma and 190 Ma from samples GTL-4 (spot 6) and GTL-9 (spot 3) are interpreted as xenocrysts. The *TuffZirc* age of ca. 94 Ma (Fig. 9d) for sample SM-1 can be interpreted as the best estimate of the crystallization age of intrusions hosting the Shimenshan deposit in Ledong area. Nevertheless, the oldest age of ca. 113 Ma for one zircon grain (spot 6) and the youngest age of ca. 84 Ma for another zircon grain (spot 11) are considered to record the earliest- and the latest stages of plutonism, based on their Th/U ratios and internal textures (Appendix A3 and Fig. 9c). This is consistent with the host granitoids being a part of the Qianjia composite pluton in Ledong area which formed between late Early Cretaceous and Late Cretaceous (ca. 101–82 Ma; Chen et al., 2008; Chen, submitted for publication). The ca. 113 Ma age at a 1σ uncertainty also overlaps with the age for the suggested, earliest stage of granitoids hosting the Gaotongling deposit in Tunchang area, and the 112–106 Ma ages for the Cretaceous volcanic rocks on Hainan Island (HBGMR, 1997; HBG, in press). When combined with the previous geochronological constraints (Chen et al., 2008; Wang et al., 2012; Jiang and Li, 2014; Chen, submitted for publication; HBG, in press), our new U–Pb ages indicate at least three stages of Mo-related magma emplacement, i.e., the late Early Cretaceous (ca. 113–108 Ma), the early Late Cretaceous (ca. 100–94 Ma), and the Late Cretaceous (ca. 90–70 Ma), on Hainan Island.

The isochron age defined by the five Re–Os analyses for five molybdenite samples from the Gaotongling deposit unambiguously points to a time of molybdenite precipitation at ca. 103 Ma (Fig. 10a). This age overlaps at 2σ uncertainty with the model ages of ca. 105 Ma for sample GTL-1 from the same deposit and ca. 104 Ma for both the Meiling and Baogaocun deposits (Appendix A4). The Re–Os isochron age of ca. 98 Ma for both the Gaotongling (Liao et al., 2008) and the Xincun deposits (Wang and Liao, 2012) is also consistent at 2σ uncertainty with the model age of ca. 100 Ma given by both the Hongling occurrence and the Luokuidong deposit (Appendix A4). Therefore this age likely represents next pulse of fluid generation and related Mo mineralization. In addition, the model age of ca. 112 Ma for one Re–Os analysis from the Xincun deposit (Wang and Liao, 2012) approximates to the late Early Cretaceous volcanism and plutonism, suggesting an earliest Mo mineralizing event. Despite the suggested minimum lifespan of a deposit between 0.5 Ma and 2.0 Ma, Zimmerman et al. (2008) warned that the exact first and last molybdenite-forming pulse is unlikely to have been sampled. Thus these obtained Re–Os ages are significant and also fall well within the emplacement age range of ca. 96–110 Ma for the host plutons in Tunchang, Qionghai, Ledong and Baoting areas. In addition, the model age of ca. 89 Ma for one Re–Os analysis from the Shimenshan deposit (Li et al., 2014) likely was a response to the ca. 90 Ma magmatic event on Hainan Island (Wang et al., 2011). This deposit also shows model ages of ca. 80 Ma for two Re–Os analyses, whereas the Hongmenling deposit gave model ages of ca. 72 Ma (Appendix A4). Because these ages lie within the emplacement age range of ca. 90–70 Ma for the Late Cretaceous plutons on Hainan Island, they might record the youngest Mo metallogenic event(s). Collectively, Mo mineralization dispersed over Hainan Island clearly cluster into three age populations (Fig. 10b): (1) late Early Cretaceous (ca. 112 Ma); (2) late Early Cretaceous to Late Cretaceous (ca. 106–95 Ma); and (3) Late Cretaceous (ca. 89–72 Ma). This indicates that the spatiotemporal association between the Mo mineralization and the granitic magmatism on Hainan Island is consistent with a Cretaceous intrusion-related ore system which resulted in multiple pulses of fluid generation and mineralization. Because most of the Mo-related deposits of economic significance formed at 106–95 Ma, this age group is considered to be a predominant episode for Mo mineralization on Hainan Island.

Irrespective of genetic types and tectonic settings, four epochs of Mo mineralization, i.e., the Lüliang (ca. 1850–1760 Ma), the Caledonian (ca. 476–425 Ma), the Indosinian (ca. 260–210 Ma), and the Yanshanian (ca. 190–70 Ma), have been identified in East China (Fig. 11), based on present and the previously published Re–Os data (Liao et al., 2008; Mao et al., 2008, 2011a,b,c; Zeng et al., 2011, 2014; Fang et al., 2012; Zhao et al., 2012; Li et al., 2013; Huang et al., 2014a,b; Wang et al., 2014; Zhai et al., 2014; Zhang et al., 2014; Mi et al., 2015; and references therein). Among these, the Yanshanian mineralization is the most important in East China and hosts the largest metal Mo reserves in China (Mao et al., 2008, 2011a). Based on the previous geochronological data, this epoch can be subdivided into two episodes (Fig. 11): (1) the Jurassic to Early Cretaceous (ca. 190–120 Ma), with a peak between 150 Ma and 130 Ma; and (2) the Early Cretaceous to Late Cretaceous (ca. 120–70 Ma), with a peak between 115 Ma and 95 Ma. The early episode of Mo mineralization were primarily present in the East Qinling–Dabie orogen and the northern margin of North China craton, and include the large- to superlarge-scale Leimengou, Jinduicheng, Nannihu, Sandaozhuang, Qian'echong, Shangfanggou, Xiaojiayingzi, Yangjiazhangzi and Lanjiagou ore deposits (Mao et al., 2008, 2011a,b). The late, ca. 120–70 Ma episode of mineralization includes the recently discovered large- to superlarge-scale deposits represented by Shapinggou in Anhui Province (ca. 110–114 Ma; Huang et al., 2011; Zhang et al., 2014), Tangjiaping in Henan Province (ca. 113 Ma; Mao et al., 2008), and Luokuidong on Hainan Island (ca. 100 Ma; Li et al., 2014). Because mineralization younger than 100 Ma has only been reported in the eastern Fujian and Hainan Provinces (Zhao et al., 2012 and this study), it likely records the youngest Mo mineralizing event in East China. However, molybdenites from the Dawan Mo–Be and Lishan Mo deposits in eastern Fujian Province yielded Re–Os isochron ages of 92.2 ± 1.3 Ma and 91.7 ± 4.9 Ma, respectively (Zhao et al., 2012), suggesting a middle Late Cretaceous mineralizing event. Therefore, the Re–Os model ages of ca. 89–72 Ma identified on Hainan Island most likely represent the youngest Mo metallogenic event recognized in East China to date.

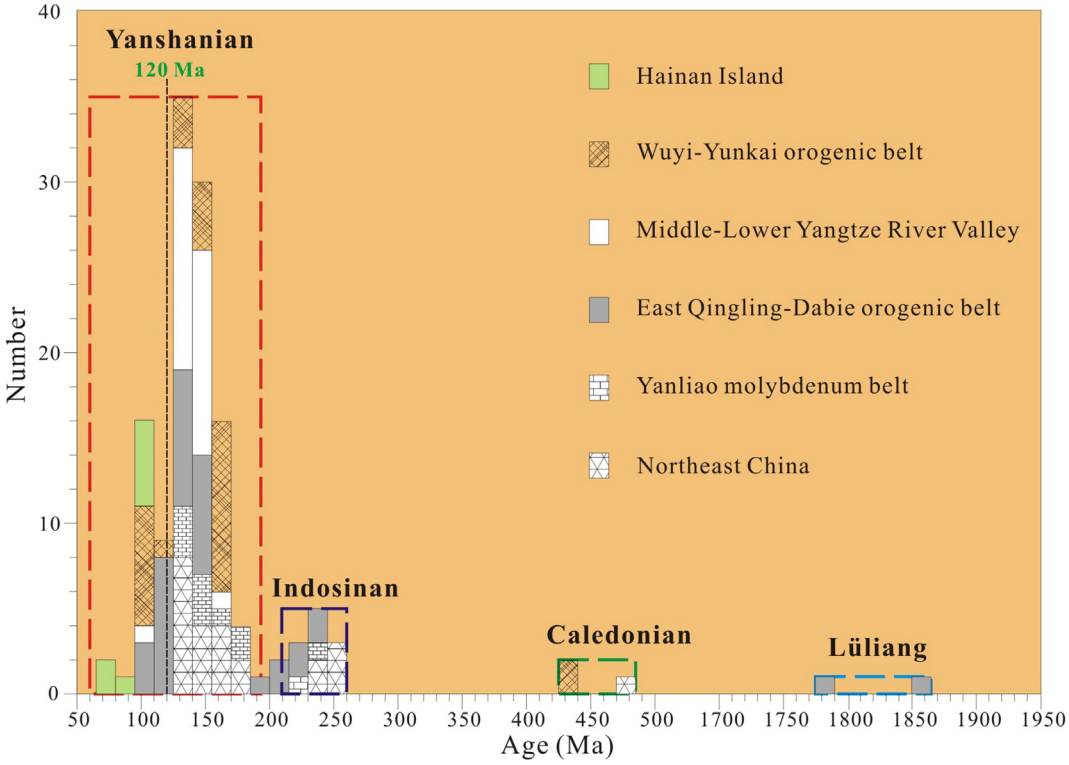

Fig. 11. Histogram of Re–Os ages for molybdenites from the Mo-related deposits in East China.
Data are from this study and Liao et al. (2008), Li et al. (2013), Mao et al. (2011a,b,c,d), Fang et al. (2012), Zhao et al. (2012), Huang et al. (2014a,b), Shu et al. (2014b), Zeng et al. (2013, 2014), Zhai et al. (2014), Zhang et al. (2014), Mi et al. (2015), and references therein.

6.2. Genetic type and origin of the Mo-hosting granitoids

The present study shows that the Cretaceous intermediate-felsic intrusions related to Mo mineralization on Hainan Island are metaluminous to weakly peraluminous, and mostly linked to magmatic centers of high-K calc-alkaline affinity (Fig. 7). Based on the contents of SiO_2 and abundances of La, Ce, Nb, Zn and Ga (Appendix A2) as well as their covariations (*not shown*), most of the Mo-hosting granitoids can be ascribed to I-type granites, with minority to A-type granites (Collins et al., 1982; Chappell, 1999). This is consistent with that P_2O_5 contents decrease significantly with increasing SiO_2 (Fig. 12a), a typical feature for the I-type granites (cf. Chappell, 1999). Combined with the negative correlation of SiO_2 with Zr, positive correlation of SiO_2 with Pb, and positive correlations of Rb with Th and Y (Fig. 12b–e), therefore the Mo-hosting granitoids on Hainan Island can be considered to be I-type granites. This also corresponds to the following lines of evidence from that: (1) the majority of the host rocks have initial $^{87}Sr/^{86}Sr$ ratios between 0.7073 and 0.7121 (Appendix A5), overlapping with ratios of 0.704–0.712 put forward by Chappell and White (1992) for I-type granites, and (2) the general occurrence of magnetite/hematite as accessory minerals in most of the Mo-related deposits (Appendix A1) is indicative of magma with relative higher oxygen fugacity (fO_2) such as I-type granites (e.g., Ishihara and Sasaki, 1989).

As the prominent features of orogenic belts (Brasilino et al., 2011), the high-K calc-alkaline, metaluminous to weakly peraluminous I-type granitoids generally have been interpreted as a mixed result of mantle-derived basaltic magma with crust-derived felsic magma via partial melting induced by underplating and injection of basaltic magma (Collins, 1998; Barbarin, 1999; Altherr and Siebel, 2002; Janoušek et al., 2004; Karsli et al., 2010; Zhang et al., 2011b; Kaygusuz et al., 2014). Two alternative models involving either the advanced assimilation-fractional crystallization of mantle-derived basaltic parental magmas or the partial melting of mafic to intermediate igneous sources have also been utilized to explain origin of this rock type (Roberts and Clemens, 1993; Sisson et al., 2005; Njanko et al., 2006). Most of the major-element oxides show well-defined linear trends (Fig. 6), suggesting the significant role of FC (fractional crystallization) processes of different mineral phases during the evolution of the Cretaceous Mo-bearing magma from low- to high-SiO_2 rocks on Hainan Island. The negative anomalies of Nb and positive anomalies of Th and Pb with concentrations generally between 11 ppm and 47 ppm (Fig. 8b; Appendix A2) are associated with subduction-related magmas and/or crustal contamination. The no correlations of SiO_2 with $(^{87}Sr/^{86}Sr)_i$ and $\varepsilon_{Nd}(t)$ (Fig. 12f–g), suggests that assimilation was less important for the generation of the Cretaceous Mo-hosting granitoids on Hainan Island. As a result, AFC (assimilation-fractional crystallization) processes can be excluded as a main factor to control the evolution of the granitoid magmas. The widespread occurrences of the coeval mafic dike swarms (Ge et al., 2003) as well as the existences of K-feldspar megacrysts and various types of intermediate to mafic microgranular enclaves in most of the Cretaceous Mo-hosting plutons (Fig. 3g–h; Wang et al., 2012; Chen, submitted for publication) thus indicate that mixing–mingling between mafic and acidic magmas likely had played a leading role in petrogenesis of the late Early Cretaceous to Late Cretaceous granitoids on Hainan Island. This is supported by that the Mo-hosting granitoids define hyperbolic arrays in the Rb vs. Sr, Rb/Sr vs. Ti/Zr and Zr/Hf, Zr/Hf vs. Nb/La, and 1/Sr vs. $(^{87}Sr/^{86}Sr)_i$ diagrams, and linear correlations of Ba and Sr, and Sr/Zr and Ti/Zr (Figs. 12h and 13), all of which are features expected for the mixing–mingling between two distinct geochemical end-members (i.e., mantle-derived and lower crust-derived components) (Kaygusuz et al., 2014). Combined with that some of the Cretaceous samples have adakitic affinities (Appendix A2), the variable geochemical compositions and gentle to steep HREE patterns as well as the approximately constant $\varepsilon_{Nd}(t)$ and $(^{87}Sr/^{86}Sr)_i$ values, and Ta/Yb vs. Th/Yb diagram (Appendices A2 and A5; Figs. 8a and 14a–b) highlight that the Mo-hosting granitoids might be formed by mixing of metasomatized sub-continental lithospheric mantle (SCLM)-derived mafic magmas with crust-derived melts (Janoušek et al., 2004). Nevertheless, the presence of

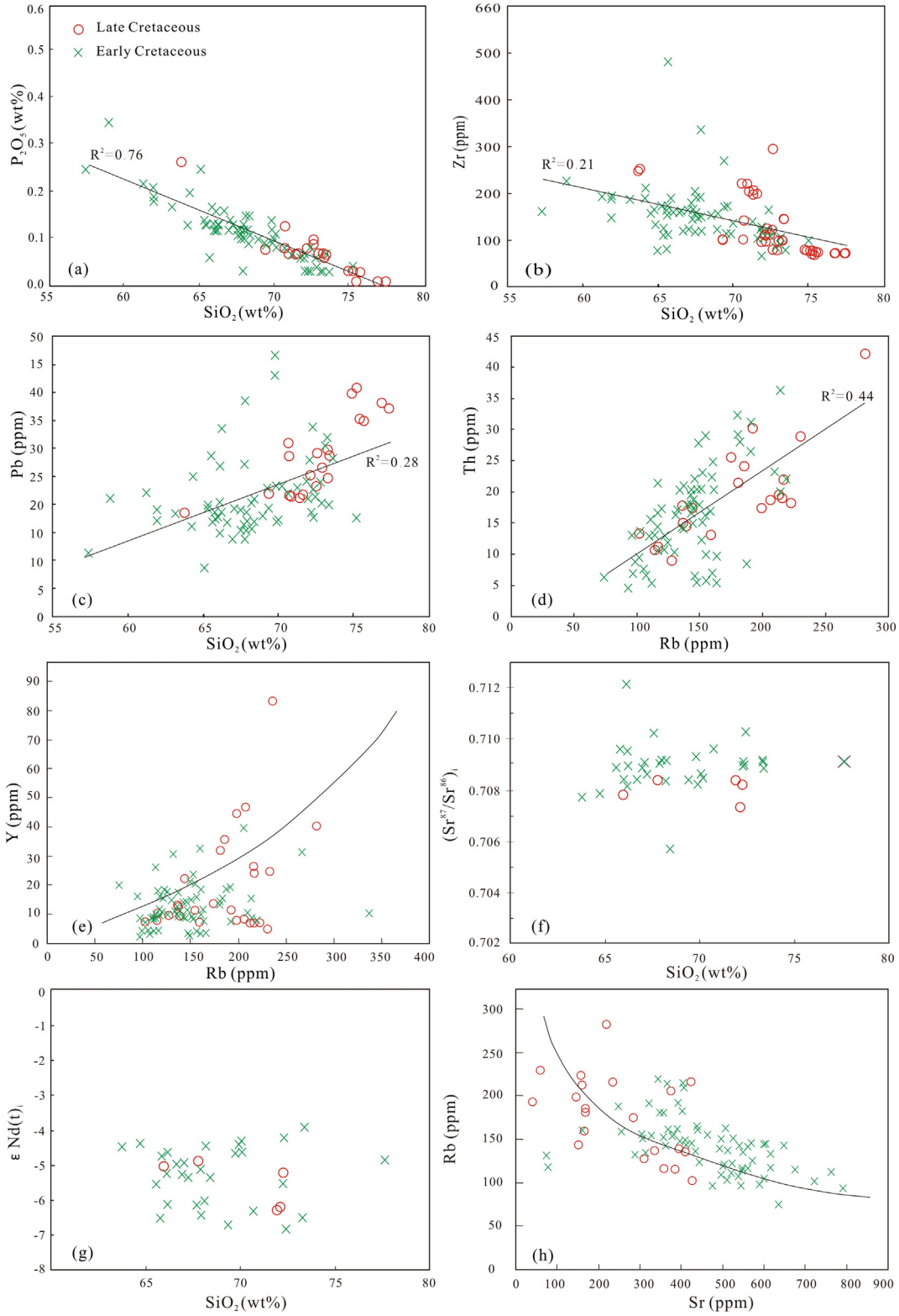

Fig. 12. Diagrams of SiO_2 vs. P_2O_5 (a), Zr (b) and Pb (c), Rb vs. Th (d) and Y (e), SiO_2 vs. $^{87}Sr/^{86}Sr_i$ (f) and $\varepsilon_{Nd}(t)$ (g), and Sr vs. Rb (h) for the Mo-hosting granitoids on Hainan Island.

various lithologies in the Mo-hosting plutons as well as the successive spatiotemporal association of the mafic and felsic magma suites during the Cretaceous on Hainan Island most likely are interpreted as a result of episodic crust–mantle interactions that occurred at depth (e.g., Zhang et al., 2011b).

The relative contributions of different end-components, i.e., crust vs. mantle are difficult to quantify, although excellent works have been made to try to understand the magma mixing–mingling mechanism (Gray and Kemp, 2009; Topuz et al., 2010). The Cretaceous Mo-hosting granitoids show distinct Nd–Sr isotopic compositions from the metamorphic basement on Hainan Island (Fig. 14b), suggesting that partial melting of the metamorphic basement was impossible to produce the Mo-hosting granitoid magma. In contrast, these granitoids not only have consistent Nd–Sr isotopic components but also share

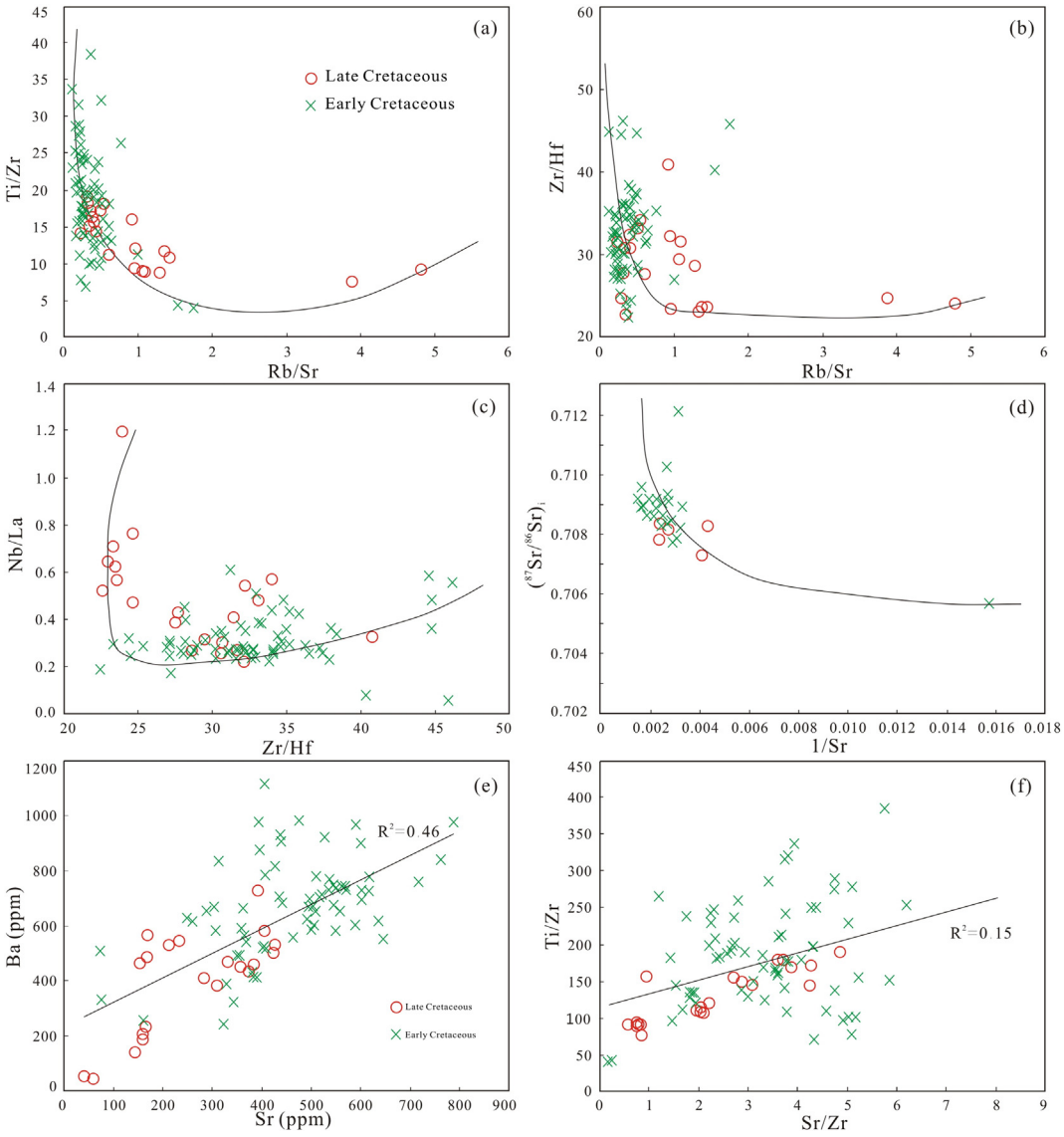

Fig. 13. Rb/Sr vs. Ti/Zr (a) and Zr/Hf (b), Zr/Hf vs. Nb/La (c), 1/Sr vs. $^{87}Sr/^{86}Sr_i$ (d), Sr vs. Ba (e), and Sr/Zr vs. Ti/Zr (f) diagrams for the Mo-hosting granitoids on Hainan Island.

similar trace element characteristics, i.e., enrichment in LREE, and variable enrichment or depletion in LILEs and HFSEs (high field strength elements), relative to primitive mantle, with the coeval mafic dike swarms (Ge et al., 2003). Such similarities indicate that the Mo-hosting granitoids on Hainan Island most plausibly had a genetic link to the coeval mafic dike swarms. Ge et al. (2003) suggested that these

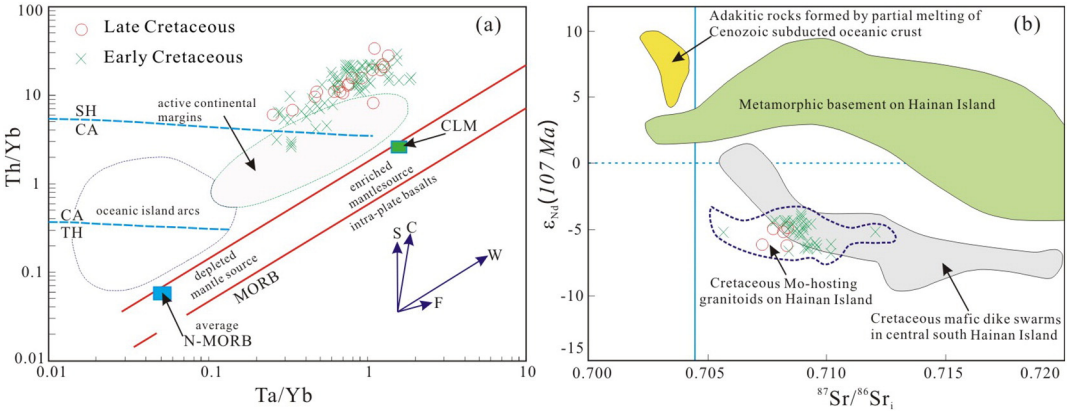

Fig. 14. Diagrams of Th/Yb vs. Ta/Yb (a; after Pearce, 1983) and $^{87}Sr/^{86}Sr_i$ vs. $\varepsilon_{Nd}(t)$ (b; modified after Wang et al., 2012) for the Mo-hosting granitoids on Hainan Island. Vectors in the panel (a) represent subduction components (S), within plate enrichment (W), crustal contamination (C) and fractional crystallization (F). CLM = continental lithospheric mantle, N-MORB = normal mid-ocean ridge basalt, SH/CA = shoshonite/calc-alkaline, and CA/TH = calc-alkaline/tholeiite. The fields in (b) for the metamorphic basement on Hainan Island and the Cretaceous (136–81 Ma) mafic dike swarms in central south Hainan Island are from Xu et al. (2001), and Ge (2003) and Wang et al. (2012), respectively.

mafic dike swarms have geochemical affinities of arc-related basalts and thus interpreted them as a result of partial melting of subduction-related metasomatized SCLM. A thermal anomaly induced by underplated basic magma into a hot crust would have caused partial melting of the lower crust (Karsli et al., 2010). Under subduction-related arc setting, the continuous upwelling of asthenosphere would have provoked partial melting of the overlying enriched mantle source (i.e., EM II), resulting in the generation of basaltic magma (Wang et al., 2012). Subsequently the basaltic magma ascended and underplated to induce partial melting of the lower crust on Hainan Island to generate high-K crust-derived melts. In this scenario, the mantle-derived basaltic melt first mixed with granitic magma of crustal origin at depth. Then, the melts, which subsequently underwent a fractional crystallization process, could ascend to shallower crustal levels to generate Mo-hosting intermediate to acidic intrusions. It is possible that several crust-derived magma pluses and the concurrent mixing between mantle-derived and crust-derived magmas finally constructed the late Early Cretaceous to Late Cretaceous granitoids on Hainan Island.

6.3. Re concentration and sulfur isotope systematics: implications for metal Mo source

Rhenium concentrations in molybdenite provide clues for the source of Re and, by association, deposit genesis (Stein et al., 2001, 2004; Stein, 2006). High, >250 ppm, to very high, >1000 ppm, Re contents suggest metal sources that involve fertile mantle or juvenile crustal, as for the case of subduction-related Cu–Au–Mo–(PGE) porphyry systems; whereas low, <100 ppm, and especially Re contents <10 ppm, indicate an evolved crustal metal source (Zimmerman et al., 2008). Contents <10 ppm and especially sub-ppm level Re are particularly characteristic of molybdenite produced during metamorphism (Bingen and Stein, 2003; Stein, 2006). By comparison with the Re concentrations in molybdenite from Mo-related deposits of different genetic types in China, Mao et al. (2008) empirically concluded that there are affinities between Re concentrations and the Mo sources, and proposed that metal Mo sources are changing from a mantle source to mixtures between mantle and crust, and then to crust with the decreasing Re concentrations in molybdenite gradually from hundreds of ppm to dozens of ppm and then to single digit ppm. Based on the Re concentrations in molybdenite (Appendix A4), the Mo sources on Hainan Island can be grouped into three types: (1) crustal source, as for the Hongmenling and Shimenshan deposits, with Re concentrations of ~0.31 ppm and ~0.35 ppm, and 1.05–1.67 ppm, respectively; (2) mixed mantle–crust source, as for the Gaotongling, Baogaocun, Luokuidong, Meiling and Xincun deposits, with Re concentrations of 3.19–13.27 ppm (mainly between 6.33 ppm and 13.27 ppm), 35.25 ppm, 28.39–31.54 ppm, 9.16 and 25.85 ppm, and 5.49–99.67 ppm (mainly between 13.39 ppm and 31.15 ppm), respectively; and (3) mantle source-dominated, such as for the Hongling occurrence, with Re contents of 135.67 ppm and 142.41 ppm. Linked to the main Mo mineralizing event, Mo sources of Mo-related deposits on Hainan Island are dominated by hybrid origins between mantle and crust, which is consistent with an origin involving the mixing of mantle-derived magma and crust-derived melts as proposed for the origin of the Mo-hosting granitoids.

However, the Re concentration in molybdenite does not provide essential proof for deposit genesis, when the molybdenite volume variable is taken into consideration (Stein et al., 2001). For examples, the Luokuidong deposit contains largest metal Mo reserves but a medium Re concentration, whereas the Shimenshan deposit has a lowest Re concentration, although both the deposits were defined as a porphyry mineral system. In contrast, the Hongling occurrence shows a highest Re concentration in molybdenite. The distinct differences for molybdenite Re concentrations at a deposit scale or among deposits (Appendix A4) likely are related to the composition and origin of ore fluids (Stein and Bingen, 2002), or the primary diffusive control by increasing natural grain size and age probably with decreasing Re content (Selby and Creaser, 2004), and/or the degree of Re dilution by molybdenite (Zimmerman et al., 2008). Combined with the molybdenite-commodity types, ore minerals (Appendix A1), ore-forming ages, metal Mo sources and tectonic settings (*discussion below*), the relatively narrow ranges of Re concentrations for the Gaotongling, Hongmenling, Baogaocun, Hongling, Shimenshan and Luokuidong mineralization indicate ore fluids whose Re compositions were stable and homogeneous throughout deposition of molybdenites (Stein and Bingen, 2002). In contrast, the highly variable Re contents for the Xincun and Meiling molybdenites most likely suggest a volume-dilution effect (Stein et al., 2001) and/or an inhomogeneous source.

Sulfur isotope studies for sulfide minerals help to constrain the possible origin of sulfur, and thus provide insights into the variations of physicochemical states of ore-forming fluids (Ohmoto, 1972; Rye and Ohmoto, 1974; Seal, 2006). The relatively narrow $\delta^{34}S$ ranges for all sulfide minerals from both the Gaotongling and Shimenshan deposits indicate a magmatic hydrothermal origin (Jensen, 1959). This is supported by the Mo-hosting granitoids on Hainan Island that show geochemical affinities of I-type granites, and that an oxidized magmatic system such as I-type granites is favored for the positive $\delta^{34}S$ values as opposed to the S-type granites with $\delta^{34}S$ values less than 0‰ (Ishihara and Sasaki, 1989). However, the slightly higher ^{34}S values for sulfides from the Shimenshan deposit than those from the Gaotongling deposit, and the difference in $\delta^{34}S$ value between chalcopyrite/pyrite and molybdenite from the Gaotongling deposit, likely reflect variable assimilation or partial melting of either pyritic sedimentary rocks with low $\delta^{34}S$ values or evaporites with high $\delta^{34}S$ values (Seal, 2006). Nevertheless, the geochemical and Nd–Sr isotopic results ruled out sulfur contamination of the magma through interactions with the unknown sedimentary rocks. The slight variation in $\delta^{34}S$ values of sulfide minerals from the Gaotongling and Shimenshan deposits thus was likely caused by the slight variation in composition, fO_2 and/or pH of ore-forming fluids during ore deposition (e.g., Ohmoto, 1972), resulting in the occurrence of isotopic disequilibrium and difference of $\delta^{34}S$ values of individual sulfide minerals (e.g., Rye and Ohmoto, 1974) in our studied deposits. This is consistent not only with the origin of the Mo-hosting granitoids but also with the Shimenshan deposit that contains lower Re contents in molybdenite than the Gaotongling deposit, suggesting a pure contribution of crust-derived melts to metal Mo source, and the Gaotongling deposit that is of variable Re concentrations, indicating a mixed crust–mantle source.

6.4. Geodynamic setting

The geodynamic setting of the high-K calc-alkaline, metaluminous to weakly peraluminous I-type granitoids has been controversial since the pioneering work of Barbarin (1999) who associated the genetic types of granitoids with the Wilson cycle. Two main tectono-magmatic models have been proposed to explain the genesis of this type rocks. The first model insists a post-orogenic lithospheric extensional origin without any relation with subduction processes (e.g., Roberts and Clemens, 1993; Rottura et al., 1998; Zhang et al., 2011b), whereas the second model suggests that the magmatism originated in an Andean-type continental margin (Altherr and Siebel, 2002; Sisson et al., 2005; Karsli et al., 2010; Kaygusuz et al., 2014). Although it has been debated as to whether or not Hainan Island was the southwardly extent of the Cathaysia Block over a long geological time scale (e.g., Li et al., 2002a, 2008a,b; Xu et al., 2014b; Wang et al., 2015), the consensus appears to be that Hainan Island was part of the Cathaysia Block since Late Permian, and after that both of them underwent a similar tectonic evolution history (Hsü et al., 1990; Li et al., 2002b; Xu et al., 2013, 2015). Moreover, most of the Chinese workers have agreed with the extensive extension and resulting large-scale magmatism and W, Sn, Bi, Mo, Cu, Pb, Zn and Au mineralization during the Late Mesozoic (180–80 Ma) in South China that were induced by subduction of the paleo-Pacific plate beneath the eastern Asian margin, and associated geodynamic processes (slab foundering or rollback or

back-arc extension) (Zhou and Li, 2000; Li, 2000; Hua et al., 2003; Zhou et al., 2006; Li and Li, 2007; Mao et al., 2011a; Wang et al., 2012; Jiang and Li, 2014). Given a broad extension-induced tectonism throughout South China during Late Mesozoic, the widespread Cretaceous magmatism and associated Mo mineralization on Hainan Island thus might be a response to slab roll-back of the Paleo-Pacific plate (e.g., Li and Li, 2007; Wang et al., 2012). The timing of magmatism and associated Mo mineralization on Hainan Island is consistent with the Late Jurassic to Cretaceous extensional event recognized in South China. Three episodes of emplacement of the Cretaceous mafic dikes on Hainan Island at ca. 135 Ma, ca. 117–105 Ma and ca. 96–81 Ma have been identified (Ge et al., 2003), which correspond to the age populations for the Cretaceous granitic magmatism and associated Mo mineralization. The Cretaceous Mo-hosting granitoids also have genetic affinities with the coeval mafic dike swarms which have been generally regarded as evidence of lithospheric extension (Ge et al., 2003). Additional evidence likely results from the emplacement of the Cretaceous mafic dikes under an extensional setting in the coastal areas of Guangdong Province of South China. Li (2000) and Cao et al. (2009) found that these mafic dikes generally occurred in three episodes during ca. 138–132 Ma, ca. 112–105 Ma and ca. 99–82 Ma. A youngest episode of ca. 75–54 Ma, which overlaps with the youngest Mo mineralizing event (ca. 72 Ma) on Hainan Island, was also reported for these mafic dikes (Cao et al., 2009). Because a Mesozoic collisional orogeny has not been recognized after the intense Indosinian orogeny in South China (Jiang and Li, 2014), Hainan Island should be affected by the principal, Cretaceous extensional event, resulting in multistage magmatism and associated Mo-polymetallic mineralization.

Re–Os data has been proven to be a valuable means to track tectonic setting and related geodynamics (Zimmerman et al., 2008). Interestingly the late Early Cretaceous to early Late Cretaceous Mo-related ore deposits show a predominant mixed mantle–crust source, whereas the Late Cretaceous was characteristic of a crustal source. Correspondingly, ore-forming ages seem to document migration of Mo metallogenesis from northeast to southwest (Fig. 1b), i.e., from Gaotongling–Meiling (105–99 Ma), via Xincun–Luokuidong–Baogaocun–Hongling (mainly 100–96 Ma), to Shimenshan and Hongmenling (89–72 Ma; Fig. 10b) on Hainan Island. This indicates that migratory pulses of the Cretaceous magmatic–hydrothermal activities and associated Mo mineralization from northeast to southwest likely were related to the Late Mesozoic tectonic evolution on Hainan Island. Zhou et al. (2006) suggested that genetically the Late Mesozoic extension in South China was linked to the NW–WNW-ward subduction of the paleo-Pacific oceanic lithosphere. In response to the flat-slab subduction (Li and Li, 2007) or the change in slab dip angle of the subduction (Zhou and Li, 2000), the Late Mesozoic magmatic rocks in the eastern South China shows a young trend from the western inland to the eastern coastal areas with the oceanward migration of magmatism to the southeast (Zhou et al., 2006; Li et al., 2007). After the Early Mesozoic subduction of the Paleo-Pacific Plate, the slab rollback of the subducted plate from west to east (Wong et al., 2009; Wang et al., 2012) led to continuous upwelling of unmetasomatized asthenosphere beneath a continental arc which likely triggered partial melting of the overlying asthenospheric and lithospheric mantle that had been metasomatized by fluids and/or melts released from the subducted oceanic crust. This process led to the Early Cretaceous basaltic magma and associated felsic magma with a signature of the subduction-related metasomatized mantle (i.e., EMII). Subsequently, the ascended mafic magma periodically underplated to induce partial melting of the preexisting lower crust. Consequently, magma mixing between mantle-derived and lower crust-derived melts occurred, which resulted in not only the Cretaceous Mo-hosting granitoids via fractional crystallization but also the approximately coeval mafic dikes. Thus mixing–mingling between mantle-derived magmas and crust-derived melts was an important process, accounting or origins of metal Mo on Hainan Island. The mixing was likely inhomogeneous, because of a large proportion of mantle-derived ore metal for the late Early Cretaceous to early Late Cretaceous (ca. 106–95 Ma) Mo mineralization, whereas almost a pure crustal source for the Late Cretaceous (ca. 89–72 Ma) Mo mineralization on Hainan Island. The migratory pluses of the Cretaceous granitic magmatism and associated Mo mineralization shown by ore-forming ages and metal Mo sources likely recorded episodic slab rollback of the westward subduction of the paleo-Pacific plate which triggered the arc system to retreat towards the Pacific Ocean (Liu et al., 2014). Alternatively, the Late Cretaceous Mo mineralization likely was a response to the transition from the common Andean-type active continental margin to the West Pacific-type continental margin at ca. 70 Ma (e.g., Jiang and Li, 2014).

7. Conclusions

Ore geological characteristics of the Mo-related deposits and occurrence on Hainan Island of South China, combined with whole-rock geochemistry, Nd–Sr and sulfur isotopic components, and zircon LA-ICP-MS U–Pb dating of the ore-bearing granitoids as well as Re–Os isotopic data of molybdenite yields the following conclusions:

1. The Cretaceous Mo-hosting granitoids were a result of three stages of magma emplacement during ca. 113–108 Ma, ca. 100–94 Ma and ca. 90–70 Ma, respectively. They belong to high-K calc-alkaline, metaluminous to weakly peraluminous I-type (magnetite series) granites and have geochemical affinities to arc-related basalts, showing derivation from subduction-related metasomatized mantle. Variable degree of magma mixing between mantle-derived and crust-derived melts was an important process for formation of the Cretaceous Mo-hosting granitoids.
2. Re–Os isotopic dating on molybdenites from the Mo-related deposits have recognized three episodes of Mo mineralization, including the main late Early Cretaceous to Late Cretaceous (ca. 106–95 Ma) event, and two subordinate events in the late Early Cretaceous (ca. 112 Ma) and the Late Cretaceous (ca. 89–72 Ma). The ca. 89–72 Ma metallogenesis in southwest Hainan Island represents the youngest Mo mineralizing event in East China.
3. The Re concentrations in molybdenite and sulfur isotopic values for sulfide minerals from the Mo-related deposits suggest that ore metal Mo was derived from a mixed mantle–crust source, with an almost pure crust source for the Late Cretaceous mineralization.
4. The intensive Cretaceous extension which led to multistage magmatism and related Mo mineralization might be ascribed to subduction of the Paleo-Pacific plate. The subduction and associated processes (e.g., episodic slab roll-back or transition from Andean-type to West Pacific-type continental margin) likely explained the migratory pluses of Mo metallogeny and associated metal Mo sources from northeast to southwest Hainan Island.

Acknowledgments

This paper is co-funded by the National Natural Science Foundation of China (41472171), and the State Key Fundamental Program (2012CB416806). We acknowledge Li Sunxiong, Yang Changsong and Zhou Yingchun from Hainan Bureau of Geology for their support during the field investigation, and Sun Yali, Li Congying and Tu Xianglin for their assistance with analyses and data processing. A particular thank is given to two anonymous reviewers for their thorough and constructive reviews, and to the editor Franco Pirajno for his editorial handling of the paper. As for the contributions of the co-authors, Xu D.R. re-wrote the present version, Wu C.J. re-represented, re-compiled and re-interpreted the analyzed data and related figures, Hu G.C. and Wang Z.L. jointly carried out all the analyses, Chen M.L. and Fu Y.R. provided the regional and ore geological data, and Chen H.Y. and Hollings P. gave very good suggestions on improvement of the manuscript and also smoothed the English.

Appendix A

Appendix A1
Ore geological characteristics of the major Mo-related ore deposits on Hainan Island.

Ore deposit and genetic classification	Longitude and latitude	Mo reserve (t)/grade (%)	Ore metal association	Host rock	Ore-controlling structure and attitude for ore body	Orebody geometry and ore occurrence	Ore- and gangue minerals	Alteration pattern
Meiling in Qionghai area Porphyry	110°32′11″–110°33′54″, 19°24′00″–19°25′23″	3311 (proven) and 18,951 (measured)/0.10%	Cu–Mo, with 1661 t metal Cu at an average grade of 0.53%	Late Cretaceous granodiorite pluton and intruded granodioritic porphyry stocks, and explosive breccias	Controlled commonly by SN- and EW-trending faults, annular fissure zones and breccia pipe, and having variable trend with variable dipping	Ring-like and lenticular orebodies, with Mo present as microcrystals adhered to cements of breccias, or as foliated or acicular aggregates disseminated in host rocks or within veinlets and stockworks crosscutting host rocks	Mo + Ccp ± Py ± Lm–Sp–Mt–Ant Qtz + Ser + Chl + Ep + Cal ± Kfs ± Amp ± Bt ± Mus, with accessory minerals Ap + Tit + Aln	Less clear alteration zoning from silicification and potassic (biotite) Mo ore zone at core outward through phyllic (sericitic, silica, pyritic) Mo–Cu ore zone, to propylitic (chloritic, epidote and carbonate) zone
Hongmenling in Ledong area Porphyry	108°43′34″–109°03′26″, 18°35′50″–18°53′11″	2164 (proven) and 20,321 (measured)/0.24%	Mo–W–(Pb–Zn), with 1530 t WO_3 at an average grade of 0.17%	Triassic biotite syenogranite pluton and intruded granite-porphyry stocks, with minor Mo and W within Late Cretaceous (ca. 94 Ma by K–Ar) porphyritic granite stocks	Controlled mostly by secondary NW- to NNW-trending fractures with dipping to NE, with minor by NE-trending fractures	Vein-type and lenticular orebodies, with Mo present as blades, laths and flaky aggregates disseminated in syenogranites and granite porphyries, or as large clots intergrown with Wol in quartz veins, or as thin smears of fissure surfaces in host rocks	Mo + Wol + Sch + Sp + Bis + Gn ± Py ± Ccp ± Apy ± Cst Qtz + Pl + Kfs + Mus + Fl ± Ser ± Amp ± Bt ± Ep ± Chl	Widespread but less strong potash feldspathization, silicification, topaz greisenization, kaolinization, sericitization, and chloritization show planar alteration, with NE-trending Pb–Zn ore veins surrounding the Mo and Mo–W orebodies
Shimenshan in Ledong area Porphyry	108°58′31″–108°59′56″, 18°29′55″–18°31′00″	10,443 (proven) and 65,804 (measured)/0.17%	Mo–(Pb–Zn–Ag), with 6877 t Pb and 1484 t Zn at average grades of 3.21% and 1.51%, respectively	Late Cretaceous (ca. 101–82 Ma by zircon U–Pb) porphyritic monzogranite pluton and intruded granite-porphyry dikes	Controlled by nearly SN- to NNW-trending faults, and having trend to SN–NNW with dipping to NWW–W	Lenticular and vein-type orebodies, with Mo present as blades and flaky aggregates or as intergrowth with Mus, Ser, Qtz and Py disseminated in greisens and host rocks of strong greisenization	Mo ± Py ± Sp ± Aq ± Wol ± Bis ± Hem ± Spe ± Gn ± Ccp Qz + Mus ± Chl ± Cal ± Fl	Strong lateral and vertical alteration zoning from central greisenization, via sericitization, silicification and pyritization, to marginal kaolinization, hematization, and chloritization, with peripheral Pb–Zn–Ag ore veins margining to the Mo mineralization
Luokuidong in Baoting area Porphyry	109°32′00″–109°35′00″, 18°24′00″–18°27′00″	254,346 (proven) and 467,663 (measured)/0.05%	Mo	Early Cretaceous volcanic rocks (ca. 112–106 Ma by zircon U–Pb), and hidden late Cretaceous porphyritic granites and quartz syenite porphyries	Controlled by annular caldera and boundary between volcanic rocks and porphyritic granites, and occurring as approximately	Tabular, vein-type and lenticular orebodies, with Mo present as (banded) blades or flaky aggregates filling fissures or margining veinlets, or as intergrowth with Py in veinlets/stockworks or with Chl disseminated in host rocks, or as	Mo + Py ± Ccp–Sp–Sch–Mt–Hem Qz + Pl + Kfs ± Bt ± Chl ± Ser ± Cal	Less strong alteration roughly showing zoning from central volcanic vent to distal host rocks are from silicification, greisenization and sericitization, via potash feldspathization and silicification, to chloritization,

(continued on next page)

Appendix A1 (*continued*)

Ore deposit and genetic classification	Longitude and latitude	Mo reserve (t)/grade (%)	Ore metal association	Host rock	Ore-controlling structure and attitude for ore body	Orebody geometry and ore occurrence	Ore- and gangue minerals	Alteration pattern
					equiaxial body	thin smears of fissure surfaces in host rocks		epidotization, pyritization and carbonatation
Baogaocun in Ledong area Porphyry	108°54′17″–108°57′00″, 18°35′50″–18°37′40″	1729 (proven) and 18,927 (measured)/0.09%	Mo	Late Cretaceous plagiogranite porphyry stocks emplaced in the Triassic syengranites and the Paleo- to Mesoproterozoic Baoban Group	Controlled by SN– and NW–NWW trending faults, and having trend to NW with dipping to SW	Mo present as radial, acicular and flaky aggregates disseminated in veins, veinlets and stockworks crosscutting host rocks or filling between Qtz and Bt grains in host rocks, or as thin smears of fissure surfaces in host rocks	Mo ± Ccp ± Py–Mt–Rt–Ilm Qz + Pl ± Kfs ± Bt ± Chl ± Ser	Mainly are silicification, potash feldspathization, biotitization and pyritization, subordinately include greisenization, sericitization, chloritization, epidotization, kaolinization and carbonatation, which show lateral zoning from orebodies to unmineralized host rocks
Xincun in Baoting area Hydrothermal vein type	109°32′40″–109°34′30″, 18°28′07″–18°29′35″	4038 (proven) and 18,967 (measured)/0.09%	Mo	Early Cretaceous rhyolitic porphyries, monzogranites and granite porphyries (ca. 112–106 Ma by zircon U–Pb), and Late Cretaceous monzogranites and granite-porphyry dikes	Controlled mainly by NNW- and NW-trending faults, with dipping to NE and NEE	Vein-type and lenticular orebodies, with Mo present as blades and clots within or marginal to quartz veins, or disseminated in gangue minerals or filling fissures of host rocks	Mo + Py ± Ccp ± Gn ± Lm ± Hem ± Mt ± Bis Qz + Pl + Kfs ± Bt ± Mus ± Chl ± Cal ± Ep, with accessory minerals Ap + Zrn + Zo + Tit	Main silicification, potash feldspathization and pyritization, with subordinate sericitization, propylitization, carbonatation, and kaolinization
Gaotongling in Tunchang area Hydrothermal vein type	110°02′30″–110°04′00″, 19°11′45″–19°13′00″	1698 (proven) and 10,847 (measured)/0.10%	Mo	Predominantly in early Late Cretaceous syenogranites, with possible occurrence in granodiorites (ca. 108–100 Ma by zircon U–Pb)	Controlled by NW-trending faults, and having trend to NW with dipping to NE	Vein-type orebodies, with Mo present as flaky or foliated aggregates disseminated in quartz veinlets crosscutting host rocks or interstitial to gangue minerals or disseminated in host rocks	Mo + Ccp ± Py–Sp–Gn–Bis Qz ± Kfs ± Bt–Chl	Main alteration with a linear zoning from central Mo mineralization, through potash feldspathization, pyritization, silicification, sericitization, to marginal chloritization
Longmenling in Lingshui area Hydrothermal vein type	109°48′30″–109°51′45″, 18°25′45″–18°28′00″	13,617 (proven) and 66,764 (measured)/0.19%	Mo	Early Cretaceous monzogranites (ca. 120 Ma by K–Ar), and intruded Late Cretaceous granodiorite stock (ca. 94 Ma by K–Ar)	Controlled mostly by NE-trending faults, and having trend to NE with steep dipping to NW	Vein-type orebodies, with most of Mo present as foliated and flaky aggregates or as intergrowth with Mt and Py interstitial to gangue minerals, or disseminated in host rocks	Mo + Py + Ccp + Mt ± Cc ± Cv ± Lm ± Ilm ± Rt Qz + Pl + Kfs + Mu + Ser ± Bt ± Chl ± Ep ± Zrn ± Ap ± And ± Tur	Strong, linear alteration including silicification, sericitization, pyritization, potash feldspathization, chloritization and carbonatation

Abbreviation of minerals: Mo = molybdenite, Py = pyrite, Ccp = chalcopyrite, Lm = limonite, Sp = sphalerite, Mt = magnetite, Ant = anatase, Qtz = quartz, Ser = sericite, Aln = allanite, Chl = chlorite, Ep = epidote, Cal = calcite, Kfs = K-feldspar, Amp = amphibole, Bt = biotite, Mus = muscovite, Ap = apatite, Ilm = ilmenite, Rt = rutile, Pl = plagioclase, Gn = galena, Bn = bornite, Fl = fluorite, Kln = kaolinite, Zrn = zircon, Zo = zoisite, Hem = hematite, Spe = specularite, Cc = chalcocite, Cv = covellite, And = andalusite, Tur = tourmaline, Toz = topaz, Wol = wolframite, Sch = scheelite, Bis = bismuthinite, Apy = arsenopyrite, Cst = cassiterite, and Aq = aquamarine.

Appendix A2

Geochemical compositions of the Cretaceous Mo-hosting granitoids on Hainan Island.

Data source: Samples with 07HN* from Gaotongling, Tunchang area were cited from Wang et al. (2012), and others from this study.

Sample	D6112-1	D3126-1	D1386-1	D1902-1	D1952-1	D2821-1	D2950-1	PM1-26-1	PM1-30-1	D3124-1	D3125-1	S006	D5207-1
Time	Late Cretaceous												
Location	Diaoluoshan, Ledong area												
Lithology	Syenogranite									Monzonitic granite			
SiO_2	76.81	75.24	72.91	75.6	70.64	71.56	73.35	70.92	71.37	75.38	74.9	72.55	73.24
TiO_2	0.09	0.14	0.25	0.15	0.29	0.3	0.27	0.33	0.32	0.12	0.15	0.32	0.24
Al_2O_3	12.61	13.01	13.83	12.78	14.45	13.82	13.59	14.11	13.79	12.8	12.85	13.51	13.76
$Fe_2O_3^T$	0.74	1.97	1.7	1.1	2.17	2.64	1.73	2.69	2.74	1.78	2.01	2.89	1.6
MnO	0.03	0.05	0.05	0.05	0.07	0.05	0.06	0.05	0.04	0.05	0.06	0.06	0.06
MgO	0.11	0.24	0.68	0.32	0.79	0.45	0.48	0.47	0.43	0.16	0.22	0.81	0.55
CaO	0.85	0.81	2.09	1.25	2.11	1.88	1.39	1.79	1.76	0.94	0.92	1.89	1.85
Na_2O	3.34	3.41	3.83	3.61	3.95	3.39	3.64	3.43	3.36	3.45	3.44	2.99	3.68
K_2O	4.82	4.68	3.69	4.52	4.5	4.84	4.74	5.23	5.37	4.58	4.42	4.16	4.16
P_2O_5	0.01	0.03	0.07	0.03	0.08	0.07	0.07	0.07	0.07	0.01	0.03	0.1	0.07
L.O.I.	0.49	0.35	0.68	0.4	0.67	0.81	0.58	0.73	0.58	0.25	0.28	0.45	0.62
Total	99.9	99.93	99.78	99.81	99.72	99.81	99.9	99.82	99.83	99.52	99.28	99.73	99.83
$Na_2O + K_2O$	8.16	8.09	7.52	8.13	8.45	8.23	8.38	8.66	8.73	8.03	7.86	7.15	7.84
Na_2O/K_2O	1.44	1.37	0.96	1.25	1.14	1.43	1.3	1.52	1.6	1.33	1.28	1.39	1.13
mg	0.13	0.11	0.29	0.23	0.27	0.15	0.22	0.15	0.14	0.08	0.10	0.22	0.26
A/NK	1.18	1.22	1.34	1.18	1.27	2.04	2.18	2.12	2.11	2.42	2.45	2.13	1.96
A/CNK	1.03	1.07	0.98	0.97	0.95	0.97	0.99	0.97	0.95	1.04	1.06	1.05	0.99
V	5.05	11.8	26.3	14	31.5	19.3	18.7	17.8	15	10.1	12.3	28.1	20.4
Cr	1.4	40.2	2.3	*	3.3	1.4	2.4	2.6	4.5	10.5	10.2	7.5	5.5
Co	0.59	1.4	3.88	2.32	4.5	3.27	2.33	3.22	2.72	1.4	1.8	3.8	2.71
Ni	0.87	18.1	3.01	2.29	3.71	3.58	2.21	0.43	0.53	4.4	4.4	3.8	1.16
Rb	230	223	115	159	139	181	175	186	144	199	213	137	128
Ba	38.3	187	456	231	726	482	412	564	458	139.1	204.7	467.2	382
Sr	59.2	157	384	165	394	168	284	170	151	145.2	159.6	332.7	310
Y	5.11	6.9	7.76	7.13	9.46	32.13	13.57	35.56	22.27	7.9	7.2	12.7	9.41
Th	28.9	18.2	10.8	13	14.5	21.5	25.6	24.1	17.1	17.3	19.4	15.1	8.86
U	8.4	7.8	2.95	6.75	9.53	4.49	4.06	3.51	2.64	6.9	7.1	3.1	2.4
Pb	38	40.9	26.5	35	28.8	21.9	28.7	21.3	21.3	35.3	39.9	23.3	29.7
Nb	12.2	13.6	8.97	13.2	10.6	16.9	19.6	16.7	14.6	12.4	15	9.4	11
Ta	0.94	1.1	0.63	0.74	0.74	0.9	1.46	1.2	0.81	1.05	1.12	0.76	1.18
Zr	71.6	78	79	74.8	102	200	146	221	206	68.5	78.3	123	100
Hf	2.9	3.3	3.2	3.2	4.5	6.8	5.3	7	6.4	2.9	3.4	4	3.1
Ga	17.5	16.6	23.6	16.5	16.3	16.7	19	18.7	20.9	18.9	12.9	14.4	17.3
La	16.02	22.1	19.07	18.67	20.35	55.4	50.86	61.53	66.94	21.9	23.3	31.2	20.28
Ce	20.45	39.2	33.64	33.12	38.76	103.8	78.47	115.5	123.9	38.5	43.1	61.6	38.18
Pr	2.52	3.9	3.96	3.56	4.99	13.18	8.66	13.65	15.01	3.5	4	6.5	4.53
Nd	7.34	11.8	14.48	11.5	16.53	45.99	27.09	50.91	56.02	11.8	12.8	22.1	15.92
Sm	1.08	1.8	2.49	1.81	2.88	9.23	4.18	9.7	9.78	1.6	1.9	3.5	2.76
Eu	0.22	0.34	0.61	0.33	0.69	0.99	0.76	1.08	1.05	0.34	0.34	0.64	0.63
Gd	0.78	1.32	1.88	1.43	2.21	7.71	3	8.33	7.51	1.23	1.4	2.47	2.26
Tb	0.12	0.2	0.26	0.2	0.32	1.17	0.45	1.25	1.03	0.19	0.17	0.36	0.31
Dy	0.73	0.98	1.42	1.11	1.7	6.56	2.3	6.66	5.19	1.02	1.03	1.86	1.63
Ho	0.18	0.21	0.29	0.24	0.35	1.35	0.49	1.39	1.01	0.22	0.22	0.37	0.33
Er	0.47	0.59	0.84	0.75	0.98	3.61	1.36	3.71	2.35	0.66	0.62	1.06	0.95
Tm	0.1	0.12	0.14	0.14	0.17	0.56	0.23	0.59	0.31	0.11	0.11	0.17	0.16
Yb	0.84	0.86	0.95	0.96	1.11	3.43	1.57	3.53	1.71	0.85	0.88	1.19	1.08
Lu	0.17	0.14	0.17	0.18	0.18	0.51	0.25	0.55	0.24	0.16	0.16	0.19	0.19
$\sum$REE	51.02	83.56	80.2	74	91.22	253.49	179.67	278.38	292.05	82.08	90.03	133.21	89.21
$(La/Yb)_N$	13.68	18.43	14.4	13.95	13.15	11.59	23.24	12.5	28.08	18.48	18.99	18.81	13.47
δEu	0.70	0.64	0.83	0.61	0.80	0.35	0.63	0.36	0.36	0.71	0.61	0.63	0.75

Note: mg = Mg / (Mg + Fe^{2+}); A/CNK = molar ratio of $Al_2O_3/(CaO + Na_2O + K_2O)$, A/NK = molar ratio of $Al_2O_3/(Na_2O + K_2O)$; δEu = Eu_N / $(Sm_N * Gd_N)^2$, N represents chondrite-normalized values from Sun and McDonough (1989).

Appendix A2 (*continued*)

Sample	D5325-1	D3128-1	S007	D5392-1	SM-1	SM-5	12HN03-4	09HN96	D0914-1	D0972-1	D1412-1	D1823-1	D3119-1
Time	Late Cretaceous								Early Cretaceous				
Location	Diaoluoshan, Ledong area				Qianjia, Ledong area				Baoting area				
Lithology	Monzonitic granite			Granite	Monzonitic granite								
SiO_2	77.34	70.7	72.14	72.52	70.67	69.34	63.74	73.27	69.93	72.82	68.99	71.2	70.68
TiO_2	0.11	0.35	0.29	0.43	0.31	0.28	0.66	0.24	0.39	0.24	0.41	0.32	0.32
Al_2O_3	11.95	14.34	13.73	13.18	14.87	15.72	15.24	14.5	14.74	14.49	14.95	14.8	14.43
$Fe_2O_3^T$	0.75	3.03	2.53	2.16	1.83	1.71	4.13	1.69	2.55	1.51	2.65	1.89	2.78
MnO	0.04	0.06	0.06	0.04	0.04	0.04	0.06	0.04	0.05	0.04	0.04	0.03	0.05
MgO	0.14	0.72	0.76	0.32	0.8	0.76	1.67	0.77	1.16	0.58	1.31	0.8	0.73
CaO	0.65	2.06	1.95	2.08	2.34	2.43	3.48	1.66	2.78	2.21	3.05	2.47	2.32
Na_2O	3.85	3.43	3.69	2.74	3.31	3.58	2.41	3.9	3.88	3.97	3.63	3.8	3.89
K_2O	4.8	4.3	3.91	5.34	4.44	4.54	3.98	2.75	3.37	3.4	3.83	3.94	3.63
P_2O_5	0.01	0.13	0.08	0.09	0.08	0.08	0.27	0.06	0.09	0.06	0.1	0.07	0.08
L.O.I.	0.24	0.29	0.38	1.33	0.73	0.94	4.62	0.33	0.84	0.5	0.82	0.43	0.68
Total	99.88	99.41	99.52	100.23	99.42	99.42	100.26	99.21	99.78	99.82	99.78	99.75	99.59
$Na_2O + K_2O$	8.65	7.73	7.6	8.08	7.75	8.12	6.39	6.65	7.25	7.37	7.46	7.74	7.52
Na_2O/K_2O	1.25	1.25	1.06	1.95	1.34	1.27	0.61	1.42	0.87	0.86	1.06	1.04	0.93
mg	0.16	0.19	0.23	0.13	0.30	0.31	0.29	0.31	0.31	0.28	0.33	0.30	0.21
A/NK	2.28	1.39	1.33	1.28	1.45	1.45	1.84	1.54	1.47	1.42	1.48	1.41	1.40
A/CNK	0.94	1.02	0.99	0.94	1.02	1.03	1.04	1.17	0.98	1.02	0.95	0.98	0.99
V	5.96	33.4	23.9	17	29.92	31.76	67.48	33.95	41.4	23.4	49.6	32.1	30.5
Cr	2.8	26.1	6.5	1.3	10.92	20.69	5.93	163.9	26.6	7.45	33.1	16.2	24.3
Co	0.59	4	3.5	1.89	2.72	3.17	6.91	2.78	6	3.54	6.92	4.44	4
Ni	0.62	10.7	3.3	3.06	3.53	3.51	6.6	6.59	6.89	4.79	9.47	6.84	8.9
Rb	193	136	116	282	205.9	215.6	216.4	103	139	162	143	137	143
Ba	50.9	581.7	445	525	432.9	498.3	543.1	528	620	407	767	780	782
Sr	40.1	406.3	355	219	375.3	423.4	233.33	426	491	390	541	511	409.4
Y	11.27	13.3	10.5	39.83	8.04	6.88	24.16	7.33	10.1	11.82	12.6	9.84	10.3
Th	30.2	17.8	11.3	42.2	18.59	19.12	22.03	13.14	17.8	20.4	16.7	20.9	19.5
U	15	3.3	4.3	8.88	6.47	9.97	4.62	2.86	6.02	6.18	3.87	3.21	5
Pb	37.2	31	25.2	29.1	21.6	21.82	18.47	24.64	16.9	20.2	17.8	22.9	21.9
Nb	22.3	13.1	8.8	20.6	11.11	9.85	17.49	8.99	11.6	10.4	9.46	9.6	10.2
Ta	1.5	0.98	0.77	1.84	1	0.91	1.22	0.72	1.01	0.89	0.66	0.71	0.86
Zr	72	141	97	295	103.8	98.82	251.24	101	171	117	152	137	115
Hf	3	4.6	3.5	10.3	3.05	2.99	6.16	3.21	6.3	4.8	5.6	5.4	3.7
Ga	24.1	21	17.8	18.7	19.4	17.8	19.04	15.48	*	*	14	20.3	20
La	18.65	51.5	20.6	77.21	19.99	20.61	54.36	22.88	37.52	32.75	32.09	33.59	38.4
Ce	33.73	92.6	41.6	147.2	40.5	38.53	105.53	42.18	66.01	49.84	57.87	59.72	69.1
Pr	3.64	9.3	4.5	17.47	4.74	4.24	11.77	4.63	7.11	5.58	6.62	6.88	6.8
Nd	10.18	32.2	15.8	61.4	16.61	14.65	43.65	15.95	23.99	18.75	22.4	22.55	23.1
Sm	1.67	5.1	2.5	10.88	2.76	2.43	7.69	2.42	3.69	2.99	3.74	3.64	3.5
Eu	0.19	0.95	0.58	1.19	0.63	0.58	1.46	0.64	0.8	0.71	0.86	0.8	0.8
Gd	1.54	3.64	1.89	9.16	1.76	1.58	5.96	1.87	2.71	2.45	2.92	2.67	2.6
Tb	0.26	0.44	0.29	1.43	0.26	0.21	0.87	0.23	0.36	0.34	0.42	0.36	0.34
Dy	1.44	2.56	1.54	7.53	1.42	1.16	4.38	1.15	1.88	1.98	2.23	1.83	1.69
Ho	0.34	0.49	0.3	1.53	0.28	0.23	0.82	0.22	0.39	0.41	0.47	0.36	0.34
Er	1.16	1.25	0.89	4.07	0.74	0.6	2.21	0.63	1.01	1.17	1.27	0.99	0.93
Tm	0.24	0.18	0.14	0.63	0.11	0.1	0.31	0.11	0.17	0.2	0.21	0.15	0.13
Yb	1.87	1.28	1.06	3.77	0.8	0.66	1.95	0.66	1.03	1.35	1.26	0.94	0.92
Lu	0.38	0.2	0.18	0.56	0.13	0.11	0.32	0.11	0.17	0.22	0.21	0.15	0.16
$\sum$REE	75.29	201.69	91.87	344.03	90.73	85.68	241.28	93.57	146.84	118.74	132.57	134.63	148.81
$(La/Yb)_N$	7.15	28.86	13.94	14.69	18.01	22.26	20.00	24.87	26.13	17.4	18.27	25.63	29.94
δEu	0.36	0.64	0.78	0.35	0.81	0.84	0.66	0.92	0.74	0.78	0.77	0.75	0.78

Appendix A2 (*continued*)

Sample	D1430-1	D0919-1	D1229-1	D3060-1	IHG8-1	D1421-1	D3117-1	D102-1	D0893	D1248	YD599-1	YD612-1	D0355
Time	Early Cretaceous												
Location	Baoting area												
Lithology	Monzonitic granite	Granodiorite			Monzonitic granite			Granodiorite		Diorite			
SiO_2	72.76	67.77	67.97	68.3	69.8	69.4	69.32	65.05	64.24	58.89	61.95	61.26	61.95
TiO_2	0.19	0.48	0.47	0.45	0.43	0.41	0.36	0.6	0.62	1.07	0.78	0.79	0.81
Al_2O_3	14.58	15.36	15.36	14.47	14.19	15.06	14.99	16.44	15.29	16.43	15.87	16.14	15.73
$Fe_2O_3^T$	1.2	3.01	2.84	3.84	2.88	2.47	3.1	3.38	4.26	5.92	5.37	5.55	5.43
MnO	0.03	0.05	0.05	0.06	0.05	0.04	0.05	0.05	0.07	0.07	0.1	0.1	0.09
MgO	0.35	1.55	1.45	1.69	0.64	1.27	1.08	1.98	2.64	3.24	3.24	3.33	3.04
CaO	1.47	3.43	3.22	3.35	1.98	3.07	2.78	4.7	4.28	5.47	5.52	5.75	5.12
Na_2O	3.64	3.56	3.48	3.13	3.08	3.51	3.76	3.09	3.25	3.1	2.77	2.81	3.2
K_2O	4.93	3.59	3.89	4.24	5.31	3.61	3.75	2.81	3.2	2.99	3.06	2.89	3.35
P_2O_5	0.04	0.12	0.1	0.15	0.14	0.09	0.09	0.25	0.13	0.35	0.21	0.22	0.18
L.O.I.	0.56	0.83	0.92	0.84	1.23	0.84	0.51	1.35	1.8	2.18	0.91	0.92	0.85
Total	99.75	99.75	99.75	100.52	99.73	99.77	99.79	99.7	99.78	99.71	99.78	99.76	99.75
$Na_2O + K_2O$	8.57	7.15	7.37	7.37	8.39	7.12	7.51	5.9	6.45	6.09	5.83	5.7	6.55
Na_2O/K_2O	1.35	1.01	1.12	1.35	1.72	1.03	1	0.91	0.98	0.96	1.1	1.03	1.05
mg	0.23	0.34	0.34	0.31	0.18	0.34	0.26	0.37	0.38	0.35	0.38	0.38	0.36
A/NK	1.29	1.58	1.54	1.48	1.31	1.55	1.46	2.02	1.73	1.97	2.01	2.08	1.77
A/CNK	1.04	0.96	0.97	0.91	0.98	0.99	0.98	0.98	0.92	0.90	0.89	0.89	0.86
V	18	56.6	52.6	60.4	25	43.6	39.7	78	93.3	125	121	122	126
Cr	6.49	38.9	39.7	236.1	8	30.6	59	14	72.5	51.6	53	58	44.6
Co	2.57	7.51	6.56	8.4	3.4	5.69	5.4	13	12.3	15	19	18	17.2
Ni	4.08	10.2	9.31	139	4.2	7.65	19.2	11	16.8	17.7	29	28	20.8
Rb	209	133	144	180	191	142	150	93	120	112	136	124	122
Ba	1113	778	900	488.8	980	742	666	976	584	841	703	683	711
Sr	405	616	601	348.9	392	561	495.8	790	500	762	435	443	523
Y	10.78	11.19	11.75	13.8	19.89	9.43	9.4	16.3	16.09	26.38	17.7	18	18.79
Th	23.3	17.1	18.5	29.1	31	17.8	20.4	4.5	17.4	5.36	14	12	12.9
U	5.37	3.26	3.41	6.8	11	4.14	5.4	1.1	4.88	0.93	2.6	2.2	3.61
Pb	23.8	16.3	15.2	16.7	43	19.3	22.9	8.6	16.1	21	19	22	18.8
Nb	10.2	8.9	9	10.6	37	8.3	9.1	11	10.5	12.3	17	18	12.4
Ta	0.75	0.76	0.74	1.07	3.6	0.58	0.84	0.5	0.57	0.66	1.1	0.7	0.82
Zr	107	163	160	149	269	157	121	157	187	224	194	192	187
Hf	3.7	5.7	5.9	4	6	5.6	4	3.5	6.1	7.4	4.2	4.3	5.8
Ga	20.9	*	*	18.7	19.9	20	20.2	*	20.9	21.4	18.4	*	17
La	35.14	35.23	36.5	38.3	76.38	32.5	33.7	30.5	29.81	53.27	30.6	31	35.28
Ce	49.33	65.59	65.15	67.2	135	57.95	64.8	50.5	59.42	97.35	60.7	60.9	66.27
Pr	9.39	8.1	8.34	7.3	14.6	6.87	6.7	6.5	7.51	12.79	7.6	7.2	8.22
Nd	33.16	27.65	26.71	24.5	45.08	22.46	23	25	28.2	48.48	25.6	25.9	29.5
Sm	5.79	4.65	4.47	4	7.18	3.78	3.5	4.6	5.17	8.9	5.1	4.8	5.53
Eu	1.44	0.99	0.95	0.67	1.2	0.84	0.71	1.5	1.03	2.37	1.2	1.2	1.28
Gd	4	3.27	3.2	2.89	5.26	2.68	2.46	4	4.17	7.44	4.1	4.2	4.67
Tb	0.53	0.48	0.48	0.39	0.78	0.38	0.34	0.6	0.6	0.99	0.7	0.6	0.66
Dy	2.65	2.42	2.47	2.43	3.78	1.87	1.74	3.1	3.35	5.35	3.3	3.4	3.72
Ho	0.48	0.49	0.49	0.47	0.71	0.4	0.34	0.6	0.68	1.01	0.6	0.6	0.72
Er	1.2	1.16	1.16	1.28	1.97	0.97	0.91	1.6	1.81	2.49	1.8	1.8	2.01
Tm	0.18	0.19	0.18	0.22	0.3	0.15	0.12	0.2	0.29	0.35	0.3	0.3	0.31
Yb	1.04	1.13	1.12	1.47	1.92	0.97	0.91	1.5	1.75	1.97	1.8	1.8	1.89
Lu	0.16	0.18	0.18	0.22	0.28	0.15	0.14	0.2	0.27	0.3	0.3	0.3	0.29
$\sum$REE	144.49	151.53	151.4	151.34	294.44	131.97	139.37	130.4	144.06	243.06	143.7	144	160.35
$(La/Yb)_N$	24.24	22.36	23.38	18.69	28.54	24.03	26.56	14.59	12.22	19.4	12.19	12.35	13.39
δEu	0.87	0.74	0.73	0.57	0.57	0.77	0.70	1.04	0.66	0.87	0.78	0.80	0.75

Appendix A2 (*continued*)

Sample	D1914-1	D0478	D0830	PM2-127-1	D3120-1	D0898	GTL-3	GTL-9	GTLY-2	GTL-4	GTL-12	07HN032*	07HN035*
Time	Early Cretaceous												
Location	Baoting area						Gaotongling, Tunchang area						
Lithology	Diorite			Granodiorite						Granite		Granodiorite	
SiO_2	57.4	63.16	61.94	67.52	65.31	66.09	68.37	65.55	66.12	72.43	72.2	64.35	66.32
TiO_2	0.91	0.73	0.78	0.47	0.58	0.53	0.39	0.49	0.43	0.14	0.16	0.91	0.75
Al_2O_3	17.46	16.19	16.33	15.6	15.95	15.68	15.19	16.19	16.38	14.87	14.53	14.74	15.29
$Fe_2O_3^T$	6.81	4.63	5.18	2.94	3.99	3.37	2.66	3.28	3.1	0.49	0.56	6.56	5.54
MnO	0.12	0.08	0.09	0.05	0.06	0.05	0.05	0.06	0.05	0.01	0.01	0.15	0.11
MgO	3.46	2.31	2.66	1.53	2.12	1.87	1.23	1.54	1.41	0.28	0.32	1.7	1.36
CaO	5.91	4.69	5.17	3.44	3.92	3.69	2.65	3.26	3.45	1.27	1.72	3.42	3.96
Na_2O	3.15	3.41	3.33	3.8	3.62	3.6	2.97	3.51	3.33	3.85	3.11	2.33	3.12
K_2O	2.45	3.52	3.24	3.67	3.45	3.7	4.3	3.75	4.1	5.06	4.64	4.37	2.63
P_2O_5	0.25	0.17	0.19	0.12	0.14	0.12	0.11	0.13	0.12	0.03	0.03	0.2	0.13
L.O.I.	1.77	0.87	0.85	0.62	0.43	1.05	1.49	1.64	0.93	0.98	2.11	1.03	0.94
Total	99.69	99.76	99.76	99.76	99.57	99.75	99.41	99.4	99.42	99.41	99.39	99.76	100.15
$Na_2O + K_2O$	5.6	6.93	6.57	7.47	7.07	7.3	7.27	7.26	7.43	8.91	7.75	6.7	5.75
Na_2O/K_2O	0.78	1.03	0.97	0.97	0.95	1.03	1.45	1.07	1.23	1.31	1.49	0.53	1.19
mg	0.34	0.33	0.34	0.34	0.35	0.36	0.32	0.32	0.31	0.36	0.36	0.21	0.20
A/NK	2.23	1.72	1.82	1.52	1.64	1.58	1.59	1.64	1.65	1.26	1.43	1.72	1.91
A/CNK	0.94	0.90	0.89	0.95	0.95	0.94	1.06	1.03	1.01	1.05	1.09	1.00	1.01
V	128	98.6	118	53.7	70.6	69.6	47.34	10.89	12.63	40.35	50.72	44.93	39.96
Cr	26.4	29.1	38	36.3	76.7	56.6	27.45	12.83	7.59	25.35	26.6	13.85	9.1
Co	17.1	12.4	15.7	7.25	9.1	9.34	5.87	0.5	0.73	3.65	6.06	8.61	7.11
Ni	10.4	12.6	15.6	8.62	20.6	13.2	6.86	0.4	0.5	5.29	6.83	6.46	4.44
Rb	74.1	122	116	135	145	146	163.1	163.7	155.8	150.8	144	187.4	154.4
Ba	616	672	580	732	729.3	743	598.1	932.3	668	921.3	550.7	623.5	386.1
Sr	636	503	550	551	601.6	568	506.8	438.4	304.4	524.4	647.8	247.4	329.7
Y	20.19	18.38	18.2	10.34	14.9	12.67	8.19	3.93	3.97	8.72	9.2	19.22	21.28
Th	6.27	10.7	14.3	14.3	15	21.9	9.63	5.3	5.77	12.22	17.35	8.34	9.76
U	1.24	2.2	3.78	2.74	3.4	3.86	2.69	3.29	3.18	5.53	5.5	3.35	3.07
Pb	11.1	18.4	17.1	15.3	19.3	14.6	20.6	28.52	26.75	21.28	18.74	25	33.48
Nb	10	11.7	12.7	8.5	10.5	10.7	9.53	6.32	7.61	9.45	9.49	11.55	12.24
Ta	0.52	0.76	0.88	1.1	0.83	0.78	0.73	0.57	0.68	0.88	0.84	0.92	1.17
Zr	162	186	148	167	164	173	118.5	76.39	79.98	121.3	126.9	206.8	189.4
Hf	4.6	6.3	4.9	5.8	5	6.2	3.42	2.71	2.84	3.38	3.63	5.88	5.56
Ga	18.3	16	23	21.1	20	19.9	*	*	19.4	*	21.89	18.5	19.76
La	34.28	37.72	37.35	32.03	38.6	40.27	33.87	15.8	16.94	17.12	26.8	26.7	27.88
Ce	64.35	67.68	69.74	59.91	78.6	72.81	57.28	29.18	32.66	34.11	50.01	53.16	56.58
Pr	8.46	8.84	8.4	6.73	8.5	8.69	6.12	3.39	3.75	4.05	5.53	6.77	7.15
Nd	29.28	29.92	32	24.07	30.9	29.76	19.66	11.83	13.05	14.57	19.42	27.62	28.77
Sm	5.71	5.57	5.82	3.81	5.7	4.94	2.92	2.1	2.32	2.68	3.17	5.5	5.87
Eu	1.42	1.29	1.39	0.92	1.03	1.05	0.79	0.58	0.59	0.71	0.83	1.2	1.09
Gd	4.8	4.64	4.71	2.99	3.88	3.59	1.98	1.33	1.3	1.95	2.18	4.65	5.01
Tb	0.69	0.68	0.68	0.4	0.52	0.48	0.28	0.15	0.16	0.28	0.31	0.74	0.82
Dy	3.87	3.58	3.76	2.02	2.72	2.62	1.53	0.75	0.75	1.55	1.7	4.07	4.49
Ho	0.77	0.71	0.74	0.41	0.52	0.53	0.3	0.14	0.14	0.33	0.34	0.79	0.86
Er	2.02	1.82	1.95	1.06	1.39	1.37	0.78	0.34	0.33	0.83	0.89	2.04	2.38
Tm	0.32	0.3	0.3	0.17	0.18	0.21	0.12	0.05	0.05	0.12	0.13	0.3	0.32
Yb	1.92	1.86	1.82	1.03	1.27	1.29	0.82	0.36	0.37	0.86	0.94	1.96	2.1
Lu	0.3	0.31	0.29	0.18	0.18	0.2	0.13	0.06	0.06	0.14	0.15	0.3	0.32
$\sum$REE	158.19	164.92	168.95	135.73	173.99	167.81	126.58	66.06	72.45	79.3	112.4	135.81	143.64
$(La/Yb)_N$	12.81	14.55	14.72	22.31	21.8	22.39	29.48	31.22	33.29	14.36	20.39	9.75	9.52
δEu	0.81	0.75	0.79	0.80	0.63	0.73	0.95	0.99	0.95	0.91	0.91	0.71	0.60

Appendix A2 (*continued*)

Sample	07HN004*	07HN005*	07HN006*	07HN007*	07HN011*	07HN013*	07HN014*	07HN025*	07HN008*	07HN009*	07HN010*	07HN019*	07HN020*	07HN028*	07HN029*	07HN030*	D776-1	D3037-1	S017
Time	Early Cretaceous																		
Location	Gaotongling, Tunchang area																Lingshui area		
Lithology	Granite								Granodiorite								Quartz monzonite		
SiO_2	72.07	71.93	70.15	71.86	73.27	73.09	73.62	72.3	65.4	66.14	67.54	65.92	67.17	65.91	66.18	67.92	65.62	67.8	75.17
TiO_2	0.28	0.23	0.29	0.26	0.14	0.14	0.13	0.19	0.53	0.53	0.51	0.52	0.54	0.52	0.52	0.49	0.31	0.23	0.18
Al_2O_3	14.76	14.81	15.89	14.9	14.66	14.61	14.56	15.1	15.69	15.96	15.98	16.13	15.87	16.11	16.02	15.69	16.76	15.87	12.67
$Fe_2O_3^T$	1.93	1.47	1.91	1.88	1.07	1.64	0.85	1.71	4.01	3.81	3.46	3.8	3.57	3.76	3.6	3.13	3.51	3.09	2.4
MnO	0.04	0.04	0.04	0.04	0.02	0.02	0.02	0.03	0.07	0.06	0.06	0.07	0.06	0.06	0.06	0.05	0.09	0.13	0.05
MgO	0.59	0.52	0.58	0.5	0.29	0.3	0.34	0.36	1.87	1.6	1.5	1.61	1.54	1.59	1.53	1.21	0.37	0.21	0.36
CaO	2.3	2.14	2.3	2.17	1.66	1.52	1.34	1.93	3.64	2.97	3.47	3.66	3.59	3.67	3.56	3.2	1.05	1.05	1.55
Na_2O	4.04	3.98	4.13	3.93	3.74	3.53	3.58	4.07	3.55	3.64	3.71	3.71	3.65	3.76	3.69	3.93	5.21	4.52	3.36
K_2O	3.43	4.02	4.11	3.94	4.66	4.55	4.74	3.78	3.57	3.55	3.55	3.46	3.46	3.46	3.58	3.3	6.05	5.78	4.32
P_2O_5	0.07	0.06	0.08	0.06	0.03	0.03	0.03	0.03	0.13	0.12	0.11	0.12	0.13	0.13	0.13	0.13	0.06	0.03	0.04
L.O.I.	0.62	0.41	0.64	0.47	0.61	0.52	1	0.68	0.89	1.72	0.62	0.97	0.94	0.7	0.67	0.68	0.51	0.47	0.62
Total	100.13	99.61	100.12	100.01	100.15	99.95	100.21	100.18	99.35	100.1	100.51	99.97	100.52	99.67	99.54	99.73	99.54	99.18	100.72
$Na_2O + K_2O$	7.47	8	8.24	7.87	8.39	8.08	8.32	7.85	7.12	7.19	7.26	7.17	7.11	7.22	7.27	7.23	11.26	10.3	7.68
Na_2O/K_2O	1.18	0.99	1	1	0.8	0.78	0.76	1.08	0.99	1.02	1.04	1.07	1.06	1.08	1.03	1.19	0.86	0.78	0.78
mg	0.23	0.26	0.23	0.21	0.21	0.15	0.29	0.17	0.32	0.30	0.30	0.30	0.30	0.30	0.30	0.28	0.10	0.06	0.13
A/NK	1.42	1.36	1.41	1.39	1.31	1.36	1.32	1.40	1.62	1.62	1.61	1.64	1.63	1.62	1.61	1.56	1.11	1.16	1.24
A/CNK	1.01	1.00	1.03	1.01	1.03	1.08	1.08	1.05	0.96	1.05	0.98	0.98	0.97	0.97	0.97	0.99	0.98	1.02	0.97
V	18.77	15.76	20.52	18.87	12.74	11.2	13.82	8.33	56.51	50.13	46.54	48.72	51.57	49.9	51.72	44.12	5	4.3	11.8
Cr	7.06	5.76	6.91	8.71	5.76	8.18	18.61	11.2	25.48	23.87	21.32	20.42	20.85	36.71	78.02	13.18	4.1	7.6	7.1
Co	2.41	5.26	2.47	2.31	1.08	1.49	0.94	1.99	7.96	6.91	6.58	6.57	6.8	7.16	7.63	5.16	2.1	1.4	1.2
Ni	3.75	3.23	3.79	3.56	1.77	2.96	10.65	4.6	10.39	8.7	10.04	7.83	8.18	17	51.54	6.7	2.1	4.1	4.1
Rb	98.74	107.4	115	105.2	146.3	160.1	148.3	96.52	109.4	96	111.7	102.5	116.2	114.6	124.6	101.7	130.7	118.2	160.2
Ba	602.3	727.7	966.6	692.3	815	903.7	875.9	981.3	698.3	746.5	703.3	651.6	648.8	672.5	724.9	757	509.5	328.4	255.1
Sr	588.7	538.3	588.7	600.8	426.2	438.1	396.1	476	496.5	545.8	520.2	511.4	559.2	546.9	570.5	720.1	74.3	76.7	161
Y	4.34	4.63	4.6	3.91	3.68	3.65	3.17	2.95	8.78	8.84	9.13	7.6	9.95	10.07	10.26	7.64	15.1	16.4	10.1
Th	9.01	6.64	10.61	7.7	6.39	6.91	5.35	6.75	12.69	13.02	15.32	13.74	16.49	12.95	11.99	9.43	10.4	10.6	24.9
U	1.51	3.62	2.29	1.08	2.09	3.65	2.22	1.03	3.32	2.77	2.71	2.68	3.49	2.83	4.05	1.71	2.2	2.4	3.4
Pb	27.79	20.99	23.18	24.05	31.76	30.06	28.14	33.76	19.8	20.25	18.93	17.44	19.18	17.85	18.75	15.87	16.7	38.5	17.7
Nb	5.8	5.01	5.93	5.21	5.98	4.39	4.31	4.68	8.02	8.68	8.92	7.32	9.49	9.44	10.13	7.7	6.1	7.1	10
Ta	0.46	0.51	0.48	0.43	0.58	0.47	0.45	0.39	0.63	0.82	0.85	0.64	0.85	0.84	0.95	0.62	0.42	0.47	1.13
Zr	124.3	65.4	113.1	102.5	86.83	84.54	78.44	103.8	131.9	151.5	122	107.9	118.1	124.5	112	116.1	481.7	334.9	96.9
Hf	4.01	2.32	3.57	3.24	3.72	3.77	3.21	3.81	4.12	4.64	3.8	3.27	3.49	3.8	3.64	3.6	10.5	8.3	3.6
Ga	18.62	17.56	20.1	18.82	19.33	20.15	18.72	20.68	18.52	18.95	19.57	17.87	20.37	20.15	20.7	20.57	15.9	16.2	13.7
La	22.72	16.29	21.98	22.07	20.24	23.25	17.49	27.06	21.59	37.41	31.23	30.58	42.75	35.23	31.31	30.39	109.3	89.9	35
Ce	42.07	32.63	42.03	40.32	37.72	41.16	31.42	49.34	41.44	65.02	56.8	53.68	72.83	62.18	57.56	58.48	185	150	59.8
Pr	4.99	3.93	4.99	4.62	4.4	4.84	3.54	5.57	5.04	7.31	6.56	5.85	7.95	7.03	6.62	6.95	17.6	14	5.4
Nd	18.13	15.11	18.42	16.71	15.95	16.1	12.74	19.92	19.13	25.48	23.9	20.9	27.98	24.66	24.53	25.71	54.7	45.8	15.9
Sm	2.84	2.75	2.99	2.56	2.86	2.63	2.17	3.19	3.43	3.82	3.91	3.16	4.27	4	4.02	4.02	6	5.3	2.2
Eu	0.74	0.67	0.83	0.77	0.67	0.6	0.63	0.73	0.98	0.98	1.03	0.85	1.08	1.02	1.03	1.05	1.27	0.96	0.42
Gd	1.83	1.68	1.85	1.58	1.71	1.71	1.4	1.91	2.66	2.96	3	2.37	3.31	3.1	2.94	2.8	3.39	3.83	1.55
Tb	0.21	0.21	0.21	0.19	0.19	0.19	0.15	0.17	0.37	0.37	0.38	0.3	0.41	0.42	0.4	0.35	0.51	0.48	0.25
Dy	0.94	1.06	1.02	0.8	0.84	0.76	0.65	0.68	1.9	1.87	1.99	1.54	2.04	2	2.06	1.69	2.46	2.53	1.39
Ho	0.16	0.19	0.17	0.14	0.14	0.12	0.11	0.11	0.36	0.35	0.36	0.28	0.38	0.37	0.39	0.29	0.49	0.54	0.29
Er	0.44	0.56	0.45	0.37	0.36	0.34	0.3	0.29	0.95	0.96	0.96	0.78	1.01	1.01	1.04	0.77	1.52	1.59	0.88
Tm	0.06	0.08	0.07	0.05	0.06	0.05	0.04	0.04	0.14	0.14	0.14	0.12	0.14	0.15	0.15	0.1	0.22	0.24	0.15
Yb	0.43	0.53	0.46	0.37	0.42	0.35	0.33	0.29	0.95	0.95	0.95	0.75	0.99	0.96	1.03	0.73	1.55	1.65	1.1
Lu	0.08	0.09	0.07	0.06	0.07	0.06	0.06	0.05	0.16	0.15	0.14	0.12	0.15	0.16	0.16	0.11	0.27	0.26	0.19
$\sum$REE	95.62	75.78	95.55	90.6	85.61	92.17	71.03	109.34	99.11	147.76	131.35	121.28	165.29	142.28	133.23	133.44	384.28	317.08	124.52
$(La/Yb)_N$	38.17	22.01	34.13	43.37	34.98	47.38	37.9	66.25	16.3	28.31	23.48	29.09	30.88	26.3	21.83	30.03	50.58	39.08	22.82
δEu	0.93	0.88	1.00	1.08	0.85	0.81	1.04	0.83	0.95	0.86	0.88	0.91	0.85	0.85	0.88	0.91	0.79	0.62	0.66

Appendix A2 (*continued*)

Sample	D3056-1	D3055-1	HNK102-09-06	HNK102-10-1	HNK103-8	HNK103-9	09HN28	09HN32	HNK24-02	HNK24-03	HNK24-05	09HN21	09HN80	12LD07-1	12LD09-2	12LD04-1	12HN17-1	12HN17-4H
Time	Early Cretaceous																	
Location	Lingshui area																	
Lithology	Granodiorite																	
SiO_2	68.22	67.72	68.09	72.29	73.37	72.24	67.01	67.91	70.02	68.16	67.89	66.92	67.76	66.64	69.9	69.77	66.15	65.76
TiO_2	0.45	0.54	0.42	0.32	0.26	0.25	0.61	0.46	0.43	0.49	0.45	0.5	0.47	0.5	0.3	0.36	0.57	0.57
Al_2O_3	14.93	14.95	14.81	13.8	13.93	14.56	15.33	15.08	14.62	15	14.85	15.03	15.49	15.66	15.24	14.94	15.98	16.16
$Fe_2O_3^T$	3.93	4.2	2.66	1.6	1.48	1.43	3.88	3.59	2.65	3.08	2.82	3.49	3.12	3.55	1.99	3.07	3.83	3.77
MnO	0.07	0.07	0.03	0.02	0.04	0.04	0.06	0.06	0.05	0.05	0.05	0.05	0.04	0.06	0.05	0.09	0.05	0.05
MgO	0.69	0.94	1.28	0.72	0.84	0.83	1.49	1.43	1.46	1.67	1.75	1.89	1.58	1.91	0.74	0.84	1.61	1.71
CaO	3.14	3.35	2.76	1.43	2.2	2.21	3.14	2.96	2.84	3.22	2.90	2.93	3.03	3.28	2.3	2.43	3.75	3.66
Na_2O	3.06	2.98	4.1	3.03	3.5	3.51	2.91	3.02	2.72	2.89	3.37	2.8	3.19	3.27	3.74	3.27	3.42	3.37
K_2O	3.59	3.65	4.29	5.1	3.38	3.85	4.38	4.05	4.32	4.02	4.63	4.35	3.65	3.99	4.42	4.12	3.6	3.73
P_2O_5	0.09	0.1	0.15	0.08	0.07	0.08	0.14	0.12	0.11	0.12	0.12	0.12	0.11	0.16	0.1	0.12	0.16	0.17
L.O.I.	0.92	0.63	0.88	0.96	0.54	0.63	0.32	0.57	0.6	1.1	0.57	1.2	0.84	1.27	0.74	1	1.15	1.34
Total	99.09	99.13	99.47	99.35	99.61	99.63	99.27	99.25	99.82	99.8	99.40	99.28	99.28	100.29	99.52	100.01	100.27	100.29
$Na_2O + K_2O$	6.65	6.63	8.39	8.13	6.88	7.36	7.29	7.07	7.04	6.91	8	7.15	6.84	7.26	8.16	7.39	7.02	7.1
Na_2O/K_2O	0.85	0.82	0.96	0.59	1.04	0.91	0.66	0.75	0.63	0.72	0.73	0.64	0.87	0.82	0.85	0.79	0.95	0.90
mg	0.15	0.18	0.32	0.31	0.36	0.37	0.28	0.28	0.36	0.35	0.38	0.35	0.34	0.35	0.27	0.21	0.30	0.31
A/NK	1.67	1.69	1.30	1.31	1.48	1.47	1.61	1.61	1.60	1.65	1.41	1.61	1.68	1.61	1.39	1.52	1.68	1.68
A/CNK	1.02	1.00	0.90	1.05	1.04	1.04	1.01	1.02	1.02	1.00	0.94	1.02	1.05	1.00	1.01	1.05	0.98	1.00
V	23.5	29	56.15	25.35	28.46	27.87	62.93	65.12	54.21	62.9	56.38	67.91	59.46	66.39	29.33	32.08	62.39	65.93
Cr	16.7	12.1	6.514	2.152	5.162	4.783	112	209.2	31.26	46.94	34.16	157.7	177.4	40.48	5.72	1.9	10.95	13.15
Co	9.3	10.6	54.8	41.82	57.28	57.87	7.306	6.931	42.55	39.68	34.46	7.6	6.2	8.43	3.26	4.33	7.21	7.86
Ni	7.2	5.5	6.29	2.75	5	5.18	10.27	9.04	10.48	15.58	10.65	13.25	11.77	13.17	2.99	1.03	3.3	3.73
Rb	131.8	158.3	143	134	191	219	152	160	180	182	214.00	155	117	149.2	214.24	149.78	154.77	153.34
Ba	650.6	613	660	833	237	320	589	538	489	517	564.00	555	720	512.83	525.35	578.67	410.98	429.17
Sr	289.8	256.5	361	313	321	344	358	369	357	402	366.00	464	617	409.72	404.05	307.39	383.26	380.1
Y	31.2	32.7	14.21	13.07	7.89	8.22	23.85	18.85	14.36	15.61	15.83	16.19	12.2	15.25	9.26	21.77	21.11	20.73
Th	16.2	16.7	20.28	20.28	26.47	22.2	23.02	22.41	32.25	28.02	36.19	29.01	21.43	27.77	19.99	17.77	16.27	15.2
U	3.1	4.9	4.73	3.84	11.32	9.65	7.43	3.81	5.15	8	9.07	9.05	5.53	8.32	7.89	3.55	5.48	5.31
Pb	20.4	27	16.15	17.64	19.86	22.64	19.15	16.91	17.13	15.62	18.50	13.75	13.63	16.57	23.26	46.62	18.19	18.17
Nb	11.2	11	10.96	13.35	12.78	12.78	12.98	10.42	11.03	11.27	12.32	10.42	8.65	11.38	11.69	11.96	13.3	13.41
Ta	0.88	1	1.25	1.39	1.33	1.36	1.35	1.03	1.3	1.29	1.37	1.12	0.76	1.12	1.01	0.87	1.07	1.05
Zr	189.7	179.9	188	161	104	116	160	152	135	146	202.00	159	143	159.96	111.93	169.83	164.52	171.76
Hf	5.9	5.7	4.9	4.23	3.33	3.52	4.83	4.01	3.96	3.99	5.82	4.39	4.19	4.65	3.36	4.54	4.59	4.93
Ga	19.1	19.3	17	14.99	18.79	19.64	18.43	17.77	17.09	17.99	17.13	16.76	19.63	18.05	18.84	16.28	18.71	18.4
La	41.4	40.2	32.45	36.9	20.94	25.03	33.53	46.17	40.93	44.22	40.31	36.04	34.17	34.46	30.4	47.07	31.3	27.69
Ce	85.5	82.9	58.37	70.49	40.55	45.47	70.08	84.53	72.77	76.87	71.66	67.13	65.32	62.26	52.75	83.42	60.63	54.96
Pr	9.5	9.3	6.61	8	4.67	5.22	8.24	9.17	8.29	8.68	8.07	7.25	7.01	6.49	5.3	8.82	6.83	6.36
Nd	36.1	35	22.73	26.59	15.63	17.12	30.12	30.01	27.03	28.65	27.21	23.92	23.81	22.79	18.47	31.05	25.52	24.21
Sm	7	7.1	3.97	4.11	2.55	2.73	5.83	4.81	4.38	4.67	4.49	4.07	3.85	3.78	2.82	5.41	4.84	4.87
Eu	1.15	1.05	1.03	0.91	0.56	0.62	1.13	0.91	0.88	0.97	0.88	0.95	0.89	0.86	0.64	0.97	1.02	0.99
Gd	5.74	5.83	3.31	3.12	1.9	2.07	5.08	3.96	3.39	3.71	3.54	3.37	3.19	3.12	2.06	4.15	3.8	4.06
Tb	0.91	0.97	0.48	0.43	0.26	0.27	0.76	0.56	0.48	0.53	0.50	0.47	0.41	0.43	0.28	0.65	0.62	0.58
Dy	5.38	5.85	2.67	2.25	1.35	1.38	4.14	2.98	2.56	2.87	2.80	2.56	2.03	2.46	1.57	3.48	3.53	3.57
Ho	1.07	1.14	0.52	0.44	0.25	0.27	0.81	0.6	0.5	0.56	0.55	0.5	0.38	0.48	0.28	0.71	0.7	0.71
Er	2.98	3.09	1.41	1.25	0.69	0.74	2.24	1.68	1.35	1.47	1.49	1.42	1.07	1.38	0.77	1.91	1.97	1.86
Tm	0.43	0.46	0.22	0.2	0.12	0.12	0.33	0.25	0.22	0.24	0.25	0.22	0.16	0.22	0.12	0.3	0.31	0.31
Yb	2.94	3.04	1.51	1.38	0.87	0.89	2.17	1.66	1.56	1.63	1.71	1.48	1.04	1.53	0.88	1.92	1.95	2.08
Lu	0.44	0.45	0.25	0.23	0.15	0.16	0.34	0.27	0.26	0.27	0.27	0.24	0.16	0.24	0.14	0.31	0.31	0.31
$\sum$REE	200.54	196.38	135.53	156.3	90.49	102.09	164.8	187.56	164.60	175.34	163.73	149.62	143.49	140.50	116.48	190.17	143.33	132.56
$(La/Yb)_N$	10.1	9.49	15.41	19.18	17.26	20.17	11.08	19.95	18.82	19.46	16.91	17.47	23.57	16.16	24.78	17.59	11.51	9.55
δEu	0.54	0.48	0.87	0.78	0.78	0.80	0.63	0.64	0.70	0.71	0.67	0.78	0.78	0.77	0.81	0.63	0.73	0.68

Appendix A3
LA-ICP-MS U–Pb data for zircons from the Mo-hosting granitoids in the Gaotongling and Shimenshan deposits.

Sample no.	Th ppm	U ppm	Th/U	$^{207}Pb/^{235}U$ ratio	$^{207}Pb/^{235}U$ 1σ	$^{206}Pb/^{238}U$ ratio	$^{206}Pb/^{238}U$ 1σ	$^{207}Pb/^{235}U$ age (Ma)	$^{207}Pb/^{235}U$ 1σ	$^{206}Pb/^{238}U$ age (Ma)	$^{206}Pb/^{238}U$ 1σ	Concordance (%)
Granodiorite from the Gaotongling deposit												
GLT4-03	263.38	724.58	0.36	0.11	0.01	0.02	0.00	108.28	5.23	100.72	1.66	92%
GLT4-05	*159.06*	*210.56*	*0.76*	*0.09*	*0.01*	*0.02*	*0.00*	*90.68*	*12.25*	*104.61*	*2.85*	*85%*
GLT4-06	399.22	466.71	0.86	0.27	0.01	0.04	0.00	241.63	10.70	237.58	3.43	98%
GLT4-09	221.12	386.95	0.57	0.11	0.01	0.02	0.00	107.89	6.76	104.42	1.97	96%
GLT4-10	845.35	2225.83	0.38	0.10	0.00	0.02	0.00	93.96	3.81	99.91	1.71	93%
GLT4-12	375.46	2499.45	0.15	0.09	0.01	0.01	0.00	91.12	4.98	89.19	2.25	97%
GLT4-16	206.96	627.30	0.33	0.11	0.01	0.02	0.00	105.93	5.90	105.82	1.88	99%
GLT4-19	431.53	587.49	0.73	0.11	0.01	0.02	0.00	103.19	5.44	97.92	1.39	94%
GLT4-20	279.58	1061.87	0.26	0.10	0.00	0.02	0.00	97.83	4.45	101.54	1.95	96%
GLT4-21	*81.12*	*349.55*	*0.23*	*0.13*	*0.01*	*0.02*	*0.00*	*124.18*	*8.46*	*106.88*	*2.05*	*85%*
GLT4-22	313.04	331.63	0.94	0.11	0.01	0.02	0.00	105.62	7.62	97.36	1.77	91%
GLT4-23	311.01	691.91	0.45	0.10	0.01	0.01	0.00	92.96	5.02	90.94	1.21	97%
GLT4-25	212.84	821.34	0.26	0.10	0.01	0.02	0.00	101.22	5.72	101.85	1.54	99%
Granite from the Gaotongling deposit												
GLT9-01	242.90	1590.22	0.15	0.10	0.00	0.02	0.00	100.01	3.79	99.19	1.15	99%
GLT9-02	125.17	218.70	0.57	0.11	0.01	0.02	0.00	103.62	12.66	102.42	2.10	98%
GLT9-03	374.03	413.50	0.90	0.23	0.01	0.03	0.00	206.69	7.87	194.02	2.81	93%
GLT9-04	*174.20*	*266.90*	*0.65*	*0.09*	*0.01*	*0.02*	*0.00*	*89.32*	*8.54*	*101.15*	*2.23*	*87%*
GLT9-05	241.99	338.03	0.72	0.12	0.01	0.02	0.00	115.75	8.47	110.51	2.96	95%
GLT9-06	*272.12*	*378.21*	*0.72*	*0.11*	*0.01*	*0.01*	*0.00*	*109.35*	*9.91*	*95.74*	*1.99*	*86%*
GLT9-07	173.45	252.71	0.69	0.10	0.01	0.02	0.00	92.43	9.83	101.09	1.96	91%
GLT9-08	237.88	332.16	0.72	0.10	0.01	0.02	0.00	92.60	6.69	96.92	1.75	95%
GLT9-10	254.82	391.28	0.65	0.11	0.01	0.02	0.00	102.10	6.63	100.41	1.69	98%
GLT9-11	321.10	752.83	0.43	0.11	0.01	0.02	0.00	102.63	5.64	99.38	1.61	96%
GLT9-12	193.18	260.68	0.74	0.09	0.01	0.02	0.00	90.30	6.72	97.04	2.02	92%
GLT9-13	280.27	536.24	0.52	0.11	0.01	0.02	0.00	105.23	6.17	96.31	1.54	91%

(continued on next page)

Appendix A3 (*continued*)

Sample no.	Th ppm	U ppm	Th/U	$^{207}Pb/^{235}U$ ratio	$^{207}Pb/^{235}U$ 1σ	$^{206}Pb/^{238}U$ ratio	$^{206}Pb/^{238}U$ 1σ	$^{207}Pb/^{235}U$ age (Ma)	$^{207}Pb/^{235}U$ 1σ	$^{206}Pb/^{238}U$ age (Ma)	$^{206}Pb/^{238}U$ 1σ	Concordance (%)
GLT9-14	143.54	250.05	0.57	0.11	0.01	0.02	0.00	108.54	9.98	108.56	2.77	99%
GLT9-15	239.07	341.20	0.70	0.11	0.01	0.02	0.00	102.24	7.24	100.20	1.78	97%
GLT9-18	*200.64*	*296.42*	*0.68*	*0.12*	*0.01*	*0.02*	*0.00*	*116.99*	*7.67*	*96.80*	*1.90*	*81%*
GLT9-19	284.38	420.01	0.68	0.10	0.01	0.02	0.00	93.19	5.73	98.88	1.81	94%
GLT9-22	294.44	350.49	0.84	0.11	0.01	0.02	0.00	101.67	7.61	100.98	2.05	99%
GLT9-23	*334.74*	*408.17*	*0.82*	*0.11*	*0.01*	*0.02*	*0.00*	*109.48*	*7.08*	*96.80*	*1.93*	*87%*
GLT9-24	266.72	428.60	0.62	0.11	0.01	0.02	0.00	103.66	7.12	100.13	1.91	96%
GLT9-25	296.98	396.22	0.75	0.10	0.01	0.02	0.00	100.02	6.62	102.48	1.88	97%
Monzonitic granite from the Shimenshan deposit												
SM-01	1174.72	1620.22	0.73	0.09	0.00	0.01	0.00	89.05	4.15	91.63	1.54	97%
SM-02	928.69	1880.68	0.49	0.09	0.00	0.01	0.00	89.34	3.48	86.55	1.14	96%
SM-03	447.96	326.02	1.37	0.09	0.01	0.01	0.00	89.38	7.00	95.32	1.78	93%
SM-04	1927.31	11,750.44	0.16	0.09	0.00	0.01	0.00	89.54	2.52	86.13	0.95	96%
SM-05	1704.49	1637.26	1.04	0.10	0.00	0.01	0.00	99.61	3.93	92.16	1.29	92%
SM-06	463.35	1503.45	0.31	0.12	0.01	0.02	0.00	115.95	5.17	112.92	1.73	97%
SM-07	2041.23	2116.72	0.96	0.10	0.00	0.01	0.00	97.14	3.79	94.58	1.61	97%
SM-08	299.08	397.06	0.75	0.09	0.01	0.01	0.00	89.39	6.10	95.66	1.75	93%
SM-09	1852.83	2250.75	0.82	0.09	0.00	0.01	0.00	90.10	3.19	88.75	1.38	98%
SM-10	868.90	1322.38	0.66	0.09	0.00	0.01	0.00	91.49	4.12	94.93	1.69	96%
SM-11	1111.85	2952.86	0.38	0.08	0.00	0.01	0.00	81.92	3.15	83.95	1.03	97%
SM-12	1072.90	1579.08	0.68	0.10	0.00	0.01	0.00	96.16	4.28	86.54	1.31	89%
SM-14	410.22	505.30	0.81	0.09	0.01	0.02	0.00	90.14	5.60	100.18	1.71	89%
SM-15	1027.56	2364.07	0.43	0.09	0.00	0.01	0.00	88.01	3.64	93.88	1.73	93%
SM-16	926.45	1322.85	0.70	0.11	0.01	0.02	0.00	101.80	4.66	97.22	1.79	95%
SM-17	1152.28	1925.65	0.60	0.10	0.00	0.01	0.00	95.18	4.02	92.46	1.52	97%
SM-18	722.35	1758.28	0.41	0.09	0.00	0.01	0.00	85.80	3.86	87.48	1.27	98%
SM-19	908.70	1584.06	0.57	0.10	0.00	0.01	0.00	94.19	3.87	93.27	1.58	99%
SM-20	*152.90*	*204.22*	*0.75*	*0.12*	*0.01*	*0.01*	*0.00*	*111.37*	*9.94*	*93.82*	*1.94*	*82%*
SM-21	506.53	871.69	0.58	0.09	0.00	0.02	0.00	88.24	4.35	96.97	1.32	90%
SM-22	1662.32	1907.62	0.87	0.10	0.00	0.01	0.00	97.79	3.73	95.53	1.22	97%
SM-23	721.53	1801.42	0.40	0.09	0.00	0.01	0.00	89.19	3.57	91.99	1.23	96%
SM-24	*806.37*	*1343.93*	*0.60*	*0.11*	*0.01*	*0.01*	*0.00*	*107.46*	*4.88*	*92.32*	*1.55*	*84%*
SM-25	451.46	1184.74	0.38	0.10	0.00	0.01	0.00	93.51	4.43	92.59	1.33	99%

Note: ① Concordance is by comparison of $^{206}Pb/^{238}U$ and $^{206}Pb/^{207}Pb$ ages; and ② for interpretation of the zircon age data, we excluded the analyses with age discordance larger and/or smaller than 10%. These excluded data are listed in italics.

Appendix A4

Re–Os isotopic data of molybdenites from the Mo-related ore deposits on Hainan Island.

Deposit/showing	Sample no.	Weight (g)	Re (ppm)	2σ	^{187}Re (ppm)	2σ	^{187}Os (ppb)	2σ	Model age (Ma)	2σ	Isochron age (Ma)	References
Gaotongling	GTL-1	0.1493	8.419	0.06	5.291	0.038	9.053	0.1057	105.09	1.4		This study
	GTL-2	0.1707	6.486	0.054	4.076	0.034	6.59	0.085	99.3	1.49	102.5 ± 1.8 Ma (2σ, MSWD = 2.0)	
	GTL-3	0.1135	6.325	0.028	3.976	0.018	6.462	0.026	99.84	0.59		
	GTL-4	0.13	10.16	0.091	6.383	0.058	10.48	0.046	98.46	0.95		
	GTL-5	0.0765	7.149	0.037	4.494	0.023	7.377	0.048	100.84	0.82		
	GTL-6	0.0997	10.71	0.076	6.731	0.048	11.22	0.034	102.39	0.77		
	GTL01-5-1	0.02284	11.58	0.11	158.8	1.5	7.28	0.07	102.4	1.5	98.4 ± 2.5 Ma (2σ), MSWD = 1.7	Liao et al. (2008)
	GTL02-1-1	0.17824	3.19	0.04	270.8	2.8	2.00	0.02	102.1	1.4		
	GTL02-1-4	0.09107	11.43	0.11	267.0	2.7	7.18	0.07	98.8	1.3		
	GTL02-10	0.07445	13.27	0.14	293.3	3.3	8.34	0.09	97.9	1.2		
	GTL02-10	0.14249	7.95	0.08	265.5	2.7	5.00	0.05	98.6	1.2		
Hongmenling	HM-1	0.3089	0.3144	0.0026	0.1976	0.0016	0.2369	0.0049	71.9	1.6		This study
	HM-2	0.3607	0.3472	0.0031	0.2182	0.002	0.2623	0.0025	72.1	0.9		
Meiling	ML-1	0.09	9.159	0.07	5.757	0.044	10.04	0.091	104.6	1.2		
	ML-2	0.0317	25.85	0.28	16.25	0.18	28.28	0.23	104.4	1.4		
Hongling	HL-1	0.0351	135.7	1.014	85.27	0.6374	143.4	0.366	100.9	0.8		
	HL-2	0.0358	142.4	1.790	89.51	1.1249	148.1	0.608	99.2	1.3		
Luokuidong	HNK100-77(1)	0.075	28.392	0.297	17.845	0.187	29.685	0.0637	99.8	1.1		Li et al. (2014)
	HNK100-77(2)	0.0714	30.810	0.073	19.365	0.056	32.171	0.131	99.6	0.5		
	HNK100-77(3)	0.0651	31.536	0.251	19.822	0.157	33.072	0.332	100.1	1.3		
Baogaocun	HNK102-09(1)	0.056	35.249	0.315	22.155	0.198	38.376	0.175	103.9	1.0		
Shimenshan	HNK103-12	0.03	1.3899	0.0055	0.8736	0.00351	1.2900	0.0137	88.6	1.0		
	HNK103-13	0.329	1.1068	0.0073	0.6957	0.00457	0.93030	0.00382	80.2	0.6		
	12LD09-8	0.10065	1.045	0.0030	0.6566	0.00210	0.8518	0.0118	77.82	1.34		This study
	12LD09-1	0.10769	1.673	0.0060	1.0514	0.00350	1.4100	0.0079	80.44	0.94		
Xincun	XC-1	0.0385	31.15	0.12	19.58	0.07	31.93	0.12	97.81	0.53	97.7 ± 1.3 Ma	Wang and Liao (2012)
	XC-2	0.069	27.24	0.17	17.12	0.11	27.61	0.20	96.71	0.91	MSWD = 1.03, with mean age of	
	XC-3	0.1094	14.56	0.07	9.15	0.05	14.54	0.11	95.57	0.89	97.15 ± 0.53 Ma (MSWD = 0.99)	
	XC-6	0.0329	99.67	0.69	62.64	0.43	101.96	0.36	97.61	0.74		
	XC-12	0.1316	13.41	0.06	8.42	0.04	13.65	0.05	97.15	0.56		
	XC-5	0.1107	5.49	0.02	3.45	0.01	6.46	0.24	112.33	4.18		

Appendix A5
Nd–Sr isotopic compositions for the Mo-hosting granitoids on Hainan Island.

Sample no.	Location	Lithology	t (Ma)	$^{87}Rb/^{86}Sr$	$^{87}Sr/^{86}Sr$	2σ	$(^{87}Sr/^{86}Sr)_i$	$\varepsilon_{Sr}(t)$	$^{147}Sm/^{144}Nd$	$^{143}Nd/^{144}Nd$	±2σ	$f_{Sm/Nd}$	$(^{143}Nd/^{144}Nd)_i$	$\varepsilon_{Nd}(t)$	T_{DM2} (Ga)	
SM-1	Qianjia, Ledong	Monzonitic granite	92	1.5469	0.710228	6	0.70821	54	0.1055	0.512316	4	−0.47	0.512253	−5.21	1.32	This study
SM-5			92	1.4358	0.709693	7	0.70782	49	0.1053	0.512326	4	−0.47	0.512263	−5.01	1.30	
09HN96			92	0.827	0.709483	14	0.70840	57	0.091764	0.512325	7	−0.53	0.512270	−4.87	1.29	
12HN03-4		Granodioritic porphyry	96	2.6847	0.712153	5	0.70834	56	0.106532	0.512257	2	−0.46	0.512187	−6.28	1.41	
12HN03-6			96	2.5784	0.710966	5	0.70730	41	0.106840	0.512261	7	−0.46	0.512191	−6.21	1.41	
09HN21		Tonalite	100	0.973	0.709969	10	0.70859	60	0.102891	0.512352	7	−0.48	0.512285	−4.39	1.26	
09HN80			98	0.549	0.709740	14	0.70898	65	0.097857	0.512338	7	−0.50	0.512275	−4.62	1.27	
12LD07-1		Monzonitic granite	99	1.4103	0.710634	5	0.70863	60	0.105420	0.512306	2	−0.47	0.512237	−5.31	1.33	
12LD09-2			100	1.0539	0.709939	5	0.70844	58	0.100360	0.512330	3	−0.49	0.512264	−4.78	1.29	
12LD04-1		Granodiorite	101	0.9877	0.709666	4	0.70826	55	0.117373	0.512349	2	−0.41	0.512272	−4.63	1.28	
12HN17-1			101	1.1689	0.711848	5	0.71019	82	0.114587	0.512231	7	−0.42	0.512156	−6.89	1.46	
12HN17-4H			101	1.1677	0.711862	5	0.71020	83	0.121563	0.512274	3	−0.38	0.512194	−6.14	1.40	
12HN11-2		Granite	100	15.2996	0.727413	6	0.70567	18	0.096667	0.512300	7	−0.51	0.512237	−5.32	1.33	
GTL-3	Gaotongling, Tunchang	Granodiorite	100	0.8108	0.710175	5	0.70902	66	0.1168	0.512304	4	−0.41	0.512228	−5.50	1.35	
GTL-9			100	0.6268	0.709758	7	0.70887	64	0.1035	0.512308	4	−0.48	0.512240	−5.25	1.33	
GTLY-2			100	0.9074	0.710171	8	0.70888	64	0.0942	0.512290	3	−0.52	0.512228	−5.48	1.35	
GTL-4		Granite	100	1.0529	0.710721	6	0.70922	69	0.1125	0.512252	4	−0.43	0.512178	−6.46	1.43	
GTL-12			100	1.4432	0.711196	5	0.70915	68	0.1127	0.512250	3	−0.43	0.512176	−6.50	1.43	
09HN32		Granodiorite	101	1.253	0.710205	17	0.70842	57	0.096899	0.512229	6	−0.51	0.512165	−6.70	1.45	
HNK24-02			99	1.459	0.710461	14	0.70842	57	0.097942	0.512319	8	−0.50	0.512256	−4.98	1.30	
HNK24-03			99	1.310	0.710120	17	0.70828	55	0.098544	0.512350	7	−0.50	0.512286	−4.38	1.26	
HNK24-05			99	1.690	0.710728	11	0.70836	56	0.099716	0.512349	7	−0.49	0.512285	−4.42	1.26	
07HN04		Granite	107	0.4854	0.710245	11	0.70951	73	0.0953	0.512256	8	−0.52	0.512189	−6.1	1.15	Wang et al. (2012)
07HN06			107	0.4936	0.710330	16	0.70958	74	0.0988	0.512234	8	−0.50	0.512165	−6.5	1.21	
07HN07			107	0.5068	0.710364	13	0.70959	74	0.0933	0.512244	7	−0.53	0.512179	−6.3	1.15	
07HN11			107	0.9935	0.710676	11	0.70917	68	0.1090	0.512247	9	−0.45	0.512171	−6.4	1.31	
07HN14			107	1.0836	0.710696	20	0.70905	66	0.1036	0.512313	7	−0.47	0.512240	−5.1	1.16	
07HN25			107	0.5868	0.710058	13	0.70917	68	0.0974	0.512259	9	−0.50	0.512191	−6.0	1.17	
07HN09		Granodiorite	107	0.5090	0.709844	11	0.70907	67	0.0912	0.512313	13	−0.54	0.512249	−4.9	1.04	
07HN10			107	0.6214	0.709540	14	0.70860	60	0.0995	0.512335	7	−0.49	0.512265	−4.6	1.09	
07HN20			107	0.6014	0.709848	18	0.70893	65	0.0928	0.512285	10	−0.53	0.512220	−5.5	1.09	
07HN28			107	0.6064	0.709822	14	0.70890	64	0.0986	0.512372	6	−0.50	0.512303	−3.9	1.03	
07HN29			107	0.6321	0.709875	10	0.70891	64	0.0996	0.512357	7	−0.49	0.512287	−4.2	1.06	
HNK102-09-06	Lingshui	Syenogranite	104	1.147	0.711027	16	0.70933	70	0.105645	0.512337	7	−0.46	0.512265	−4.66	1.28	This study
HNK102-10-1			104	1.361	0.714086	16	0.71208	109	0.093446	0.512300	8	−0.52	0.512236	−5.22	1.33	
HNK103-8	Baoting	Monzonitic granite	100	1.725	0.710310	14	0.70786	49	0.098555	0.512350	9	−0.50	0.512286	−4.37	1.26	
HNK103-9			100	1.842	0.710340	13	0.70772	47	0.096334	0.512343	7	−0.51	0.512280	−4.47	1.26	
09HN28		Granodiorite	100	1.224	0.710853	13	0.70911	67	0.116918	0.512338	8	−0.41	0.512261	−4.83	1.29	

Appendix A6
Sulfur isotopic compositions for sulfides from the Gaotongling and Shimenshan deposits on Hainan Island.

Deposit	Sample no.	Mineral	$\delta^{34}S_{V\text{-}CDT}$ (‰)	References
Gaotongling	GTL-1	Molybdenite	4.39	This study
Gaotongling	GTL-2	Molybdenite	4.49	This study
Gaotongling	GTL-4	Molybdenite	4.6	This study
Gaotongling	GTL-6	Molybdenite	4.76	This study
Gaotongling	GTL-11	Chalcopyrite	3.86	This study
Gaotongling	2GTL-12-1	Chalcopyrite	2.93	This study
Gaotongling	2GTL-12-2	Chalcopyrite	1.36	This study
Gaotongling	GTL01-5-1	Pyrite	3.0	Liao et al. (2008)
Gaotongling	GTL01-5-1	Molybdenite	5.5	Liao et al. (2008)
Gaotongling	GTL01-5-4	Pyrite	2.9	Liao et al. (2008)
Gaotongling	GTL02-1-2	Molybdenite	4.4	Liao et al. (2008)
Shimenshan	SM-004	Pyrite	4.77	This study
Shimenshan	SMM-006	Molybdenite	5.29	This study
Shimenshan	SMF-006	Pyrite	5.73	This study
Shimenshan	SMM-008	Molybdenite	5.32	This study
Shimenshan	SMF-008	Pyrite	5.46	This study

References

Altherr, R., Siebel, W., 2002. I-type plutonism in a continental back-arc setting: Miocene granitoids and monzonites from the central Aegean Sea, Greece. Contrib. Mineral. Petrol. 143, 397–415.

Andersen, T., 2002. Correction of common lead in U–Pb analyses that do not report ^{204}Pb. Chem. Geol. 192 (1), 59–79.

Barbarin, B., 1999. A review of the relationships between granitoid types, origins and their geodynamic environments. Lithos 46, 605–626.

Bingen, B., Stein, H., 2003. Molybdenite Re–Os dating of biotite dehydration melting in the Rogaland high-temperature granulites, S Norway. Earth Planet. Sci. Lett. 208, 181–195.

Black, L.P., Kamo, S.L., Allen, C.M., Aleinikoff, J.N., Davis, D.W., Korsch, R.J., Foudoulis, C., 2003. TEMORA1: a new zircon standard for Phanerozoic U–Pb geochronology. Chem. Geol. 200, 155–170.

Brasilino, R.G., Sial, A.N., Ferreira, V.P., Pimentel, M.M., 2011. Bulk rock and mineral chemistries and ascent rates of high-K calc-alkalic epidote-bearing magmas, Northeastern Brazil. Lithos 127, 441–454.

Cannell, J., Cooke, D., Walshe, J., Stein, H., 2005. Geology, mineralization, alteration, and structural evolution of the El Teniente porphyry Cu–Mo deposit. Econ. Geol. 100, 979–1003.

Cao, J.J., Hu, R.Z., Xie, G.Q., Liu, S., 2009. Geochemistry and genesis of mafic dikes from the coastal areas of Guangdong Province, China. Acta Petrol. Sin. 25 (3), 984–1000 (in Chinese with English abstract).

Carten, R.B., White, W.H., Stein, H.J., 1993. High-grade granite-related molybdenum systems; classification and origin. In: Kirkham, R.V., Sinclair, W.D., Thorpe, R.I., Duke, J.M. (Eds.), Mineral Deposit Modeling. Geological Association of Canada Special Paper 40, pp. 521–554.

Chappell, B., 1999. Aluminium saturation in I- and S-type granites and the characterization of fractionated haplogranites. Lithos 46 (3), 535–551.

Chappell, B., White, A., 1992. I- and S-type granites in the Lachlan Fold Belt. Trans. R. Soc. Edinb. Earth Sci. 83 (1–2), 1–26.

Chen, M.L., 2015. Petrogenesis and Geological Implications of the Qianjia Complex, Hainan Island and Its Relationship With Mineralization (Dissertation), China University of Geosciences for the Doctor Degree of Philosophy (submitted for publication, 1–114 pp.) (in Chinese with English abstract).

Chen, M.L., Li, S.X., Zeng, Y.L., Zhou, J.B., 2008. Petrochemical characteristics and metallogenic analysis of the Cretaceous Qianjia rockbodies in Hainan Island. Miner. Resour. Geol. 22 (1), 36–42 (in Chinese with English abstract).

Collins, W.J., 1998. Evaluation of petrogenetic models for Lachlan Fold Belt granitoids: implications for crustal architecture and tectonic models. Aust. J. Earth Sci. 45, 483–500.

Collins, W.J., Beams, S.D., White, A.J.R., Chappell, B.W., 1982. Nature and origin of A-type granites with particular reference to southeastern Australia. Contrib. Mineral. Petrol. 80, 189–200.

Corfu, F., Hanchar, J.M., Hoskin, P.W.O., Kinny, P., 2003. Altas of zircon textures. Rev. Mineral. Geochem. 53, 469–500.

Defant, M.J., Drummond, M.S., 1990. Derivation of some modern arc magmas by melting of young subducted lithosphere. Nature 347, 662–665.

Ding, S.J., Fu, Y.R., Zhou, T.H., Dong, G.Y., 2005. The high-grade Baolun gold deposit, Hainan Island, China. In: Mao, J.W., Bierlein, F.P. (Eds.), Mineral Deposit ResearchMeeting the Global Challenge (Proceedings of the Eighth Biennial SGA Meeting, Beijing, China) vol. 3. Springer-Verlag, Berlin Heidelberg (1521–1522 pp.).

Du, A.D., He, H.L., Yin, N.W., Zou, X.Q., Sun, Y.L., Sun, D.Z., Chen, S.Z., Qu, W.J., 1993. Direct dating of molybdenites using the Re–Os geochronometer. Chin. Sci. Bull. 38, 1319–1320.

Du, A.D., He, H.L., Yin, N.W., Zou, X.Q., Sun, Y.L., Sun, D.Z., Chen, S.Z., Qu, W.J., 1994. A study on the rhenium–osmium geochronometry of molybdenites. Acta Geol. Sin. 68, 339–347.

Fang, J.Q., Nie, F.J., Zhang, K., Liu, Y., Xu, B., 2012. Re–Os isotopic dating on molybdenite separates and its geological significance from the Yaojiagou molybdenum deposit, Liaoning Province. Acta Petrol. Sin. 28 (2), 372–378 (in Chinese with English abstract).

Fedo, C.M., Sircombe, K.N., Rainbird, R.H., 2003. Detrital zircon analysis of the sedimentary record. Rev. Mineral. Geochem. 53, 277–303.

Ge, X.Y., 2003. Mesozoic magmatism in Hainan Island (SE China) and its tectonic significance: geochronology, geochemistry and Sr-Nd isotope evidences. (Dissertation) 2003, the graduate school of the Chinese Academy of Sciences for the Doctor Degree of Philosophy. pp. 1–87 (in Chinese with English abstract).

Ge, X.Y., Li, X.H., Zhou, H.W., 2003. Geochronologic, geochemistry and Sr–Nd isotopes of the Late Cretaceous mafic dike swarms in southern Hainan Island. Geochimica 32 (1), 11–20 (in Chinese with English abstract).

Gray, C.M., Kemp, A.I.S., 2009. The two-component model for the genesis of granitic rocks in southeastern Australia—nature of the metasedimentary-derived and basaltic end members. Lithos 111, 113–124.

Gruen, G., Heinrich, C.A., Schroeder, K., 2010. The Bingham Canyon porphyry Cu–Mo–Au deposit. II. Vein geometry and ore shell formation by pressure-driven rock extension. Econ. Geol. 105, 69–90.

HBG (Hainan Bureau of Geology), 2015. Geology in Hainan Province. Geological Publishing House, Beijing (in press, in Chinese).

HBGMR (Hainan Bureau of Geology and Mineral Resources), 1997. Lithostratigraphy of Hainan Province. Chinese University of Geosciences Press, Wuhan (1–125 pp. in Chinese).

Hou, W., Chen, H.F., Wang, K.F., Peng, G.L., Tang, H.F., Liang, X.Q., Xu, D.R., 1996. Geotectonics of Hainan Island and Gold Metallogeny. Science Press, Beijing (618 pp. in Chinese).

Hsü, K.J., Li, J., Chen, H., Wang, Q., Sun, S., Sengör, A., 1990. Tectonics of South China: key to understanding West Pacific geology. Tectonophysics 183 (1), 9–39.

Hua, R.M., Chen, P.R., Zhang, W.L., Liu, X.D., Lu, J.J., Lin, J.F., Yao, J.M., Qi, H.W., Zhang, Z., Gu, S.Y., 2003. Metallogenic systems related to Mesozoic and Cenozoic granitoids in South China. Sci. China Ser. D 46 (8), 816–829.
Huang, F., Wang, D.H., Lu, Y.M., Chen, Y.C., Wang, B.H., Li, C., 2011. Molybdenite Re–Os isotopic age of Shapinggou Mo deposit in Anhui Province and Mesozoic Mo ore-forming stages in East Qinling–Dabie Mountain region. Mineral Deposits 30 (6), 1039–1057 (in Chinese with English abstract).
Huang, F., Wang, D.H., Chen, Z.Y., Wang, C.H., Liu, S.B., Chen, Z.H., 2014a. Preliminary study on metallogenic specialization of the granites related to the molybdenum deposits in the Nanling region. Geotecton. Metallog. 38 (2), 239–254 (in Chinese with English abstract).
Huang, F., Wang, D.H., Santosh, M., Wang, C.H., Zeng, Z.L., Liu, S.B., Wang, L.Q., Zhang, Y.Z., 2014b. Genesis of the Yuanlingzhai porphyry molybdenum deposit, Jiangxi province, South China: constraints from petrochemistry and geochronology. J. Asian Earth Sci. 79, 759–776.
Ishihara, S., Sasaki, A., 1989. Sulfur isotopic ratios of the magnetite-series and ilmenite-series granitoids of the Sierra Nevada batholith—a reconnaissance study. Geology 17, 788–791.
Janoušek, V., Braithwaite, C.J.R., Bowes, D.R., Gerdes, A., 2004. Magma-mixing in the genesis of Hercynian calc-alkaline granitoids: an integrated petrographic and geochemical study of the Sázava intrusion, Central Bohemian Pluton, Czech Republic. Lithos 78, 67–99.
Jensen, M.L., 1959. Sulfur isotopes and hydrothermal mineral deposits. Econ. Geol. 54, 374–394.
Jiang, X.Y., Li, X.H., 2014. In situ zircon U–Pb and Hf–O isotopic results for ca. 73 Ma granite in Hainan Island: Implications for the termination of an Andean-type active continental margin in southeast China. J. Asian Earth Sci. 82, 32–46.
Karsli, O., Dokuz, A., Uysal, I., Aydin, F., Chen, B., Kandemir, R., Wijbrans, J., 2010. Relative contributions of crust and mantle to generation of Campanian high-K calc-alkaline I-type granitoids in a subduction setting, with special reference to the Harşit Pluton, Eastern Turkey. Contrib. Mineral. Petrol. 160, 467–487.
Kaygusuz, A., Arslan, M., Siebel, W., Sipahi, F., İlbeyli, N., Temizel, İ., 2014. LA-ICP MS zircon dating, whole-rock and Sr–Nd–Pb–O isotope geochemistry of the Camiboğazı pluton, Eastern Pontides, NE Turkey: implications for lithospheric mantle and lower crustal sources in arc-related I-type magmatism. Lithos 192–195, 271–290.
Landtwing, M.R., Dillenbeck, E.D., Leake, M.H., Heinrich, C.A., 2002. Evolution of the breccia-hosted porphyry Cu–Mo–Au deposit at Agua Rica, Argentina: progressive unroofing of a magmatic hydrothermal system. Econ. Geol. 97, 1273–1292.
Lawley, C., Richards, J., Anderson, R., Creaser, R., Heaman, L., 2010. Geochronology and geochemistry of the MAX porphyry Mo deposit and its relationship to Pb–Zn–Ag mineralization, Kootenay Arc, Southeastern British Columbia, Canada. Econ. Geol. 105 (6), 1113–1142.
Laznicka, P., 2010. Chapter 7: Cordilleran granitoids in convergent continental margins (lower, plutonic levels). Giant Metallic Deposits, 2nd ed. Springer-Verlag, Berlin Heidelberg (169–262 pp.).
Lee, J.W., Williams, I.S., Ellis, D.J., 1997. Pb, Th, and U diffusion in natural zircon. Nature 390, 151–162.
Li, X.H., 2000. Cretaceous magmatism and lithospheric extension in southeast China. J. Asian Earth Sci. 18 (3), 293–305.
Li, X.H., Li, Z.X., Li, W.X., Liu, Y., Yuan, C., Wei, G.J., Qi, C.S., 2007. U–Pb zircon, geochemical and Sr–Nd–Hf isotopic constraints on age and origin of Jurassic I- and A-type granites from central Guangdong, SE China: A major igneous event in response to foundering of a subducted flat-slab? Lithos 96 (2007), 186–204.
Li, Z.X., Li, X.H., 2007. Formation of the 1300-km-wide intracontinental orogen and postorogenic magmatic province in Mesozoic South China: a flat-slab subduction model. Geology 35 (2), 179–182.
Li, X.H., McCulloch, M.T., 1996. Secular variation in the Nd isotopic composition of Neoproterozoic sediments from the southern margin of the Yangtze Block: evidence for a Proterozoic continental collision in southeast China. Precambrian Res. 76, 67–76.
Li, Z.X., Zhang, L., Powell, C.M.A., 1995. South China in Rodinia: part of the missing link between Australia–East Antarctica and Laurentia? Geology 23, 407–410.
Li, Z.X., Li, X.H., Kinny, P.D., Wang, J., 1999. The breakup of Rodinia: did it start with a mantle plume beneath South China? Earth Planet. Sci. Lett. 173, 171–181.
Li, X.H., Zhou, H.W., Chung, S.L., Ding, S.J., Liu, Y., Lee, C.Y., Ge, W.C., Zhang, Y.M., Zhang, R.J., 2002a. Geochemical and Sm–Nd isotopic characteristics of metabasites from central Hainan Island, South China and their tectonic significance. Island Arc 11, 193–205.
Li, Z.X., Li, X.H., Zhou, H.W., Kinny, P.D., 2002b. Grenvillian continental collision in south China: new SHRIMP U–Pb zircon results and implications for the configuration of Rodinia. Geology 30, 163–166.
Li, X.H., Li, Z.X., Li, W.X., Wang, Y.J., 2006. Initiation of the Indosinian orogeny in South China: evidence for a Permian magmatic arc on Hainan Island. J. Geol. 114, 341–353.
Li, Z.X., Bogdanova, S.V., Collins, A.S., Davidson, A., De Waele, B., Ernst, R.E., Fitzsimons, I.C.W., Fuck, R.A., Gladkochub, D.P., Jacobs, J., Karlstrom, K.E., Lu, S., Natapov, L.M., Pease, V., Pisarevsky, S.A., Thrane, K., Vernikovsky, V., 2008a. Assembly, configuration, and break-up history of Rodinia: a synthesis. Precambrian Res. 160, 179–210.
Li, Z.X., Li, X.H., Li, W.X., Ding, S.J., 2008b. Was Cathaysia part of Proterozoic Laurentia? New data from Hainan Island, south China. Terra Nova 20, 154–164.
Li, C.Y., Wang, F.Y., Hao, X.L., Ding, X., Zhang, H., Ling, M.X., Zhou, J.B., Li, Y.L., Fan, W.M., Sun, W.D., 2012. Formation of the world's largest molybdenum metallogenic belt: a plate-tectonic perspective on the Qinling molybdenum deposits. Int. Geol. Rev. 54 (9), 1093–1112.
Li, N., Chen, Y.J., Pirajno, F., Ni, Z.Y., 2013. Timing of the Yuchiling giant porphyry Mo system, and implications for ore genesis. Mineral. Deposita 48, 505–524.
Li, S.X., Chen, M.L., Yang, D.S., Wang, Y.H., 2014. The molybdenite Re–Os age and analysis of geodynamic background in Hainan island. Geol. Miner. Resour. South China 30 (3), 272–279 (in Chinese with English abstract).
Liao, X.J., Wang, P.A., Qin, H.C., Lu, X.K., Dong, F.X., Liu, X.C., Shu, B., 2008. Geology, geochemistry and ore-forming age of the Gaotongling molybdenum deposit, Tunchang area, Hainan, China. Geol. Bull. China 27 (4), 560–570 (in Chinese with English abstract).
Liu, Y.S., Hu, Z.C., Gao, S., Günther, D., Xu, J., Gao, C.G., Chen, H.H., 2008. In situ analysis of major and trace elements of anhydrous minerals by LA-ICP-MS without applying an internal standard. Chem. Geol. 257 (1–2), 34–43.
Liu, L., Xu, X.S., Xia, Y., 2014. Cretaceous Pacific plate movement beneath SE China: evidence from episodic volcanism and related intrusions. Tectonophysics 614, 170–184.
Lowell, J.D., Guilbert, M., 1970. Lateral and vertical alteration–mineralization zoning in porphyry ore deposits. Econ. Geol. 65 (4), 373–408.
Ludington, S., Plumlee, G.S., 2009. Climax-type porphyry molybdenum deposits. U.S. Geological Survey Open-File Report 2009-1215, pp. 1–16.
Ludwig, K.R., 2003. Isoplot 3.00, a geochronological toolkit for Microsoft Excel. Berkeley Geochronology Center, Special Publication 4, pp. 1–70.
Ludwig, K.R., Mundil, R., 2002. Extracting reliable U–Pb ages and errors from complex populations of zircons from Phanerozoic tuffs. Journal of Conference Abstracts, 12th Goldschmidt Conference Paper A663.
Ma, D.Q., Wang, X.D., Chen, Z.P., Xiao, Z.F., Zhang, W.C., Zhong, S.Z., 1997. New achievements about Baoban Group in Hainan Island. Reg. Geol. China 16 (2), 130–136 (in Chinese with English abstract).
Maniar, P.D., Piccoli, P.M., 1989. Tectonic discrimination of granitoids. Geological Society of America Bulletin 101, 635–643.
Mao, J.W., Xie, G.Q., Bierlein, F., Qu, W.J., Du, A.D., Ye, H.S., Pirajno, F., Li, H.M., Guo, B.J., Li, Y.F., Yang, Z.Q., 2008. Tectonic implications from Re–Os dating of Mesozoic molybdenum deposits in the East Qinling–Dabie orogenic belt. Geochim. Cosmochim. Acta 72 (18), 4607–4626.
Mao, J.W., Pirajno, F., Cook, N., 2011a. Mesozoic metallogeny in East China and corresponding geodynamic settings—an introduction to the special issue. Ore Geol. Rev. 43, 1–7.
Mao, J.W., Pirajno, F., Xiang, J.F., Gao, J.J., Ye, H.S., Li, Y.F., Guo, B.J., 2011b. Mesozoic molybdenum deposits in the east Qinling–Dabie orogenic belt: characteristics and tectonic settings. Ore Geol. Rev. 43, 264–293.
Mao, J.W., Xie, G.Q., Duan, C., Pirajno, F., Ishiyama, D., Chen, Y.C., 2011c. A tectono-genetic model for porphyry-skarn-stratabound Cu–Au–Mo–Fe and magnetite–apatite deposits along the Middle-Lower Yangtze River Valley, Eastern China. Ore Geol. Rev. 43, 294–314.
Metcalfe, I., 2013. Gondwana dispersion and Asian accretion: tectonic and palaeogeographic evolution of eastern Tethys. J. Asian Earth Sci. 66, 1–33.
Metcalfe, I., Shergold, I.H., Li, Z.X., 1994. IGCP 321 Gondwana dispersion and Asian accretion:field-work on Hainan Island. Episodes 16 (4), 443–447.
Mi, M., Chen, Y.J., Yang, Y.F., Wang, P., Li, F.L., Wan, S.Q., Xu, Y.L., 2015. Geochronology and geochemistry of the giant Qian'echong Mo deposit, Dabie Shan, eastern China: implications for ore genesis and tectonic setting. Gondwana Res. 27, 1217–1235.
Mutschler, F.E., Wright, E.G., Ludington, S.D., Abbott, J.T., 1981. Granite molybdenite systems. Econ. Geol. 76, 874–897.
Njanko, T., Nédélec, A., Affaton, P., 2006. Synkinematic high-K calc-alkaline plutons associated with the Pan-African Central Cameroon shear zone (W-Tibati area): petrology and geodynamic significance. J. Afr. Earth Sci. 44, 494–510.
Ohmoto, H., 1972. Systematics of sulfur and carbon isotopes in hydrothermal ore deposits. Econ. Geol. 67, 551–578.
Pearce, J.A., 1983. Role of the sub-continental lithosphere in magma genesis at active continental margins. In: Hawkesworth, C.J., Norry, M.J. (Eds.), Continental Basalt and Mantle Xenoliths. Shiva Publishing, Nantwich, UK, Shiva (230–249 pp.).
Pirajno, F., 2009. Chapter 4 Intrusion-related hydrothermal mineral systems. Hydrothermal Processes and Mineral Systems. Springer Science+Business Media B.V. (205–354 pp.).
Raith, J.G., Stein, H.J., 2000. Re–Os dating and sulfur isotope composition of molybdenite from W–Mo deposits in western Namaqualand, South Africa: implications for ore genesis and low-P high-grade metamorphism. Mineral. Deposita 35, 741–753.
Rickwood, P.C., 1989. Boundary lines within petrologic diagrams which use oxides of major and minor elements. Lithos 22, 247–263.
Roberts, M.P., Clemens, J.D., 1993. Origin of high-potassium, calc-alkaline, I-type granitoids. Geology 21, 825–828.
Rottura, A., Bargossi, G.M., Caggianelli, A., Del Moro, A., Visonà, D., Tranne, C.A., 1998. Origin and significance of the Permian high-K calc-alkaline magmatism in the central-eastern Southern Alps, Italy. Lithos 45, 329–348.
Rye, R.O., Ohmoto, H., 1974. Sulfur and carbon isotopes and ore genesis: a review. Econ. Geol. 69, 826–842.
Seal II, R.R., 2006. Sulfur isotope geochemistry of sulfide minerals. Rev. Mineral. Geochem. 61, 633–677.
Seedorff, E., Einaudi, M.T., 2004. Henderson porphyry molybdenum system, Colorado. I. Sequence and abundance of hydrothermal mineral assemblages, flow paths of evolving fluids. Econ. Geol. 99, 3–38.
Seedorff, E., Dilles, J.H., Proffett, J.M., Einaudi, M.T., Zurcher, L., Stavast, W.J.A., Johnson, D.A., Barton, M.D., 2005. Porphyry deposits: characteristics and origin of hypogene features. Econ. Geol. 100 (29), 251–298.
Selby, D., Creaser, R.A., 2004. Macroscale NTIMS and microscale LA-MC-ICP-MS Re–Os isotopic analysis of molybdenite: testing spatial restrictions for reliable Re–Os age determinations, and implications for the decoupling of Re and Os within molybdenite. Geochim. Cosmochim. Acta 68, 3897–3908.
Shu, L.S., Jahn, B.M., Charvet, J., Santosh, M., Wang, B., Xu, X.S., Jiang, S.Y., 2014a. Early Paleozoic depositional environment and intraplate tectono-magmatism in the Cathaysia Block (South China): evidence from stratigraphic, structural, geochemical and geochronological investigations. Am. J. Sci. 314, 154–186.
Shu, Q.H., Lai, Y., Wang, C., Xu, J.J., Sun, Y., 2014b. Geochronology, geochemistry and Sr–Nd–Hf isotopes of the Haisugou porphyry Mo deposit, northeast China, and their geological significance. J. Asian Earth Sci. 79, 777–791.

Sillitoe, R.H., 1980. Types of porphyry molybdenum deposits. Min. Mag. 142 (6), 550–553.
Sisson, T.W., Ratajeski, K., Hankins, W.B., Glazner, A.F., 2005. Voluminous granitic magmas from common basaltic sources. Contrib. Mineral. Petrol. 148, 635–661.
Smoliar, M.I., Walker, R.J., Morgan, J.W., 1996. Re–Os ages of group IIA, IIIA, IVA, and IVB iron meteorites. Science 271, 1099–1102.
Stein, H.J., 2006. Low-rhenium molybdenite by metamorphism in northern Sweden: recognition, genesis, and global implications. Lithos 87, 300–327.
Stein, H.J., Bingen, B., 2002. 1.05–1.01 Ga Sveconorwegian metamorphism and deformation of the supracrustal sequence at Saesvatn, South Norway: Re–Os dating of Cu–Mo mineral occurrences. Geol. Soc. Lond. Spec. Publ. 204, 319–335.
Stein, H.J., Sundblad, K., Morgan, J.W., Markey, R.J., Motuza, G., 1998. Re–Os ages for Archean molybdenite and pyrite, Kuittila, Finland and Proterozoic, Kabeliai, Luthuania: a metamorphic and metasomatic test for the chronometer. Mineral. Deposita 33, 329–345.
Stein, H.J., Markey, R.J., Morgan, J.W., Hannah, J.L., Schersten, A., 2001. The remarkable Re–Os chronometer in molybdenite: how and why it works. Terra Nova 13, 479–486.
Stein, H.J., Scherstén, A., Hannah, J.L., Markey, R.J., 2003. Sub-grain scale decoupling of Re and ^{187}Os and assessment of laser ablation ICP-MS spot dating in molybdenite. Geochim. Cosmochim. Acta 67 (19), 3673–3686.
Stein, H.J., Hannah, J.L., Zimmerman, A., Markey, R.J., Sarkar, S.C., Pal, A.B., 2004. A 2.5 Ga porphyry Cu–Mo–Au deposit at Malanjkhand, central India: implications for Late Archean continental assembly. Precambrian Res. 134, 189–226.
Sun, S.S., McDonough, W.F., 1989. Chemical and isotopic systematics of oceanic basalts: implications for mantle composition and processes. In: Saunders, A.D., Norry, M.J. (Eds.), Magmatism in the Ocean Basins. Geological Society Special Publications 42, pp. 313–345.
Sun, Y.L., Xu, P., Li, J., He, K., Chu, Z., Wang, C.Y., 2010. A practical method for determination of molybdenite Re–Os age by inductively coupled plasma-mass spectrometry combined with Carius tube-HNO_3 digestion. Anal. Methods 2 (5), 575–581.
Tang, L.M., Chen, H.L., Dong, C.W., Yang, S.F., Shen, Z.R., Chen, X.G., Fu, L.L., 2013. Middle Triassic post-orogenic extension on Hainan Island: chronology and geochemistry constraints of bimodal intrusive rocks. Sci. China Earth Sci. 56 (5), 783–793.
Topuz, G., Altherr, R., Siebel, W., Schwarz, W.H., Zack, T., Hasözbek, A., Barth, M., Satlr, M., Şen, C., 2010. Carboniferous high-potassium I-type granitoid magmatism in the Eastern Pontides: the Gümüşhane pluton (NE Turkey). Lithos 116, 92–110.
USGS (U.S. Geological Survey), 2011. Mineral commodity summaries 2011. USGS Sciences for a Changing World (198 pp.).
Wang, L., Liao, X.J., 2012. Geological characteristics and genesis of Xincun molybdenum deposit in Baoting County, Hainan Province. Geol. Miner. Resour. South China 28 (3), 203–212.
Wang, X.F., Ma, D.Q., Jiang, D.H., 1991. Geology of Hainan Island (II): Magmatic Rocks. Geological Publishing House, Beijing (274 pp. in Chinese).
Wang, Z.L., Xu, D.R., Zhang, Y.Q., Chen, F.X., Wang, L., Wu, J., 2011. Zircon LA-ICP-MS U–Pb dating of the granodiorite porphyry from Shilu iron ore deposit, Hainan Province and its geological implication. Geotecton. Metallog. 35 (2), 292–299 (in Chinese with English abstract).
Wang, Q., Li, X.H., Jia, X.H., Wyman, D., Tang, G.J., Li, Z.X., Ma, L., Yang, Y.H., Jiang, Z.Q., Gou, G.N., 2012. Late Early Cretaceous adakitic granitoids and associated magnesian and potassium-rich mafic enclaves and dikes in the Tunchang–Fengmu area, Hainan Province (South China): partial melting of lower crust and mantle, and magma hybridization. Chem. Geol. 328, 222–243.
Wang, Y.J., Fan, W.M., Zhang, G.W., Zhang, Y., 2013. Phanerozoic tectonics of the South China Block: key observations and controversies. Gondwana Res. 23 (4), 1273–1305.
Wang, Y.H., Zhao, C.B., Zhang, F.F., Liu, J.J., Wang, J.P., Peng, R.M., Liu, B., 2014. SIMS zircon U–Pb and molybdenite Re–Os geochronology, Hf isotope, and whole-rock geochemistry of the Wunugetushan porphyry Cu–Mo deposit and granitoids in NE China and their geological significance. Gondwana Res. http://dx.doi.org/10.1016/j.gr.2014.10.001.
Wang, Z.L., Xu, D.R., Hu, G.C., Yu, L.L., Wu, C.J., Zhang, Z.C., Cai, J.X., Shan, Q., Hou, M.Z., Chen, H.Y., 2015. Detrital zircon U–Pb ages of the Proterozoic metaclastic-sedimentary rocks in Hainan Province of South China: new constraints on the depositional time, source area, and tectonic setting of the Shilu Fe–Co–Cu ore district. J. Asian Earth Sci. http://dx.doi.org/10.1016/j.jseaes.2015.04.014.
Westra, G., Keith, S.B., 1981. Classification and genesis of stockwork molybdenum deposits. Econ. Geol. 76 (4), 844–873.
White, W.H., Bookstrom, A.A., Kamilli, R.J., Ganster, M.W., Smith, R.P., Ranta, D.E., Steininger, R.C., 1981. Character and origin of Climax-type molybdenum deposits. Econ. Geol. 75th Anniversary Volume, 270–316.
Wong, J., Sun, M., Xing, G., Li, X.-h., Zhao, G., Wong, K., Yuan, C., Xia, X., Li, L., Wu, F., 2009. Geochemical and zircon U–Pb and Hf isotopic study of the Baijuhuajian metaluminous A-type granite: extension at 125–100 Ma and its tectonic significance for South China. Lithos 112 (3–4), 289–305.
Xu, D.R., Fan, W.M., Liang, X.Q., Tang, H.F., 2001. Characteristics of Proterozoic metamorphic basement in Hainan Island and its implications for crustal growth: Nd and Pb isotope constraints. Geol. J. China Univ. 7 (2), 146–157 (in Chinese with English abstract).
Xu, D.R., Wang, Z.L., Cai, J.X., Wu, C.J., Bakun-Czubarow, N., Wang, L., Chen, H.Y., Baker, M.J., Kusiak, M.A., 2013. Geological characteristics and metallogenesis of the Shilu Fe-ore deposit in Hainan Province, South China. Ore Geol. Rev. 53, 318–342.
Xu, D.R., Wang, Z.L., Chen, H.Y., Hollings, P., Jansen, N.H., Zhang, Z.C., Wu, C.J., 2014a. Petrography and geochemistry of the Shilu Fe–Co–Cu ore district, South China: implications for the origin of a Neoproterozoic BIF system. Ore Geol. Rev. 57, 322–350.
Xu, Y.J., Cawood, P.A., Du, Y.S., Zhong, Z.Q., Hughes, N.C., 2014b. Terminal suturing of Gondwana along the southern margin of South China Craton: evidence from detrital zircon U–Pb ages and Hf isotopes in Cambrian and Ordovician strata, Hainan Island. Tectonics 2490–2504 http://dx.doi.org/10.1002/2014TC003748.
Xu, D.R., Kusiak, M.A., Wang, Z.L., Chen, H.Y., Bakun-Czubarow, N., Wu, C.J., Konečný, P., Hollings, P., 2015. Microstructural observation and chemical dating on monazite from the Shilu Group, Hainan Province of South China: implications for origin and evolution of the Shilu Fe–Co–Cu ore district. Lithos 216–217, 158–177.
Zeng, Q., Yuan, C., Guo, Z., Lin, J., Wu, W., Cai, D., Zhuang, S., Huang, H., Fu, C., Wu, T., Wang, W., Yun, P., 1992. Fundamental Geological Investigation of Sanya, Hainan Island. The Press of the China University of Geosciences, Wuhan (174 pp. in Chinese with English abstract).
Zeng, Q.D., Liu, J.M., Zhang, Z.L., Chen, W.J., Zhang, W.Q., 2011. Geology and geochronology of the Xilamulun molybdenum metallogenic belt in eastern Inner Mongolia, China. Int. J. Earth Sci. (Geol. Rundsch.) 100, 1791–1809.
Zeng, Q.D., Liu, J.M., Qin, K.Z., Fan, H.R., Chu, S.X., Wang, Y.B., Zhou, L.L., 2013. Types, characteristics, and time–space distribution of molybdenum deposits in China. Int. Geol. Rev. 55 (11), 1311–1358.
Zeng, Q.D., Liu, J.M., Chu, S.X., Wang, Y.B., Sun, Y., Duan, X.X., Zhou, L.L., Qu, W.J., 2014. Re–Os and U–Pb geochronology of the Duobaoshan porphyry Cu–Mo–(Au) deposit, northeast China, and its geological significance. J. Asian Earth Sci. 79, 895–909.
Zhai, D.G., Liu, J.J., Wang, J.P., Yang, Y.Q., Zhang, H.Y., Wang, X.L., Zhang, Q.B., Wang, G.W., Liu, Z.J., 2014. Zircon U–Pb and molybdenite Re–Os geochronology, and whole-rock geochemistry of the Hashitu molybdenum deposit and host granitoids, Inner Mongolia, NE China. J. Asian Earth Sci. 79, 144–160.
Zhang, Y.M., Zhang, R.J., Rao, H.Z., Ma, G.G., 1997. The Precambrian crustal tectonic evolution in Hainan Island. Earth Sci. 22 (4), 395–400 (in chinese with English abstract).
Zhang, F.F., Wang, Y.J., Chen, X.Y., Fan, W.M., Zhang, Y.H., Zhang, G.W., Zhang, A.M., 2011a. Triassic high-strain shear zones in Hainan Island (South China) and their implications on the amalgamation of the Indochina and South China Blocks: kinematic and ^{40}Ar/^{39}Ar geochronological constraints. Gondwana Res. 19, 910–925.
Zhang, X.H., Mao, Q., Zhang, H.F., Zhai, M.G., Yang, Y.H., Hu, Z.C., 2011b. Mafic and felsic magma interaction during the construction of high-K calc-alkaline plutons within a metacratonic passive margin: the Early Permian Guyang batholith from the northern North China Craton. Lithos 125, 569–591.
Zhang, H., Li, C.Y., Yang, X.Y., Sun, Y.L., Deng, J.H., Liang, H.Y., Wang, R.L., Wang, B.H., Wang, Y.X., Sun, W.D., 2014. Shapinggou: the largest Climax-type porphyry Mo deposit in China. Int. Geol. Rev. 56 (3), 313–331.
Zhao, Z., Chen, Z.H., Wang, C.H., Yang, W.P., 2012. Molybdenite Re–Os age of the Dawan Mo–Be deposit, East Fujian—a discussion on the tempo-spatial distribution and tectonic setting of the molybdenite deposit in Fujian Province. Geotecton. Metallog. 36 (3), 399–405 (in Chinese with English abstract).
Zhou, X.M., Li, W.X., 2000. Origin of late Mesozoic igneous rocks in Southeastern China: implications for lithosphere subduction and underplating of mafic magmas. Tectonophysics 326 (3–4), 269–287.
Zhou, X.M., Sun, T., Shen, W.Z., Shu, L.S., Niu, Y.L., 2006. Petrogenesis of Mesozoic granitoids and volcanic rocks in South China: a response to tectonic evolution. Episodes 29 (1), 26–33.
Zimmerman, A., Stein, H.J., Hannah, J.L., Kozelj, D., Bogdanov, K., Berza, T., 2008. Tectonic configuration of the Apusini–Banat–Timok–Srednogorie belt, Balkans–South Carpathians,constrained by high precision Re–Os molybdenite ages. Mineral. Deposita 43, 1–21.